DEVELOPMENT OF A SHELL FINITE ELEMENT FOR LARGE DEFORMATION ANALYSIS OF LAMINATED COMPOSITES

A THESIS SUBMITTED TO
THE GRADUATE SCHOOL OF NATURAL AND APPLIED SCIENCES
OF
MIDDLE EAST TECHNICAL UNIVERSITY

BY

TUBA YILDIZ

IN PARTIAL FULFILLMENT OF THE REQUIREMENTS
FOR
THE DEGREE OF MASTER OF SCIENCE
IN
MECHANICAL ENGINEERING

SEPTEMBER 2008

Approval of the thesis:

DEVELOPMENT OF A SHELL FINITE ELEMENT FOR LARGE DEFORMATION ANALYSIS OF LAMINATED COMPOSITES

submitted by **TUBA YILDIZ** in partial fulfillment of the requirements for the degree of **Master of Science in Mechanical Engineering Department, Middle East Technical University** by,

Prof.Dr. Canan Özgen
Dean, Graduate School of **Natural and Applied Sciences** _____

Prof.Dr. S.Kemal İder
Head of Department, **Mechanical Engineering** _____

Prof.Dr. Haluk Darendeliler
Supervisor, **Mechanical Engineering Dept., METU** _____

Examining Committee Members

Prof. Dr. Mustafa İlhan Gökler _____
Mechanical Engineering Dept., METU

Prof. Dr. Haluk Darendeliler _____
Mechanical Engineering Dept., METU

Prof. Dr. Suha Oral _____
Mechanical Engineering Dept., METU

Prof. Dr. Suat Kadıoğlu _____
Mechanical Engineering Dept., METU

Prof. Dr. Can Çoğun _____
Mechanical Engineering Dept., Gazi University

Date: September 2nd, 2008

I hereby declare that all information in this document has been obtained and presented in accordance with academic rules and ethical conduct. I also declare that, as required by these rules and conduct, I have fully cited and referenced all material and results that are not original to this work.

Name, Last name : Tuba Yıldız

Signature :

ABSTRACT

DEVELOPMENT OF A SHELL FINITE ELEMENT
FOR LARGE DEFORMATION ANALYSIS OF
LAMINATED COMPOSITES

Yıldız, Tuba

M.Sc., Department of Mechanical Engineering

Supervisor: Prof. Dr. Haluk Darendeliler

September 2008, 110 Pages

The objective of the present work is to investigate the behavior of laminated fiber - reinforced polymer matrix composite shell structures under bending load with the help of a modified finite element computer code which was previously developed for the analysis of pseudo-layered single material shells. The laminates are assumed to be orthotropic and the formulation is adapted to first order shear deformation theory. The aim is to determine the large deformation characteristics numerically, and to predict the modes of failure by the illustration of the critical elements of the model. Therefore, several failure theories are also integrated to the code to detect first ply failure. Triangular shell elements are used and all the related data are generated from the mid-plane. Laminates under transverse loading are analyzed through several boundary conditions and ply orientations. To verify the numerical results obtained, a commercial finite element program is used to compare the outputs of the study, and the comparison is found to have shown good agreement. The onset of damage is investigated by using different failure criteria consisting of maximum stress, Tsai-Wu, and Tsai- Hill theories and close results are obtained.

Keywords: Laminated Composite Shell, First Ply Failure, Finite Element Analysis, Elastic Deformation

ÖZ

TABAKALI KOMPOZİTLERİN BÜYÜK ŞEKİL DEĞİŞTİRME ANALİZİ AMACIYLA BİR KABUK SONLU ELEMANININ GELİŞTİRİLMESİ

Yıldız, Tuba

Yüksek Lisans, Makine Mühendisliği Bölümü

Tez Yöneticisi: Prof. Dr. Haluk Darendeliler

Eylül 2008, 110 Sayfa

Yapılan yüksek lisans çalışmasında, polimer matrisli tabakalı kabuk kompozitlerin eğilme yükü altındaki davranışlarını incelemek amacıyla, daha önce hayali tabaklı tek malzemeli kabukların analizi için yazılmış sonlu elemanlar programı geliştirilmiştir. Laminalar ortotropik kabul edilmiş ve çalışmada birinci derece kayma gerilmesi teoremi kullanılmıştır. Çeşitli fiber yönleri ve sınır koşullarındaki birçok plakanın büyük deformasyon analizi sayısal olarak gerçekleştirilmiş hasar başlangıçlarının oluştuğu kritik elemanlar tespit edilmiştir. Üçgen sonlu elemanların kullanılması tercih edilmiştir. Programın doğruluğunu kontrol etmek amacıyla, ticari bir sonlu elemanlar analizi programı kullanılmıştır. Her iki programdan da elde edilen deformasyon değerleri karşılaştırılmış ve uyumlu oldukları gözlenmiştir. Hasar analizi sonucu ulaşılan veriler, maksimum gerilme, Tsai-Wu ve Tsai-Hill kriterleri ile ayrı ayrı incelenmiş ve yakın sonuçlar elde edildiği görülmüştür.

Anahtar Kelimeler: Tabaklı Kompozit Kabuk, Hasar Modu, Sonlu Elemanlar Analizi, Elastik Deformasyon

ACKNOWLEDGMENTS

I would like to thank my supervisor Prof. Dr. Haluk Darendeliler for his guidance, patience, advice, criticism, encouragements, and insight through the research.

TABLE OF CONTENTS

LIST OF TABLES

TABLES

LIST OF FIGURES

FIGURES

CHAPTER 1

INTRODUCTION

Composites are advanced engineering materials with superior mechanical properties that can be tailored and diversified among the purpose of application. The requirements of the design are accomplished by the combination of two or more distinct materials on macroscopic scale in order to improve the desired properties like strength, stiffness, corrosion resistance, fatigue life, weight, attractiveness, thermal insulation or conductivity. The advanced improvements generally result in challenging design applications which require professional expertise. Their high-strength-to-weight ratio exceeding that of the constituents is the main attribute which makes mechanics of composite materials a more popular area of interest.

1.1 Types

The need for fiber placement in different directions according to the particular application has led to various types of composites. In the continuous fiber reinforced laminate, individual-continuous-fiber/matrix laminae is oriented in the required directions and bonded together to form a laminate. Although the continuous fiber laminate is used extensively, the potential for delamination, or separation of the laminae is still a major problem because the interlaminar strength is matrix-dominated.

Woven composites do not have distinct laminae and are not susceptible to delamination, but strength and stiffness are sacrificed due to the fact that the fibers are not so straight as in the continuous fiber laminate.

Chopped fiber composites may have short fibers randomly dispersed in the matrix. These are used extensively in high volume applications due to low manufacturing cost, but their mechanical properties are considerably poorer than those of continuous fiber composites.

Hybrid composites consist of mixed chopped and continuous fibers or mixed fiber types such as glass/graphite. They greatly expand the range of properties that can be achieved with advanced composites. Hybrid composites generally suffer from delamination.

Another common composite configuration, the sandwich structure, consists of high strength composite facing sheets bonded to a lightweight foam or honeycomb core. Sandwich structures have extremely high flexural stiffness-to-weight ratios and are widely used in aerospace structures. The design flexibility offered by these and other composite configurations is obviously quite attractive to designers, and the potential now exists to design not only the structure but also the structural material itself.

Particulate composites have an additive constituent which is essentially one or two dimensional and macroscopic. They differ from the fiber and flake types in that distribution of the additive constituent is usually random rather than controlled. Particulate composites are therefore usually isotropic. This family of composites includes dispersion-hardened alloys and cermets.

1.2 Constituents

1.2.1 Fibers and Flakes

Fibers are the principle constituent of a composite material. They occupy the largest volume fraction in a composite laminate and share the major portion of the load acting on a composite structure. Proper selection of the type, amount and orientation

of fibers is very important because it influences the following characteristics of a composite laminate:

- Specific gravity
- Tensile strength and modulus
- Compressive strength and modulus
- Fatigue strength and failure mechanisms
- Electric and thermal conductivities
- Cost

Although the strength and one-dimensional nature of the fibers make them highly useful in composite structures, particularly where anisotropy is desirable, there are applications where two-dimensional elements or flakes, are preferable. With nondestructive flakes such as glass or mica, it is possible to obtain good dielectric properties and resistance to heat. Compared with fibers, flakes are relatively inexpensive to produce and can be handled in batch quantities.

1.2.1.1 Fiber Types

Glass fibers are the most common of all reinforcing fibers for polymeric matrix composites since they are strong, low in cost, nonflammable, nonconductive and corrosion resistant. The disadvantages are low tensile modulus, relatively high specific gravity, low fatigue resistance, sensitivity to abrasion and high hardness. Glass fiber is made by melting the raw materials (silicon dioxide and metallic-oxide-modifying elements) in a high temperature furnace and then drawing the molten material into filaments. There are three main categories of glass fiber which are E-glass, S-glass and C-glass. E-glass (named for its electrical properties) accounts for most of the glass fiber production and is the most widely used reinforcement for composites. The second most popular glass fiber, S-glass, has roughly 30 percent greater tensile strength and 20 percent greater modulus of elasticity than E-glass, but

is not as widely used because of its high cost. C-glass is used in the areas where particularly chemical resistance is necessary.

Carbon fibers account for the advanced group of fibers and preferred among the advantages of high tensile strength-to-weight and tensile modulus-to-weight ratios, high fatigue strengths and lower specific gravities. Their high cost has so far excluded them from widespread commercial applications, but they are used mostly in aerospace industry where weight savings is considered more critical than cost. Carbon fibers are manufactured from two types of precursors, namely textile precursor (polyacrylonitrile –PAN, or rayon) and pitch precursors (a by-product of petroleum refining or coal coking). After a sequence of heat treatments, the precursor is converted to carbon.

Aramid fibers possess a tensile strength seven to eight times that of the steel wire and have an excellent stability against the temperature change. Therefore, aramid fibers are widely used in the automotive industry for tire cords, timing belts, and break friction materials. In addition, these fibers have been used as concrete reinforcing materials and in high-performance ropes. The major disadvantages of aramid fiber-reinforced composites are their low compressive strength and the difficulty in cutting and machining them. Fibers are produced by extruding an acidic solution of a proprietary precursor from a spinneret.

The most prominent feature of boron fibers is their extremely high tensile modulus which is in the range 379-414 GPa. Because of the relatively large diameter, boron fibers offer excellent resistance to buckling, which contributes to high compressive strength for boron fiber-reinforced composites whereas main disadvantage is the high cost. Boron fibers are manufactured by chemical vapor deposition of boron into a heated substrate (a tungsten wire or a carbon monofilament).

Ceramic fibers are notable for their high temperature applications in metal and ceramic matrix composites. SiC and Al_2O_3 are the examples of ceramic fibers suitable for reinforcing metal matrices in which carbon and boron exhibit transverse reactivities.

Properties of an arbitrary set of fibers are listed in Table 1.2.1

Table 1.2.1 Properties of Selected Reinforcing Fibers [2]

Fiber	***Typical Diameter (μm)***	***Specific Gravity (g/cm^3)***	***Tensile Modulus (GPa)***	***Tensile Strength (GPa)***	***Strain to Failure (%)***	***Coefficient of Thermal Expansion ($10^{-6}/^oC$)***
Glass						
E-glass	10	2.54	72.4	3.45	4.8	5
S-glass	10	2.49	86.9	4.30	5.0	2.9
PAN Carbon						
T-300	7	1.76	231	3.65	1.4	-0.6
T-40	5.1	1.81	290	5.65	1.8	-0.75
AS-1	8	1.80	228	3.10	1.32	
AS-4	7	1.80	248	4.07	1.65	
Pitch Carbon						
P-55	10	2.0	380	1.90	0.5	-1.3
P-100	10	2.15	758	2.41	0.32	-1.45
Aramid						
Kevlar 49	11.9	1.45	131	3.62	2.8	-2.59
Boron	140	2.7	393	3.1	0.79	5
SiC						
Monofilament	140	3.08	400	3.44	0.86	1.5

Fiber diameters classify the various fiber morphologies, which consist of whiskers (<1 μm), continuous multifilament yarn (5-25 μm), and continuous monofilament (>100 μm). Whiskers are discontinuous reinforcements with high aspect ratio. Because of their small diameters, they have very few defects to initiate fracture and as a result, have much higher strengths than the discontinuous fibers. Silicon carbide, silicon nitride, carbon and potassium titanate whiskers are currently in use.

1.2.2 Matrices

Depending on the application, it is possible to view the role of the matrix in two distinct ways, namely, as the binder that contains the major structural elements (fibers) and transfers load between them, or as the primary phase which is merely reinforced by the secondary fiber phase. Fibers are of little use without the presence of a matrix material or a binder. The important functions of a matrix material also include the following:

- The matrix isolates the fibers so that individual fibers can act separately. This stops or slows the propagation of the crack.
- The matrix provides a good surface quality and aids in the production of net-shape or near-net-shape parts.
- The matrix provides protection to reinforcing fibers against chemical attack and mechanical damage (wear).
- Depending on the matrix material selected, performance characteristics such as ductility, impact strength, etc. are also influenced. A ductile matrix will increase the toughness of the structure. For higher toughness requirements, thermoplastic based composites are selected.
- The failure mode is strongly affected by the type of matrix material as well as its compatibility with the fiber.

1.2.2.1 Matrix Materials

Matrix materials are categorized in three groups which are mainly polymers, metals and ceramics.

1.2.2.1.1 Polymers

A polymeric material is a collection of a large number of polymer molecules of similar chemical structure. In the solid state, these molecules are frozen in space either in a random fashion or in a mixture of random and orderly fashions. Polymers are divided into two categories: thermoplastics and thermosets.

In a thermoplastic polymer, individual molecules are linear in structure with no chemical linking between them. Thus, with the application of heat and pressure, a thermoplastic polymer can be softened, melted, and reshaped as many times as desired. The most important advantage of thermoplastic polymers over thermosets is their high impact strength and fracture resistance, which in turn impart excellent damping characteristics to the composite material. On the contrary, thermoplastics exhibit poor creep resistance, especially at elevated temperatures, and they are more susceptible to solvents as compared to thermosets. The higher viscosity of thermoplastic resins makes some manufacturing processes more difficult. The examples of thermoplastic matrix materials are nylon, polypropylene, polyetheretherketone (PEEK) and polyphenylene sulfide.

In a thermoset polymer on the other hand, the molecules are chemically joined together by cross-links. Once these rigid, three-dimensional structures are formed during polymerization reaction, the thermoset polymer can not be melted and reshaped. However, if the number of cross-links is low, it may be possible to soften it. Thermosets are brittle in nature and are used with some form of filler and reinforcement. They provide easy processability and better fiber impregnation,

because the liquid resin is used at room temperature for various processes. Thermosets offer greater thermal and dimensional stability, better rigidity, and higher electrical, chemical and solvent resistance. The most common resin materials used in thermoset composites are epoxy, polyester, vinylester, phenolics, polyamides and bismaleimides.

1.2.2.1.2 Metals

The metal matrix composites (MMCs) are materials consisting of metal alloys reinforced with continuous fibers, particulates or whiskers. Because of their ability to provide the needed strength at the lowest weight and least volume, they are attractive for the structural and nonstructural applications. MMCs are superior to polymers with their high shear modulus and ductility, tensile strength, small coefficient of expansion, resistance to moisture and dimensional stability.

The two most commonly used metal matrices are based on aluminum and titanium, since these metals have comparatively low specific gravities and are available in a variety of alloy forms. MMC engine applications are produced and used for automobile engine cylinders die-cast from a carbon fiber-aluminum-Al_2O_3 material. Titanium MMCs are used in applications where performance is demanded without regard to cost-effectiveness. This is where one obtains high-temperature performance unattainable with conventional materials.

1.2.2.1.3 Ceramics

Ceramic fibers such as SiC and SiN_4 use polysilane as the base material. Ceramic matrix composites (CMCs), in which ceramic or glass matrices are reinforced with continuous fibers, chopped fibers, whiskers or particulates, are emerging as a class of advanced engineering structural materials. CMCs currently have limited temperature applications but a large potential for much wider use in military, aerospace, and

commercial applications such as energy-efficient systems and transportation with their superior dielectric properties.

There are also other specialty CMCs such as nanocomposites (made form reactive powders) and electroceramics. CMCs are unique in that they combine low density with high modulus, strength and toughness (contrasted with monolithic ceramics), and strength retention at high temperatures. They are among the stiffest materials and have high stiffness-to-weight ratios. Many have good corrosion and erosion characteristics for high temperature applications. Industrial uses of CMCs include furnace materials, energy conversion systems, gas turbines, and heat engines. They have been also used in jet fighters. Ceramic matrix composites mainly suffer from brittleness.

1.3 Applications

The primary usage of advanced composite materials is for aerospace applications. Aircraft are distinguished from the other vehicles by the fact that structural factors of safety are low and power-to-weight ratios are high. These levels are achieved by using materials with high specific material properties and precise design procedures. Airplanes, rockets missiles and various structural components of these, including engines and also satellite applications have been routinely produced with glass, carbon and kevlar composites. Composite components in aircraft applications are given in Table 1.3.1.

The construction and civil structure industries are the second major users of composite materials. The driving force for the use of glass- and carbon-reinforced plastics for bridge applications is reduced installation, handling, repair, and life-cycle costs as well as improved corrosion and durability. It also saves a significant amount of time for repair and installation, and thus minimizes the blockage of traffic. Composite usage in earthquake and seismic retrofit activities is also popular. The

columns wrapped by glass/epoxy, carbon/epoxy and aramid/epoxy show good potential for these applications.

Table 1.3.1 Composite Components in Aircraft Applications [3]

	Composite Components
F-14	Doors, horizontal tails, fairings, stabilizer skins
F-15	Fins, rudders, vertical and horizontal tails, speed breaks, stabilizer skins
F-16	Vertical and horizontal tails, fin leading edge, skins on vertical fin box
B-1	Doors, vertical and horizontal tails, flaps, slats, inlets
AV-8B	Doors, rudders, vertical and horizontal tails, ailerons, flaps, fin box, fairings
Boeing 737	Spoilers, horizontal stabilizers, wings
Boeing 757	Doors, rudders, elevators, ailerons, spoilers, flaps, fairings
Boeing 767	Doors, rudders, elevators, ailerons, spoilers, fairings

The use of composites in marine industry dates back to World War II, when the first experiments with reinforced plastics were initiated. It has been realized that the most promising combination for marine applications would utilize glass fibers reinforced with either epoxy or polyester resins. Today the combination of thermosetting polyester resin reinforced with glass fabric is almost universally accepted as the principal marine composite, taking the advantages of resistance to environment including corrosion, rusting, and other forms of degradation, ability to mold seamless, nonleaking structures of complex shape, excellent weight and durability characteristics together with low maintenance cost and ease of repair.

Glass fibers are most often used in production of parts for passenger cars and commercial vehicles. The excellent impact and corrosion resistance of composites make them ideal materials for the vulnerable valance panel below the front or rear bumper. Nonmetallic composites are also finding many applications in parts like radiator fan shrouds, front fender inner panels, and splash panels that have traditionally been made from sheet steel. Since the automotive sector is cost sensitive, carbon fiber composites are not yet accepted due to their high material cost.

Sports and recreation equipment suppliers are becoming major users of composite materials. The growth in structural composite usage has been the greatest interest in high-performance racing boats and sports goods, like golf shafts, tennis rackets, bicycle frames, snow skis, and fishing roads. These products are light in weight and provide superior performance, which helps the user easy handling and increased comfort.

Appliance and equipment field using fiber-glass-reinforced plastics (FRP) is expanding. FRP bulk molding compounds (BMC) and sheet molding compounds (SMC) have proved effective for high-volume automotive exterior components and are finding increasing applications for bulkheads, base pans and enclosures of many different configurations in the appliance and equipment industry. Fiberglass reinforced thermoplastics are finding significant applications in components used in dishwashers, home laundry equipment, sewing machines, and doors as well as business machines, computers and pumps.

1.4 Drawbacks

Drawbacks of the composites are as follows:

- The relationships between forces and deformations are much more complicated for anisotropic composites than they are for conventional

isotropic materials, and this can lead unexpected behavior. While a normal stress induces only normal strains, and a shear induces only shear strains in an isotropic material, a normal or shear stress may induce both normal and shear strains in an anisotropic composite.

- A temperature change in an isotopic material causes expansion or contraction that is uniform in all directions, whereas a temperature change in anisotropic material may cause nonuniform expansion or contraction plus distortion. These so-called "coupling" effects have important implications for not only the analytical mechanics of composites but for the experimental characterization of composite behavior as well.
- Directionally dependent properties make the analysis and design applications more difficult and require special expertise.
- The material cost for composite materials is very high compared to that of steel and aluminum.
- The lack of high-volume production methods limits the widespread use of composite materials.
- Classical ways of designing products with metals depend on the use of machinery and metals handbooks, and design data handbooks. Designing parts with composites lack such books because of the lack of database.
- Since a large portion of composites uses polymer based matrices, temperature resistance is limited by the plastic's properties.
- Solvent resistance, chemical resistance and environmental stress cracking of composites depend on the properties of polymers. Some polymers have low resistance to solvents and environmental stress cracking.
- Composites absorb moisture which affects the properties and dimensional stability of the composites [1, 2, 3, 4, 5].

1.5 Scope of the Current Study

In this study, a finite element program is developed to analyze the nonlinear behavior of the laminated composite flat shells under transverse loading. The deformed coordinates of the laminates having various combinations of ply orientations are plotted within the elastic range until the first ply failure. The initiation of the damage is detected through three different failure theories which are integrated to the developed code, and the results are verified by the help of the commercial finite element program, ANSYS.

The outline of the thesis is briefly as follows: After the introductory part Chapter 1, which includes the basic information about composite materials as properties, application areas, constituents, and their manufacturing techniques together with drawbacks; the literature survey is presented in Chapter 2. Chapter 3 is the part where the plate/shell theories are clarified according to the level of complexity. First order shear deformation theory, constituting the backbone of the current analysis is also presented in this content. Chapter 4 is the part that deals with the failure criteria. In Chapter 5, the governing equations of the analysis are derived starting from the virtual work principle and the constitutive relations are given. Chapter 6 is the section of output data, their comparisons and discussion of the results, and the conclusions are given in the Chapter 7.

CHAPTER 2

LITERATURE REVIEW

Literature review can be roughly categorized in two parts: In the first group of researches, the mainly concentrated subject is to construct the appropriate computational model and to implement the constitutive equations, most commonly to the finite element programs. The second group deals with the extension of the previous studies to work on failure based criteria. This concept can also be subtitled into many variations including: (1) limit theories, (2) polynomial theories, (3) strain energy theories, which are generally used to detect the failure initiation, or namely the first ply failure, and (4) property degradation models which are employed to inspect the total collapse of the laminate.

Masud, Tham and Liu [6] presented a continuum based shear deformable finite element formulation of thick composite shells assuming the displacements and rotations finite while the strains are infinitesimal. The model was cast into a co-rotational framework which had been derived from updated Lagrangian procedure. The algorithm was based on the idea that if the load increment was small enough with respect to the element dimensions, consequently the incremental strains were also small and of the magnitude of small strains, so the quadratic terms in Green-Lagrange strain tensor could be omitted. Numerical examples were carried on flat, cylindrical and spherical geometries with different boundary conditions and mesh densities using eight-node hexahedral mesh elements. Before operating with orthotropic composites, the model was tested with isotropic plates and shells.

Kumar and Palaninathan [7] studied the exact through thickness integration of laminated shells with constant and linearly varying Jacobian inverses. They found out that, the conventional degenerated shell element failed to converge during the three-dimensional integration, especially when the number of layers in the laminate increased. Four computational models were developed for transversely isotropic layers, including numerical integration in three dimensions in each layer, linear Jacobian inverse across the thickness, constant Jacobian inverse through the thickness and a fourth model was offered with further approximation of the second. The performances of the models were evaluated for numerical accuracy and computational efficiency and it was concluded that fourth model was the best to fit.

Hossain, Sinha and Sheikh [8] analyzed anisotropic, doubly curved, moderately thick composite shells. The approach was based on MITC (Mixed Interpolation of Tensorial Components) technique. With the imposition of higher order MITC elements, three dimensional integration was reduced into two dimensions and by this way, computational time was decreased since the quantities involved in the element matrices were independent of the thickness variable. Out-of-plane stresses have been plotted with different ply orientations, curvatures, loading conditions and element types.

Dau, Polit and Touratier [9] analyzed the nonlinear behavior of composite and sandwich plate/shell structures with von-Karmann assumptions. Five degrees of freedom were assumed to obtain a cosine distribution of transverse shear stresses avoiding shear correction factors. Triangular elements were introduced to the finite element mesh. Boundary conditions were satisfied at top and bottom surfaces of the shells. Continuity conditions between layers of the laminate for both shear and transverse stresses were ensured. Transverse shear deflection through thickness was numerically evaluated with different meshes and boundary conditions, and compared with experimental results of the former studies.

Klinkel, Gruttmann and Wagner [10] derived a continuum based three-dimensional shell element. Finite element procedure was based on enhanced assumed strain and assumed natural strain methods in order to prevent shear locking. Eight-node brickelement mesh within linear elastic orthotropic layers was analyzed. In the model tri-linear shape functions were imposed to interpolate the geometric configuration.

Brank and Carrera [11] presented a model for composite structures introducing C^0-continuity of displacements into the first order shear deformation theory satisfying the continuity of the interlaminar equilibrium conditions, taking into account discontinuity of derivatives of displacements and proposing a piecewise linear variation of displacement field across the thickness. Reissner's mixed variational formulation was used and assumed natural strain method was imposed to the constitutive equations. Also, shear stresses were assumed according to a layerwise independent model. Linear and nonlinear examples were compared throughout the developed submodels.

Alfano, Auricchio, Rosati and Sacco [12] formulated 4 and 9-node MITC (Mixed Interpolated Tensorial Components) elements of laminated composite plates. The aim was to evaluate the out-of-plane stresses by the regularization of the extensional and flexural strain fields. They rearranged the displacement fields of second and third derivatives using least square techniques to work with MITC elements, since this approach provides continuity of displacement and rotation fields only up to their first derivatives. Numerical results were compared with regular and highly distorted meshes as well as analytical solutions.

Yu, Hogdes and Volovoi [13] simplified three dimensional anisotropic elasticity problem into two dimensions (an equivalent single layer theory) with a formulation based on asymptotic analysis. The resulting algorithm was a Reissner-like plate theory which can also be implemented in a one-dimensional commercial finite

element program. Results of the developed theory are compared with the exact solutions in terms of stress components.

Wung [14] studied a first-order shear/fourth-order transverse deformation theory of laminated composite shells. The assumption of zero transverse shear stress and ignorance of non-zero surface tractions in the first order shear and classical plate theories were found unrealistic for failure prediction. Since the omission of the normal stress would not just yield less accurate results but also would take more computational effort to satisfy the numerical convergence criterion, higher order shear deformations were introduced to compensate these defects. To improve the computational efficiency, explicit through thickness integration depending upon the updated Lagrangian formulation was used.

Rohwer and Rolfes [15] derived a procedure for fiber reinforced composites in plane stress condition accounting for all six components of stress tensor. Equilibrium conditions were applied to locally determine the stress components in transverse direction. In this way, transverse shear stresses with first derivatives and transverse normal stresses with second derivatives of the membrane stress were imposed. To ease the computational efficiency, in-plane derivatives of the membrane and twisting forces and mixed derivatives of the membrane forces were omitted. The procedure was observed to work well with plates and shells as well as cylinders even under thermal loads.

Goswami [16] presented a finite element formulation for three-dimensional stress analysis of thick and thin plates with higher order shear deformation theory. Parabolic shear strains and linearly distributed normal strains did not require any shear correction factors during the analysis. Comparisons under different mesh refinements, ply orientations, boundary conditions and loadings provided satisfactory convergence.

Chaudhuri and Hsia [17] analyzed the effect of thickness on the large deformation analysis of the curved laminated shells. Total Lagrangian formulation was adapted to a nonlinear theory accounting for layerwise linear displacement distribution through thickness.

Malekzadeh and Setoodeh [18] employed DQ (differential quadrature) method to investigate the large deformation characteristics of thin and moderately thick laminated plates. In this way, the nonlinear equations and boundary conditions were constructed by DQ rules. Constitutive equations were rearranged in order to work for cross-ply lamina orientations since the study only concentrated on symmetric and anti-symmetric cross-ply laminates.

Limit analyses are generally recovered by the use of Mises-like theories, especially with Tsai-Wu criterion, which is the adaptation of failure envelopes used in isotropic elasticity to anisotropy. While the investigation of damage onset is generally carried out with maximum stress, Tsai-Wu, Tsai-Hill, Azzi-Tsai theories or in some cases with the modified or combined versions of these popular criteria, the property degradation and the ultimate collapse of the laminates are determined with the implementation of Hashin or Chang-like theories.

Parhi, Bhattacharyya and Sinha [19] indicated the first ply failure of the laminate by the direct implementation of Tsai-Wu theory to their model.

Huang [20] applied bridging model technique to characterize nonlinearity of composites undergoing inelastic deformation. He constructed the compliance matrix as a combination of fiber and matrix materials instead of the treating the structure with the united properties of the two constituents. The model was incorporated into a commercial finite element program. Laminates under bending and in-plane loads were analyzed with triangular and quadrilateral meshes and outputs were verified with experiments.

Huang et al. [21] also presented another version of bridging model dealing with the effect of matrix plasticity on ultimate strength of composite laminates introducing instantaneous stiffness of the lamina using its constituent properties and fiber volume fraction. Tsai-Wu criterion was applied to the lamina level and maximum normal stress criterion was applied to constituent level. In this micromechanical model, fibers were treated as transversely isotropic and linearly elastic until rupture while matrix was isotropically elasic-plastic.

Lin and Hu [22] introduced a mixed failure criterion which was composed of Tsai-Wu and Maximum Stress theories. This criterion was used to determine the failure onset and proposed degrading model was used to represent post-damage mode. The material was assumed to behave elastic-plastic and brittle to failure. Nonlinear constitutive behavior was analyzed under in-plane loading, and the outputs of the subroutine attached to a commercial finite element program was observed to agree with the experimental ones.

The formulation generated by Padhi, Shenoi, Moy and Hawkins [23] is one of the few studies dealing with progressive failure of laminated plates under transverse loading. Nonlinear response of composite plates with linear elastic material properties was analyzed with a number failure criterion including Hashin, Tsai-Wu, Hoffman, Azzi-Hill and maximum stress. In this way, an algorithm based on stiffness reduction of the failed element was progressed and integrated to a commercial finite element program in order to determine first ply failure and ultimate collapse of the structures with different aspect ratios. Achieved numerical results were found to correlate well with the experimental data.

Spottswood and Palazotto [24] worked on the initial and progressive failure of the curved composite panel designed to resist transverse loading through the use of Hashin failure criterion. As the composite shell failed, corresponding stiffness was reduced and constitutive equations were rearranged in the computer program. Fiber

failure, matrix failure and delamination were considered upon the developed SLR (simplified large rotation/displacement) theory.

Prusty, Satsangi and Ray [25] integrated eight-noded isoparametric quadratic shell element to the first order shear deformation theory in order to investigate first ply failure analysis of laminated panels under transverse loading. Yeh-Stratton criterion was used to determine the failure loads together with the well known theories maximum stress, maximum strain, Tsai-Wu, Tsai-Hill and Hoffman. Simply supported boundary condition was considered for cross-ply and anti-symmetric angle ply plates with different lamination schemes while a thirteen-layer shell roof was analyzed for varying ratio of radius of curvature to the span. The results were compared with those of the previously published studies.

In [26] and [27], a finite element based progressive failure analysis dealing with the transverse loading of composite plates was presented. The formulation was carried out for linear and elastic range. After estimating the failure onset, the related stiffness of the failed lamina had been discounted completely, i.e., the model was degradated according to the failure mode of the weakest layer. Then, the stiffness matrix was rearranged with the remaining laminae and stresses and strains were recalculated together with the displacements to compute the failure load of the second weakest lamina which would fail immediately under increased share of stresses. After a ply-by-ply analysis, ultimate failure load of the laminate was achieved.

CHAPTER 3

COMPOSITE PLATE/SHELL THEORIES

There are several theories dealing with composite plates and shells, which are basically extensions of isotropic elasticity theories. These can be classified among the complexity of stress-strain field assumptions they propose.

3. 1 Equivalent Single Layer (ESL) Theories

Composite laminae are bonded together to form a laminate with desired thickness and stiffness. In most applications, the thickness of the laminate is small compared to the planar dimensions [28]. For this reason, 3-D elasticity theories are reduced into that of 2-D ones by making assumptions concerning with the variation of displacements and stresses among the thickness of the laminate.

In the ESL approach, all material layers constructing the structure are treated as one equivalent anisotropic layer and classical plate theory is employed ignoring the transverse shear [6]. The displacements u and v are assumed to vary linearly through the thickness of the laminate while ω is constant across the transverse direction and hence the shear strains are continuous at the interface between two adjacent layers. The main advantage is the low computational cost, but the main deficiency is that continuity of the shear strains at the interfaces results in inherent shear stress discontinuity in the model [29].

3.1.1 Classical Plate Theory

Classical plate theory is an extension of Euler-Bernoulli beam theory to plates, and is known as the Kirchhoff plate theory. This theory is based on the assumptions that a straight line perpendicular to the plane of the plate is 1) inextensible, 2) remains straight, and 3) rotates such that it remains perpendicular to the tangent to the deformed surface. These assumptions are equivalent to specifying [30]

$$\varepsilon_z = 0, \quad \varepsilon_{yz} = 0, \quad \varepsilon_{xz} = 0 \tag{3.1.1.1}$$

Classical plate theory does not account for transverse shear deformation. It is extensively used to analyze plates whose length-to-thickness ratio is of the order of 25 or greater (thin plates). When the plate's properties are anisotropic and the length-to-thickness ratio is less than 25, the effect of transverse shear deformation is significant. Thus, to avoid underestimation of the deflections and overprediction of the natural frequencies and the critical buckling loads, a refined theory must be selected [31]. This theory is inadequate for the analysis of composite plates/shells due to high ratio of in-plane Young's modulus to the transverse shear modulus. In addition, ignorance of interlaminar shear strains and stresses, which play a vital role in delamination mode gives rather unreliable results [16]. So, it is not very practical to use classical plate theory in industrial applications for convenience.

3.1.2 First Order Shear Deformation Theory

First order shear deformation theory has the most widespread application area in the literature since it provides a good compromise between equivalent single layer and layerwise theories. The theory is built up with the idea that transverse normals do not remain perpendicular to the midsurface after deformation, which introduces shear strains to the model and gives improved response as compared to the classical plate theory. Other assumptions can be summarized as follows:

1. The transverse normal does not stretch, setting out of plane normal stress σ_{33} zero which requires that ω not be function of thickness coordinate, z. Consequently, it can be concluded that, the degrees of freedom are automatically reduced to five including three translations and two rotations.
2. Transverse shear strain components are constant through the thickness, which yields a constant value of shear strain through the thickness coordinate and needs shear correction factors, which are dimensionless quantities to compensate the effects of constant state of shear strains in the first order shear deformation theory and the quadratic or higher order distribution of shear strains in the elasticity theories.
3. Shear stresses are continuous piecewise quadratic functions of the thickness coordinate.

Like classical plate theory, first order shear deformation theory yields poor interlaminar shear stresses too. The interlaminar shear stresses obtained from the FSDT through constitutive relations are layerwise constant values which can not satisfy the shear stress continuity conditions and the equilibrium conditions at the interlaminar interfaces. To overcome this deficiency, the theory can be improved in the form of higher-order shear deformation theories [14].

3.2 Three Dimensional Elasticity Theories

3.2.1 Traditional 3-D Elasticity Formulations

As the laminates get thicker, shear deformable models are mostly inadequate and three dimensional theories enter the scene to provide improved response. The point is to express the through thickness component of the displacement field in higher order terms which leads to the omission of shear correction factors automatically. By the implementation of 3-D elasticity equations, a more reliable stress field is obtained and warping problems that are impossible to solve with 2-D theories can also be

practiced. The formulation concludes more precise results and consequently a more realistic failure prediction but the model is difficult to construct and also expensive.

3.2.2 Layerwise Theories

Equivalent single layer theories are often inadequate to represent the 3-D stress domain or even global response accurately for thicker structures. For thin laminates, the error introduced due to discontinuous interlaminar stresses (transverse stresses at the interface of two layers) can be negligible. However, for thick laminates, the ESL theories can give erroneous results for all stresses, requiring the use of more sophisticated theories like layerwise ones. To overcome this issue, layerwise theories are proposed by Reddy [28], which assume separate displacement field within each layer. The displacement-based layerwise theories can be subdivided into two classes:

1. *The partial layerwise theories* that use layerwise theories which use layerwise expansions for the in-plane displacement components but not the transverse displacement component, and
2. *The full layerwise theories* that use layerwise expressions for all three displacement components.

They lead to accurate results, especially for very thick laminates and are particularly useful for analyzing local effects [12]. On the other hand, finite element formulations in order to construct layerwise analyses need serious expertise are expensive in terms of CPU time.

3.3 Multiple Model Methods

The ESL theories, partial and full layerwise models have their own advantages and disadvantages in terms of solution accuracy, economy and ease of implementation. Used alone, none of these three types of models is suitable for general laminate

analysis since each is restricted to a limited portion of the laminate modeling spectrum due mainly to the heterogeneous nature of composite materials and the wide range of scales of interest. However, by combining all three model types in a multiple model analysis which denotes any analysis method that uses different mathematical models or different levels of discretization for different subregions of the finite element domain; or global-local analysis, a wide variety of laminate problems can be solved with maximum accuracy and minimum cost. Global-local analysis is typically used when there exists a particular subregion of interest that occupies a small portion of the computational domain. Typically, the global region (the entire computational domain) is analyzed with an economical, yet adequate model, the local region might be modeled with 3-D finite elements. The task often requires the joining of incompatible finite element meshes and/or incompatible finite element mathematical models. In the case of incompatibility, the numerical model used to implement the mathematical models may be same or different; often it is the finite element method.

Multiple model method is simply the superimposition of two or more displacement fields in the same finite element domain with the integration of different mathematical models in order to capture localized 3-D stress regions in a tractable manner. In this way, solution economy can be maximized without sacrificing solution accuracy [28].

CHAPTER 4

FAILURE THEORIES

Failure analysis of a laminate is much more complex than that of a single lamina. The first ply failure indicates the failure of the weakest lamina where the stress exceeds the allowable strength level [26]. The determination of first ply failure load is very essential in understanding the failure process leading to total collapse. The initial failure of a lamina is governed by the exceeding limit prescribed by a failure criterion [19].

The damage modes are dependent on loading, stacking sequence and specimen geometry. There are many theories to predict the onset of failures and their progression. Most of the failure criteria are based on the stress state in the lamina. An accurate kinematic model of the laminate is necessary to determine the stress and strain fields which are the key parameters of the design to be controlled [28].

In this study, first ply failures of several laminates are analyzed among the maximum stress, Tsai-Wu and Tsai-Hill criteria. During the execution of all the theories mentioned, stresses are transformed from global coordinates to material directions in each ply. Laminates are considered orthotropic and analyzed with a macroscopic approach.

4.1 Maximum Stress Criterion

This criterion predicts failure when any stress component along a principle axis exceeds the corresponding strength in that direction. When σ_1, σ_2, σ_6 are the stress

components in a lamina along the principal material axes, the criterion is expressed as

$$\sigma_1 = \begin{cases} X_T \\ -X_C \end{cases} \begin{matrix} when \\ \end{matrix} \begin{matrix} \sigma_1 > 0 \\ \sigma_1 < 0 \end{matrix}, \ \sigma_2 = \begin{cases} Y_T \\ -Y_C \end{cases} \begin{matrix} when \\ \end{matrix} \begin{matrix} \sigma_2 > 0 \\ \sigma_2 < 0 \end{matrix} \text{ and } |\sigma_6| = S \tag{4.1}$$

The failure surfaces for $\sigma_6 = 0$ take the form of a rectangle. Due to the different values of longitudinal and transverse tensile and compressive strengths, the rectangle is not symmetrical with respect to both σ_1 and σ_2 axes. The criterion does not account for interaction between the stress components, that is, the critical value of a stress component is independent of the values of the other stresses. Failure is predicted by the least of the three equations [32].

4.2 Tsai-Wu Criterion (Interactive Tensor Polynomial)

The failure surface for this quadratic polynomial is of the form of an ellipse, independent of ply orientations and thickness of the laminate. The Tsai-Wu failure envelope is expressed as:

$$F_i \sigma_i + F_{ij} \sigma_i \sigma_j = 1 \quad (i, j = 1,...6) \tag{4.2}$$

where σ_i is the stress tensor component in the material coordinates and F_i, F_{ij} are the strength tensor components [6]. Points lying on the domain boundary locate stress states at which the material has exhausted its strength capabilities [33].

For plane stress condition the equation reduces to:

$$F_{11}\sigma_1^2 + 2F_{12}\sigma_1\sigma_2 + F_{22}\sigma_2 + F_{66}\sigma_6^2 + F_1\sigma_1 + F_2\sigma_2 = 1 \tag{4.3}$$

In the above expression, the constants X_T, X_C, Y_T, Y_C represent longitudinal strength in tension, longitudinal strength in compression, transverse strength in tension and transverse strength in compression, respectively. This criterion is regarded as a superior one compared to maximum stress theory since it includes additional interactive terms. It is also found mathematically convenient for any kind of programming.

The stress tensor components F_i and F_{ij} are written in their explicit form as:

$$\begin{aligned} F_1 &= \frac{1}{X_T X_C}, \quad F_{11} = \frac{1}{X_T} - \frac{1}{X_C} \\ F_2 &= \frac{1}{Y_T Y_C}, \quad F_{22} = \frac{1}{Y_T} - \frac{1}{Y_C} \\ F_{12} &= \frac{-1}{2}\left(X_T X_C Y_T Y_C\right)^{1/2}, \quad F_{66} = \frac{1}{S^2} \end{aligned} \tag{4.4}$$

The term F_{12} is sometimes omitted form the general equation representing the failure surface, since it is difficult and expensive to determine experimentally because it needs biaxial testing. Another important limitation of this approach is that it has no provision to include the effect of the operating failure mechanism during the failure process [34].

4.3 Tsai-Hill Criterion (Distortional Strain Energy Polynomial)

This criterion is an extension of distortional strain energy or Von Mises yield criterion to account for anisotropy. For biaxial state of stress, it is modified as:

$$\frac{\sigma_1^2}{X^2} - \frac{\sigma_1 \sigma_2}{X^2} + \frac{\sigma_2^2}{Y^2} + \frac{\sigma_6^2}{S^2} = 1 \tag{4.5}$$

denoting a failure surface where stresses $\sigma_1, \sigma_2, \sigma_6$ refer to the principle material axes. For the failure to be avoided, left hand side of the equation should not exceed 1. (4.3.1) does not distinguish between the tensile and compressive strengths. However, it is suggested that the strengths X and Y take the values X_T or X_C and Y_T or Y_C being compatible with the signs of the corresponding stresses [32].

It has been experimentally proved that Tsai-Hill theory appears to be much more applicable to failure prediction for glass-epoxy composites than maximum stress or maximum strain theories [35].

CHAPTER 5

GOVERNING EQUATIONS OF THE ANALYSIS

5.1 Variational Formulation

The relation between the deformed (initial) and undeformed states of a body of volume V_0 and surface area A_0 is defined as

$$x_i = X_i + u_i \tag{5.1}$$

where x_i is the Eulerian (spatial) and X_i is the Lagrangian (material) coordinates. When the reference surface of the undeformed body coincides with its middle surface, it follows that [13]

$$\boldsymbol{x = x\ (X,\ t)} \tag{5.2}$$

If the virtual work principle is applied over a virtual displacement δx_i

$$\int_{V_0} S_{ij}\delta E_{ij} dV_0 = \int_{A_0} T_k \delta x_k dA_0 \tag{5.3}$$

In the equation above, S_{ij} is the second Piola-Kirchoff stress tensor, E_{ij} is the Lagrangian strain tensor, T_k is the surface traction vector at a spatial point referred to the undeformed area. The material time derivative of (5.3) gives

$$\int_{V_0}\left(\dot{S}_{ij}\,\delta E_{ij} + S_{ij}\,\delta \dot{E}_{ij} \right) dV_0 = \int_{A_0} \dot{T}_{ik}\,\delta x_k \, dA_0 \tag{5.4}$$

Imposing the well-known equations

$$E_{ij} = \frac{1}{2}\left(\frac{\partial x_k}{\partial X_i}\frac{\partial x_k}{\partial X_j} - \delta_{ij} \right) \tag{5.5}$$

and

$$S_{ij} = \frac{\rho_0}{\rho}\frac{\partial X_i}{\partial x_k}\sigma_{kl}\frac{\partial X_j}{\partial x_l} \tag{5.6}$$

where ρ and ρ_0 are densities in deformed and reference configurations respectively, and σ_{kl} is the Cauchy stress tensor. One obtains

$$\int_{V_0}\frac{\rho_0}{\rho}\left(\overline{\sigma}_{kl}\frac{\partial \delta v_k}{\partial x_l} + \sigma_{ml}\frac{\partial v_k}{\partial x_l}\frac{\partial \delta v_k}{\partial x_m} \right) dV_0 = \int_{A_0} \dot{T}_{ik}\,\delta x_k \, dA_0 \tag{5.7}$$

where $\overline{\sigma}_{kl}$ is the Truesdell stress rate and v_k is the velocity.

The velocity gradient can also be divided into its symmetric and skew-symmetric parts D_{ij}, the rate of deformation, and W_{ij}, the spin tensor as

$$\frac{\partial v_k}{\partial x_l} = D_{kl} + W_{kl} \tag{5.8}$$

$\overline{\sigma_{kl}}$ can be written using the mentioned property of the velocity gradient through the existence of the Jaumann rate of Cauchy stress tensor, σ_{kl}^{*} as

$$\overline{\sigma}_{kl} = \sigma_{kl}^{*} + \frac{\partial v_m}{\partial x_m}\sigma_{kl} - \sigma_{km}D_{lm} - \sigma_{ml}D_{km} \tag{5.9}$$

Imposing (5.9) into (5.7) gives

$$\begin{aligned}&\int_{V_0}\frac{\rho_0}{\rho}\left[\left(\sigma_{kl}^{*} + \frac{\partial v_m}{\partial x_m}\sigma_{kl}\right)\delta D_{kl} - 2\sigma_{ml}D_{km}\delta D_{kl} + \sigma_{ml}\frac{\partial v_k}{\partial x_l}\frac{\partial \delta v_k}{\partial x_m}\right]dV_0 \\ &= \int_{V_0}\dot{T}_k\delta v_k\, dA_0\end{aligned} \tag{5.10}$$

Cauchy and Kirchoff stress tensors σ_{kl} and τ_{kl}, and their Jaumann rates are related each other as

$$\tau_{kl} = \frac{\rho_0}{\rho}\sigma_{kl} \tag{5.11}$$

$$\tau_{kl}^{*} = \sigma_{kl}^{*} + \frac{\partial v_m}{\partial x_m}\sigma_{kl} \tag{5.12}$$

Assuming $\rho_0/\rho \approx 1$, and $\partial v_m/\partial x_k << 1$, for incompressible materials, σ_{kl} and τ_{kl} become identical. One can write

$$\tau_{kl}^{*} = C_{klmn}D_{mn} \tag{5.13}$$

where Q_{klmn} is the constitutive relation for composites. Equation 5.10 finally becomes

$$\int_V \left(Q_{klmn} D_{mn} \delta D_{kl} - 2\sigma_{ml} D_{km} \delta D_{kl} + \sigma_{ml} \frac{\partial v_k}{\partial x_l} \frac{\partial \delta v_k}{\partial x_m} \right) dV = \int_{V_0} \dot{T}_k \delta v_k \, dA \tag{5.14}$$

or

$$\int_V \left(\delta D^T Q D - 2\delta D^T \hat{\sigma} D + \delta W^T \tilde{\sigma} \right) dV = \int_A \delta v^T \dot{T} \, dA \tag{5.15}$$

5.2 Kinematic Displacement Fields

According to the shear-deformable theory of Mindlin, displacement field of any point in a shell whose midsurface coincides with the xy-plane can be written as [10]:

$$U_x = u_x(x, y) + z\theta_y(x, y) \tag{5.16}$$

$$U_y = u_y(x, y) + z\theta_x(x, y) \tag{5.17}$$

$$U_z = u_z(x, y) \tag{5.18}$$

where u_x, u_y, u_z are displacements of the midpoint of the laminate; θ_x and θ_y are rotations of transverse normal about x and y axes respectively. From the above equation set, velocity field is expressed as:

$$V_x = v_x(x, y) + z\dot{\theta}_y(x, y) \tag{5.19}$$

$$V_y = v_y(x, y) + z\dot{\theta}_x(x, y) \tag{5.20}$$

$$V_z = v_z(x, y) \tag{5.21}$$

In order to prevent shear locking, anisoparametric approach is considered and shape functions are redefined according to the quadratic deflection assumption suggested

by Tessler and Huges. Hence, velocity field v_i and rotations θ_i are written in terms of triangular area coordinates ξ_i for $i = 1,2,3$; $j = 2,3,1$; $k = 3,1,2$:

$$v_x = \xi_i v_x^i \tag{5.22}$$

$$v_y = \xi_i v_y^i \tag{5.23}$$

$$v_z = \xi_i v_z^i + \frac{1}{2}(b_j \xi_k \xi_i - b_k \xi_i \xi_j)\dot{\theta}_x^i + \frac{1}{2}(a_j \xi_k \xi_i - a_k \xi_i \xi_j)\dot{\theta}_y^i \tag{5.24}$$

$$\dot{\theta}_x = \xi_i \dot{\theta}_x^i \tag{5.25}$$

$$\dot{\theta}_y = \xi_i \dot{\theta}_y^i \tag{5.26}$$

The quadratically interpolated function v_z can also be expressed in compact form using quadratic shape functions N_i as

$$v_z = N_i v_z^i \tag{5.27}$$

where

$$N_1 = \xi_1(2\xi_1 - 1) \tag{5.28}$$

$$N_2 = \xi_2(2\xi_2 - 1) \tag{5.29}$$

$$N_3 = \xi_3(2\xi_3 - 1) \tag{5.30}$$

$$N_4 = 4\xi_1\xi_2 \tag{5.31}$$

$$N_5 = 4\xi_2\xi_3 \tag{5.32}$$

$$N_6 = 4\xi_3\xi_1 \tag{5.33}$$

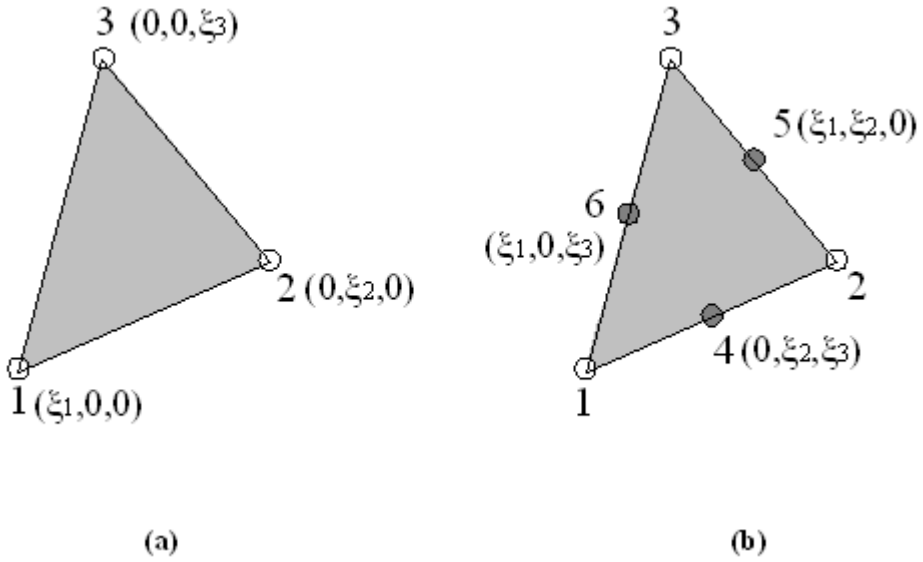

Figure 5.2.1 Representation of a) isoparametric b) anisoparametric triangular element

Table 5.2.1 Natural Coordinates for Isoparametric and Anisoparametric Approach (The coordinates are linearly independent and $\xi_1 + \xi_2 + \xi_3 = 1$ for each node in each set (see Figure 5.2.1))

	ξ_1	ξ_2	ξ_3
Isoparametric	1	1	1
Anisoparameric	$1/2$	$1/2$	$1/2$

It is also possible to establish the velocity vector $\boldsymbol{v}$ in terms of the element degrees of freedom vector $\boldsymbol{q}$:

$$\boldsymbol{v} = \boldsymbol{N}\,\boldsymbol{q} \tag{5.34}$$

In the above expression:

$$q^T = \begin{bmatrix} v_x^1 & v_y^1 & v_z^1 & \dot{\theta}_x^1 & \dot{\theta}_y^1 & 0 & v_x^2 & v_y^2 & v_z^2 & \dot{\theta}_x^2 & \dot{\theta}_y^2 & 0 & v_x^3 & v_y^3 & v_z^3 & \dot{\theta}_x^3 & \dot{\theta}_y^3 & 0 \end{bmatrix} \tag{5.35}$$

$$N = \begin{bmatrix} \xi_1 & 0 & 0 & 0 & 0 & 0 & \xi_2 & 0 & 0 & 0 & 0 & 0 & \xi_3 & 0 & 0 & 0 & 0 & 0 \\ 0 & \xi_1 & 0 & 0 & 0 & 0 & 0 & \xi_2 & 0 & 0 & 0 & 0 & 0 & \xi_3 & 0 & 0 & 0 & 0 \\ 0 & 0 & \xi_1 & \zeta_1 & \zeta_4 & 0 & 0 & 0 & \xi_2 & \zeta_2 & \zeta_5 & 0 & 0 & 0 & \xi_3 & \zeta_3 & \zeta_6 & 0 \\ 0 & 0 & 0 & \xi_1 & 0 & 0 & 0 & 0 & 0 & \xi_2 & 0 & 0 & 0 & 0 & 0 & \xi_3 & 0 & 0 \\ 0 & 0 & 0 & 0 & \xi_1 & 0 & 0 & 0 & 0 & 0 & \xi_2 & 0 & 0 & 0 & 0 & 0 & \xi_3 & 0 \end{bmatrix} \tag{5.36}$$

$$\zeta_i = \frac{1}{2}\left(-b_k \xi_i \xi_j + b_j \xi_i \xi_k\right) \tag{5.37}$$

$$\zeta_{i+3} = \frac{1}{2}\left(a_j \xi_i \xi_k - b_k \xi_i \xi_j\right) \tag{5.38}$$

for $i = 1,2,3$; $j = 2,3,1$; $k = 3,1,2$

From Equation 5.8, the tensors D_{ij} and W_{ij} defined in contracted notation gives

$$D_{mn} = \frac{1}{2}\left(\frac{\partial v_m}{\partial v_n} + \frac{\partial v_n}{\partial v_m}\right) \tag{5.39}$$

$$W_{mn} = \frac{1}{2}\left(\frac{\partial v_m}{\partial v_n} - \frac{\partial v_n}{\partial v_m}\right) \tag{5.40}$$

Introducing the rate of deformation matrix $\boldsymbol{D}$

$$D_{xx} = \frac{1}{2}\left(\frac{\partial v_x}{\partial x} + \frac{\partial v_x}{\partial x}\right) = v_{x,x} + z\dot{\theta}_{y,x} \tag{5.41}$$

$$D_{yy} = \frac{1}{2}\left(\frac{\partial v_y}{\partial y} + \frac{\partial v_y}{\partial y}\right) = v_{y,y} - z\dot{\theta}_{x,y} \tag{5.42}$$

$$D_{zz} = \frac{1}{2}\left(\frac{\partial v_z}{\partial z} + \frac{\partial v_z}{\partial z}\right) = 0 \tag{5.43}$$

$$D_{xy} = \frac{1}{2}\left(\frac{\partial v_x}{\partial y} + \frac{\partial v_y}{\partial x}\right) = \frac{1}{2}\left(v_{x,y} + v_{y,x} + z\dot{\theta}_{y,y} - z\dot{\theta}_{x,x}\right) \tag{5.44}$$

$$D_{yz} = \frac{1}{2}\left(\frac{\partial v_y}{\partial z} + \frac{\partial v_z}{\partial y}\right) = \frac{1}{2}\left(-\dot{\theta}_x + v_{z,y}\right) \tag{5.45}$$

$$D_{zx} = \frac{1}{2}\left(\frac{\partial v_x}{\partial z} + \frac{\partial v_z}{\partial x}\right) = \frac{1}{2}\left(\dot{\theta}_y + v_{z,x}\right) \tag{5.46}$$

$$\begin{bmatrix} D_{xx} \\ D_{yy} \\ 2D_{xy} \\ 2D_{yz} \\ 2D_{xz} \end{bmatrix} = \begin{bmatrix} v_{x,x} + z\dot{\theta}_{y,x} \\ v_{y,y} - z\dot{\theta}_{x,y} \\ v_{x,y} + v_{y,x} + z\dot{\theta}_{y,y} - z\dot{\theta}_{x,x} \\ v_{z,y} - \dot{\theta}_x \\ v_{z,x} + \dot{\theta}_y \end{bmatrix} \tag{5.47}$$

$$\boldsymbol{D} = \boldsymbol{H}\,\boldsymbol{D}^* = \begin{bmatrix} D_{xx} \\ D_{yy} \\ 2D_{xy} \\ 2D_{yz} \\ 2D_{xz} \end{bmatrix} = \begin{bmatrix} 1 & 0 & 0 & z & 0 & 0 & 0 & 0 \\ 0 & 1 & 0 & 0 & -z & 0 & 0 & 0 \\ 0 & 0 & 1 & 0 & 0 & z & 0 & 0 \\ 0 & 0 & 0 & 0 & 0 & 0 & 1 & 0 \\ 0 & 0 & 0 & 0 & 0 & 0 & 0 & 0 \end{bmatrix} \begin{bmatrix} v_{x,x} \\ v_{y,y} \\ v_{x,y} + v_{y,x} \\ \dot{\theta}_{y,x} \\ \dot{\theta}_{x,y} \\ \dot{\theta}_{y,y} - \dot{\theta}_{x,x} \\ v_{z,y} - \dot{\theta}_x \\ v_{z,x} - \dot{\theta}_y \end{bmatrix} \tag{5.48}$$

If the matrix $\boldsymbol{D}^*$ is written in terms of nodal variables in the form

$$\boldsymbol{D}^* = \boldsymbol{B}\boldsymbol{q} \tag{5.49}$$

Equation 5.48 is refined as

$$\boldsymbol{D = HBq} \tag{5.50}$$

where

$$\boldsymbol{B} = \begin{bmatrix} \xi_{1,x} & 0 & 0 & 0 & 0 & 0 & \xi_{2,x} & 0 & 0 & 0 & 0 & 0 & \xi_{3,x} & 0 & 0 & 0 & 0 & 0 \\ 0 & \xi_{1,y} & 0 & 0 & 0 & 0 & 0 & \xi_{2,y} & 0 & 0 & 0 & 0 & 0 & \xi_{3,Y} & 0 & 0 & 0 & 0 \\ \xi_{1,y} & \xi_{1,x} & 0 & 0 & 0 & 0 & \xi_{2,y} & \xi_{2,x} & 0 & 0 & 0 & 0 & \xi_{3,Y} & \xi_{3,x} & 0 & 0 & 0 & 0 \\ 0 & 0 & 0 & 0 & \xi_{1,x} & 0 & 0 & 0 & 0 & 0 & \xi_{2,x} & 0 & 0 & 0 & 0 & 0 & \xi_{3,x} & 0 \\ 0 & 0 & 0 & \xi_{1,y} & 0 & 0 & 0 & 0 & 0 & \xi_{2,y} & 0 & 0 & 0 & 0 & 0 & \xi_{3,y} & 0 & 0 \\ 0 & 0 & 0 & -\xi_{1,x} & \xi_{1,y} & 0 & 0 & 0 & 0 & -\xi_{2,x} & \xi_{2,y} & 0 & 0 & 0 & 0 & -\xi_{3,x} & \xi_{3,y} & 0 \\ 0 & 0 & \xi_{1,y} & F_1 - \xi_1 & F_4 & 0 & 0 & 0 & \xi_{2,y} & F_2 - \xi_2 & F_5 & 0 & 0 & 0 & \xi_{3,y} & F_3 - \xi_3 & F_6 & 0 \\ 0 & 0 & \xi_{1,x} & F_7 & F_{10} + \xi_1 & 0 & 0 & 0 & \xi_{2,x} & F_8 & F_{11} + \xi_2 & 0 & 0 & 0 & \xi_{3,x} & F_9 & F_{12} + \xi_3 & 0 \end{bmatrix} \tag{5.51}$$

and the spin tensor, W_{ij}

$$\boldsymbol{W} = \begin{bmatrix} V_{x,x} \\ V_{x,y} \\ V_{x,z} \\ V_{y,x} \\ V_{y,y} \\ V_{y,z} \\ V_{z,x} \\ V_{z,y} \end{bmatrix} = \begin{bmatrix} v_{x,x} + z\dot{\theta}_{y,x} \\ v_{x,y} + z\dot{\theta}_{y,y} \\ \dot{\theta}_y \\ v_{y,x} - z\dot{\theta}_{x,x} \\ v_{y,y} - z\dot{\theta}_{x,y} \\ -\dot{\theta}_x \\ v_{z,x} \\ v_{z,y} \end{bmatrix} \tag{5.52}$$

or

$$\boldsymbol{W} = \boldsymbol{G}\boldsymbol{W}^{*} = \begin{bmatrix} 1 & 0 & 0 & 0 & 0 & 0 & 0 & 0 & 0 & 0 & z & 0 \\ 0 & 1 & 0 & 0 & 0 & 0 & 0 & 0 & 0 & 0 & 0 & z \\ 0 & 0 & 0 & 0 & 0 & 0 & 0 & 1 & 0 & 0 & 0 & 0 \\ 0 & 0 & 0 & 1 & 0 & 0 & 0 & 0 & -z & 0 & 0 & 0 \\ 0 & 0 & 0 & 0 & 1 & 0 & 0 & 0 & 0 & -z & 0 & 0 \\ 0 & 0 & 0 & 0 & 0 & 0 & -1 & 0 & 0 & 0 & 0 & 0 \\ 0 & 0 & 0 & 0 & 1 & 0 & 0 & 0 & 0 & 0 & 0 & 0 \\ 0 & 0 & 0 & 0 & 0 & 1 & 0 & 0 & 0 & 0 & 0 & 0 \end{bmatrix} \begin{bmatrix} v_{x,x} \\ v_{x,y} \\ v_{y,x} \\ v_{y,y} \\ v_{z,x} \\ v_{z,y} \\ \dot{\theta}_{x} \\ \dot{\theta}_{y} \\ \dot{\theta}_{x,x} \\ \dot{\theta}_{x,y} \\ \dot{\theta}_{y,x} \\ \dot{\theta}_{y,y} \end{bmatrix} \tag{5.53}$$

where

$$\boldsymbol{W}^{*} = \boldsymbol{R}\boldsymbol{q} \tag{5.54}$$

and

$$\boldsymbol{R} = \begin{bmatrix} \xi_{1,x} & 0 & 0 & 0 & 0 & 0 & \xi_{2,x} & 0 & 0 & 0 & 0 & 0 & \xi_{3,x} & 0 & 0 & 0 & 0 & 0 \\ \xi_{1,y} & 0 & 0 & 0 & 0 & 0 & \xi_{2,y} & 0 & 0 & 0 & 0 & 0 & \xi_{3,y} & 0 & 0 & 0 & 0 & 0 \\ 0 & \xi_{1,x} & 0 & 0 & 0 & 0 & 0 & \xi_{2,x} & 0 & 0 & 0 & 0 & 0 & \xi_{3,x} & 0 & 0 & 0 & 0 \\ 0 & \xi_{1,y} & 0 & 0 & 0 & 0 & 0 & \xi_{2,y} & 0 & 0 & 0 & 0 & 0 & \xi_{3,y} & 0 & 0 & 0 & 0 \\ 0 & 0 & \xi_{1,x} & \boldsymbol{F}_{1} & \boldsymbol{F}_{4} & 0 & 0 & 0 & \xi_{2,x} & \boldsymbol{F}_{2} & \boldsymbol{F}_{5} & 0 & 0 & 0 & \xi_{3,x} & \boldsymbol{F}_{3} & \boldsymbol{F}_{6} & 0 \\ 0 & 0 & \xi_{1,y} & \boldsymbol{F}_{7} & \boldsymbol{F}_{10} & 0 & 0 & 0 & \xi_{2,y} & \boldsymbol{F}_{8} & \boldsymbol{F}_{11} & 0 & 0 & 0 & \xi_{3,y} & \boldsymbol{F}_{9} & \boldsymbol{F}_{12} & 0 \\ 0 & 0 & 0 & -\xi_{1} & 0 & 0 & 0 & 0 & 0 & -\xi_{2} & 0 & 0 & 0 & 0 & 0 & -\xi_{3} & 0 & 0 \\ 0 & 0 & 0 & 0 & \xi_{1} & 0 & 0 & 0 & 0 & 0 & \xi_{2} & 0 & 0 & 0 & 0 & 0 & \xi_{3} & 0 \\ 0 & 0 & 0 & \xi_{1,x} & 0 & 0 & 0 & 0 & 0 & \xi_{2,x} & 0 & 0 & 0 & 0 & 0 & \xi_{3,x} & 0 & 0 \\ 0 & 0 & 0 & \xi_{1,y} & 0 & 0 & 0 & 0 & 0 & \xi_{2,y} & 0 & 0 & 0 & 0 & 0 & \xi_{3,y} & 0 & 0 \\ 0 & 0 & 0 & 0 & \xi_{1,x} & 0 & 0 & 0 & 0 & 0 & \xi_{2,x} & 0 & 0 & 0 & 0 & 0 & \xi_{3,x} & 0 \\ 0 & 0 & 0 & 0 & \xi_{1,y} & 0 & 0 & 0 & 0 & 0 & \xi_{2,y} & 0 & 0 & 0 & 0 & 0 & \xi_{3,y} & 0 \end{bmatrix} \tag{5.55}$$

finally

$$\boldsymbol{W = GRq} \tag{5.56}$$

In both matrices $\boldsymbol{B}$ and $\boldsymbol{R}$

$$F_1 = 0.5\left(-\left(y_1 - y_2\right)\left(\xi_{1,y}\xi_2 + \xi_{2,y}\xi_1\right) + \left(y_3 - y_1\right)\left(\xi_{1,y}\xi_3 + \xi_{3,y}\xi_1\right)\right) \tag{5.57}$$

$$F_2 = 0.5\left(-\left(y_2 - y_3\right)\left(\xi_{2,y}\xi_3 + \xi_{3,y}\xi_2\right) + \left(y_1 - y_2\right)\left(\xi_{2,y}\xi_1 + \xi_{1,y}\xi_2\right)\right) \tag{5.58}$$

$$F_3 = 0.5\left(-\left(y_3 - y_1\right)\left(\xi_{3,y}\xi_1 + \xi_{1,y}\xi_3\right) + \left(y_2 - y_3\right)\left(\xi_{3,y}\xi_2 + \xi_{2,y}\xi_3\right)\right) \tag{5.59}$$

$$F_4 = 0.5\left(-\left(x_1 - x_3\right)\left(\xi_{1,y}\xi_3 + \xi_{3,y}\xi_1\right) - \left(x_2 - x_1\right)\left(\xi_{1,y}\xi_2 + \xi_{2,y}\xi_1\right)\right) \tag{5.60}$$

$$F_5 = 0.5\left(-\left(x_2 - x_1\right)\left(\xi_{2,y}\xi_1 + \xi_{1,y}\xi_2\right) - \left(x_3 - x_2\right)\left(\xi_{2,y}\xi_3 + \xi_{3,y}\xi_2\right)\right) \tag{5.61}$$

$$F_6 = 0.5\left(-\left(x_3 - x_2\right)\left(\xi_{3,y}\xi_2 + \xi_{2,y}\xi_3\right) - \left(x_1 - x_3\right)\left(\xi_{3,y}\xi_1 + \xi_{1,y}\xi_3\right)\right) \tag{5.62}$$

$$F_7 = 0.5\left(-\left(y_1 - y_2\right)\left(\xi_{1,x}\xi_2 + \xi_{2,x}\xi_1\right) - \left(y_3 - y_1\right)\left(\xi_{1,x}\xi_3 + \xi_{3,x}\xi_1\right)\right) \tag{5.63}$$

$$F_9 = 0.5\left(-\left(y_2 - y_3\right)\left(\xi_{2,x}\xi_3 + \xi_{3,x}\xi_2\right) + \left(y_1 - y_2\right)\left(\xi_{2,x}\xi_1 + \xi_{1,x}\xi_2\right)\right) \tag{5.64}$$

$$F_9 = 0.5\left(-\left(y_3 - y_1\right)\left(\xi_{3,x}\xi_1 + \xi_{1,x}\xi_3\right) + \left(y_2 - y_3\right)\left(\xi_{3,x}\xi_2 + \xi_{2,x}\xi_3\right)\right) \tag{5.65}$$

$$F_{10} = 0.5\left(\left(x_1 - x_3\right)\left(\xi_{1,x}\xi_3 + \xi_{3,x}\xi_1\right) - \left(x_2 - x_1\right)\left(\xi_{1,x}\xi_2 + \xi_{2,x}\xi_1\right)\right) \tag{5.66}$$

$$F_{11} = 0.5\left(\left(x_2 - x_1\right)\left(\xi_{2,x}\xi_1 + \xi_{1,x}\xi_2\right) - \left(x_3 - x_2\right)\left(\xi_{2,x}\xi_3 + \xi_{3,x}\xi_2\right)\right) \tag{5.67}$$

$$F_{12} = 0.5\left(\left(x_3 - x_2\right)\left(\xi_{3,x}\xi_2 + \xi_{2,x}\xi_3\right) - \left(x_1 - x_3\right)\left(\xi_{3,x}\xi_1 + \xi_{1,x}\xi_3\right)\right) \tag{5.68}$$

x_i and $y_i\,(i = 1,2,3)$, are the local coordinates of the nodes.

Enforcing 5.50 and 5.54 into 5.15 gives

$$\int_A (\boldsymbol{\delta q}^T \boldsymbol{B}^T \overline{\boldsymbol{Q}} \boldsymbol{Bq} - 2\boldsymbol{\delta q}^T \boldsymbol{B}^T \ \overline{\hat{\boldsymbol{\sigma}}} \boldsymbol{Bq} + \boldsymbol{\delta q}^T \boldsymbol{R}\ \overline{\tilde{\boldsymbol{\sigma}}} \boldsymbol{Rq})\, dA = \int_A \boldsymbol{\delta q}^T \boldsymbol{N}^T \dot{\boldsymbol{T}}\, dA \tag{5.69}$$

$$\overline{\boldsymbol{Q}} = \sum_{n=1}^{N} \int_{h_n}^{h_{n+1}} \boldsymbol{H}^T \boldsymbol{Q} \boldsymbol{H} \, dz \tag{5.70}$$

$$\overline{\hat{\boldsymbol{\sigma}}} = \sum_{n=1}^{N} \int_{h_n}^{h_{n+1}} \boldsymbol{H}^T \hat{\boldsymbol{\sigma}} \boldsymbol{H} \, dz \tag{5.71}$$

$$\overline{\tilde{\boldsymbol{\sigma}}} = \sum_{n=1}^{N} \int_{h_n}^{h_{n+1}} \boldsymbol{G}^T \tilde{\boldsymbol{\sigma}} \boldsymbol{G} \, dz \tag{5.72}$$

N denotes the total number of layers and h_n, the distance from the midsurface of the shell to the bottom of the nth [36].

5.3 Constitutive Equations

The stress-strain relations for an orthotropic material in principal material coordinates can be written in matrix form as follows:

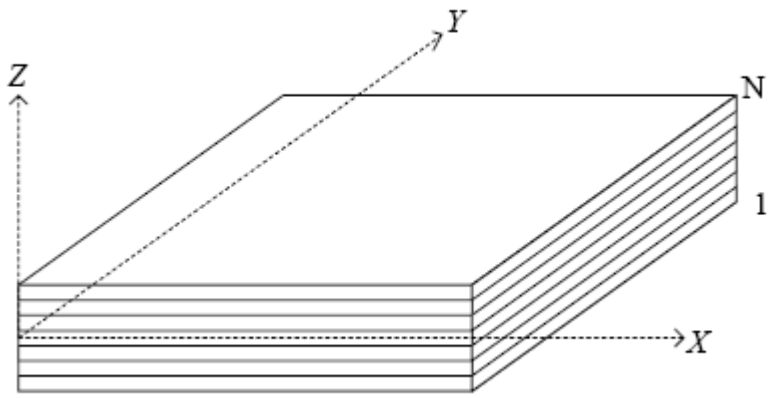

Figure 5.3.1 Laminated flat shell and global reference axes with N denoting number of layers [37]

In material coordinates l, t, z

$$\begin{Bmatrix} \sigma_l \\ \sigma_t \\ \sigma_z \\ \sigma_{tl} \\ \sigma_{tz} \\ \sigma_{lz} \end{Bmatrix} = \begin{Bmatrix} \sigma_1 \\ \sigma_2 \\ \sigma_3 \\ \sigma_4 \\ \sigma_5 \\ \sigma_6 \end{Bmatrix} = \begin{bmatrix} C_{11} & C_{12} & C_{13} & 0 & 0 & 0 \\ C_{12} & C_{22} & C_{23} & 0 & 0 & 0 \\ C_{13} & C_{23} & C_{33} & 0 & 0 & 0 \\ 0 & 0 & 0 & C_{44} & 0 & 0 \\ 0 & 0 & 0 & 0 & C_{55} & 0 \\ 0 & 0 & 0 & 0 & 0 & C_{66} \end{bmatrix} \begin{Bmatrix} \varepsilon_1 \\ \varepsilon_2 \\ \varepsilon_3 \\ \varepsilon_4 \\ \varepsilon_5 \\ \varepsilon_6 \end{Bmatrix} \tag{5.73}$$

Imposing the assumption $\sigma_3 = 0$:

$$\begin{Bmatrix} \sigma_1 \\ \sigma_2 \\ \sigma_6 \\ \sigma_4 \\ \sigma_5 \end{Bmatrix} = \begin{bmatrix} Q_{11} & Q_{12} & 0 & 0 & 0 \\ Q_{12} & Q_{22} & 0 & 0 & 0 \\ 0 & 0 & Q_{66} & 0 & 0 \\ 0 & 0 & 0 & k^2 Q_{44} & 0 \\ 0 & 0 & 0 & 0 & k^2 Q_{55} \end{bmatrix} \begin{Bmatrix} \varepsilon_1 \\ \varepsilon_2 \\ \varepsilon_6 \\ \varepsilon_4 \\ \varepsilon_5 \end{Bmatrix} \tag{5.74}$$

where the contracted notation Q_{ij} represents the elements of the reduced stiffness matrix , and k^2 is the shear correction factor which is taken here as $5/6$.

$$Q_{11} = \frac{E_1}{1 - \upsilon_{12}\upsilon_{21}} \quad Q_{12} = \frac{\upsilon_{21} E_1}{1 - \upsilon_{12}\upsilon_{21}} \quad Q_{22} = \frac{E_2}{1 - \upsilon_{12}\upsilon_{21}} \tag{5.75}$$

$$Q_{44} = G_{23} \qquad Q_{55} = G_{13} \qquad Q_{66} = G_{12}$$

In local coordinates x, y, z

$$\begin{Bmatrix} \sigma_x \\ \sigma_y \\ \sigma_{xy} \\ \sigma_{yz} \\ \sigma_{xz} \end{Bmatrix} = \begin{bmatrix} \overline{Q}_{11} & \overline{Q}_{12} & \overline{Q}_{16} & 0 & 0 \\ \overline{Q}_{12} & \overline{Q}_{22} & \overline{Q}_{26} & 0 & 0 \\ \overline{Q}_{16} & \overline{Q}_{26} & \overline{Q}_{66} & 0 & 0 \\ 0 & 0 & 0 & \overline{Q}_{44} & \overline{Q}_{45} \\ 0 & 0 & 0 & \overline{Q}_{45} & \overline{Q}_{55} \end{bmatrix} \begin{Bmatrix} \varepsilon_x \\ \varepsilon_y \\ \varepsilon_{xy} \\ \varepsilon_{yz} \\ \varepsilon_{xz} \end{Bmatrix} = [\overline{Q}]\{\varepsilon\} \tag{5.76}$$

Introducing the transformed reduced stiffness matrix

$$\overline{\boldsymbol{Q}} = \boldsymbol{T}^T \boldsymbol{Q} \boldsymbol{T} \tag{5.77}$$

where

$$\boldsymbol{T} = \begin{bmatrix} \cos^2\theta & \sin^2\theta & 0 & 0 & -2\cos\theta\sin\theta \\ \sin^2\theta & \cos^2\theta & 0 & 0 & 2\cos\theta\sin\theta \\ \cos\theta\sin\theta & -\cos\theta\sin\theta & 0 & 0 & \cos^2\theta - \sin^2\theta \\ 0 & 0 & \cos\theta & \sin\theta & 0 \\ 0 & 0 & -\sin\theta & \cos\theta & 0 \end{bmatrix} \tag{5.78}$$

The matrix $\boldsymbol{T}$ transfers the local coordinate system of the shell by defining the angle θ between the triangular element mesh and the fiber angle orientation as follows

$$\boldsymbol{i}_k^{'} \cdot \boldsymbol{i}_l = \left|\boldsymbol{i}_k^{'}\right| \left|\boldsymbol{i}_l\right| \cos\theta \tag{5.79}$$

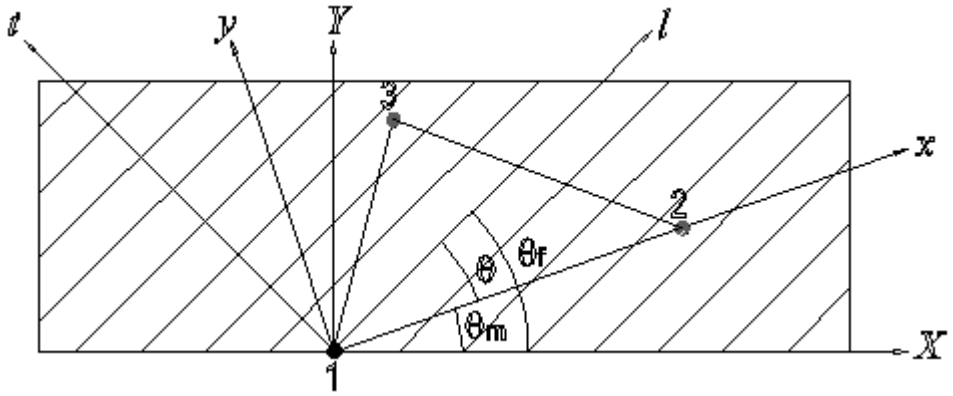

Figure 5.3.2 Definition of transform angle

θ_m : Angle between global axis *X* and local axis *x*

θ_f : Fiber angle (Angle between global axis, *X* and principal material direction, *l*)

θ : Transformation angle (Angle between local axis, *x* and principal material direction, *l*)

5.4 Coordinate Transformation

Triangular area coordinates or natural coordinates are related to that of Cartesian system by the equation 5.4.1. This transformation is necessary in order to switch from one system to the other. Local quantities are transformed to global one to construct a proper stiffness matrix using the mapping relationships below

$$x = \sum_{i=1}^{3} x_i \psi_i(\xi, \eta) \tag{5.80}$$

$$y = \sum_{i=1}^{3} y_i \psi_i(\xi, \eta) \tag{5.81}$$

The following correlation can also be specified in global coordinates that

$$\begin{bmatrix} 1 \\ x \\ y \end{bmatrix} = \begin{bmatrix} 1 & 1 & 1 \\ x_1 & x_2 & x_3 \\ y_1 & y_2 & y_3 \end{bmatrix} \begin{bmatrix} \xi_1 \\ \xi_2 \\ \xi_3 \end{bmatrix} \tag{5.82}$$

The inverse of 5.4.1 yields:

$$\begin{bmatrix} \xi_1 \\ \xi_2 \\ \xi_3 \end{bmatrix} = \frac{1}{2A} \begin{bmatrix} x_2 y_3 - x_3 y_2 & y_2 - y_3 & x_3 - x_2 \\ x_3 y_1 - x_1 y_3 & y_3 - y_1 & x_1 - x_3 \\ x_1 y_2 - x_3 y_1 & y_1 - y_2 & x_2 - x_1 \end{bmatrix} \begin{bmatrix} 1 \\ x \\ y \end{bmatrix} = \begin{bmatrix} a_1 & b_1 & c_1 \\ a_2 & b_2 & c_2 \\ a_3 & b_3 & c_3 \end{bmatrix} \begin{bmatrix} 1 \\ x \\ y \end{bmatrix} \tag{5.83}$$

or

$$\xi_i = \frac{1}{2A}\left(a_i + b_i x + c_i y\right) \quad i = 1,2,3 \tag{5.84}$$

where

$$A = A_1 + A_2 + A_3 \tag{5.85}$$

$$a_1 = x_2 y_3 - x_3 y_2 \qquad a_2 = x_3 y_1 - x_1 y_3 \qquad a_3 = x_1 y_2 - x_2 y_1 \tag{5.86}$$

$$b_1 = y_2 - y_3 \qquad b_2 = y_3 - y_1 \qquad b_3 = y_1 - y_2 \tag{5.87}$$

$$c_1 = x_3 - x_2 \qquad c_2 = x_1 - x_3 \qquad c_3 = x_2 - x_1 \tag{5.88}$$

The Jacobian is derived from 5.80 to 5.83 as

$$J = 2A = \det \begin{bmatrix} 1 & 1 & 1 \\ x_1 & x_2 & x_3 \\ y_1 & y_2 & y_3 \end{bmatrix} == \begin{bmatrix} x_2 - x_1 & y_2 - y_1 \\ x_3 - x_1 & y_3 - y_1 \end{bmatrix} = \begin{bmatrix} c_3 & -b_3 \\ -c_2 & b_2 \end{bmatrix} \tag{5.89}$$

In the form of partial derivatives of the shape functions via the chain rule

$$\begin{bmatrix} \frac{\partial}{\partial \xi} \\ \frac{\partial}{\partial \eta} \end{bmatrix} = \begin{bmatrix} \frac{\partial x}{\partial \xi} & \frac{\partial y}{\partial \xi} \\ \frac{\partial x}{\partial \eta} & \frac{\partial y}{\partial \eta} \end{bmatrix} \begin{bmatrix} \frac{\partial}{\partial x} \\ \frac{\partial}{\partial y} \end{bmatrix} = J \begin{bmatrix} \frac{\partial}{\partial x} \\ \frac{\partial}{\partial y} \end{bmatrix} \tag{5.4.90}$$

$$\begin{bmatrix} \frac{\partial}{\partial x} \\ \frac{\partial}{\partial y} \end{bmatrix} = J^{-1} \begin{bmatrix} \frac{\partial}{\partial \xi} \\ \frac{\partial}{\partial \eta} \end{bmatrix} \tag{5.91}$$

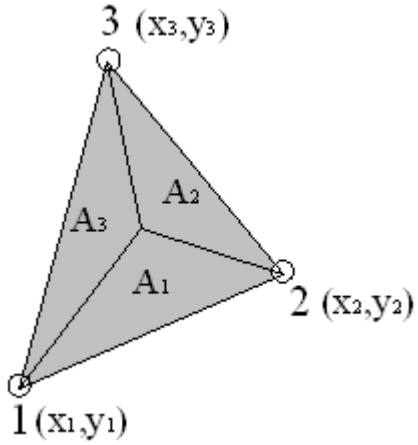

Figure 5.4.1 Configuration of the element

5.5 Numerical Integration

In order to evaluate the derived functions and to adapt them into a computer algorithm, the integral forms must be analytically calculated in a practical and convenient way over the finite element domain. The global stiffness matrix is constituted in this way with the employment of Gauss quadrature formula.

The integrated functions are approximated by computing the function values at the Gaussian points $\psi_i(\xi,\eta)$, the abscissas of the quadrature points within the element or simply integration points, through the equation

$$\int_{\Omega} F(\xi,\eta)\, d\xi\, d\eta = \sum_{i=1}^{n} w_i\, F(\xi_i,\eta_i) \tag{5.92}$$

where n is the number of integration points and w_i denotes the weighting functions that varies according to n. In the present formulation; $n = 3$, $w_1 = w_2 = w_3 = 1/3$. It should also be pointed out that in the case of quadratic triangle

$$\int_{\Omega} F(\xi,\eta)\, d\xi\, d\eta = \int_{\Omega} F(\xi_1,\xi_2,\xi_3)\, d\xi_1\, d\xi_2 \tag{5.93}$$

$$\int_{\Omega} F(\xi_1,\xi_2,\xi_3)\, d\xi_1\, d\xi_2 = \sum_{i=1}^{n} w_i F(\xi_{1i},\xi_{2i},\xi_{2i}) \tag{5.94}$$

The jacobian is imposed to the element stiffness matrix K_e, and the term dV in the K_e is written in the form of natural coordinates as

$$dV = \det \mathrm{J}\ \xi_1\xi_2\xi_3 \tag{5.95}$$

5.6 Convergence Criterion

Throughout the solution procedures of a nonlinear analysis, the basic equation to be solved is [38]

$$^{t+\Delta t}\boldsymbol{R} - {}^{t+\Delta t}\boldsymbol{F} = \boldsymbol{0} \tag{5.96}$$

In the expression above, $^{t+\Delta t}\boldsymbol{R}$ stores the externally applied loads and $^{t+\Delta t}\boldsymbol{F}$ is the vector of nodal point forces that are equivalent to the element stress. Since the nodal point forces $^{t+\Delta t}\boldsymbol{F}$ vary according to the nodal point displacements, equation 5.96

should be iterated. The aim is to evaluate the element configuration at time $t+\Delta t$, and it is assumed that the deformation state at time t is known, then

$$^{t+\Delta t}\boldsymbol{F} = {}^{t}\boldsymbol{F} + \boldsymbol{F} \tag{5.97}$$

where $\boldsymbol{F}$ is the increment in nodal point forces corresponding to the increment in element displacements and stresses from time t to $t+\Delta t$. This matrix can be approximated using the stiffness $^{t}\boldsymbol{K}_T$ as

$$\boldsymbol{F} \cong {}^{t}\boldsymbol{K}_T \boldsymbol{U} \tag{5.98}$$

where $\boldsymbol{U}$ is the vector of incremental nodal point displacements and

$$^{t}\boldsymbol{K}_T = \partial^{t}\mathbf{F} / \partial^{t}\boldsymbol{U} \tag{5.99}$$

Substituting (5.98) to (5.97) gives

$$^{t}\boldsymbol{K}_T \boldsymbol{U} = {}^{t+\Delta t}\boldsymbol{R} - {}^{t}\boldsymbol{F} \tag{5.100}$$

and solving for $\boldsymbol{U}$, an approximation of the displacements at time $t+\Delta t$ can be calculate by

$$^{t+\Delta t}\boldsymbol{U} \cong {}^{t}\boldsymbol{U} + \boldsymbol{U} \tag{5.101}$$

Having calculated an approximation to the displacements corresponding to time $t+\Delta t$, one can proceed to the next time increment with the Newton-Raphson equations

$$ {}^{t}\boldsymbol{K}_T\,\boldsymbol{U} = {}^{t+\Delta t}\boldsymbol{R} - {}^{t}\boldsymbol{F} $$

$$ {}^{t+\Delta t}\boldsymbol{U}^{(i)} \cong {}^{t+\Delta t}\boldsymbol{U} + \boldsymbol{\Delta U}^{(i)} \tag{5.102} $$

In order for the incremental solution scheme based on iterative methods to be effective, a realistic criterion should be used for termination of the iteration to see whether the solution has converged within the present tolerances or it is diverging from the true value [17]

The following inequality

$$ \frac{\left\| \Delta U^{(i)} \right\|}{\left\| {}^{t+\Delta t}U \right\|} \leq CON \tag{5.103} $$

is employed to be satisfied within the user determined tolerance range, *CON*. In Equation 5.103, ${}^{t+\Delta t}\boldsymbol{U}$ is the nodal point displacement and it is approximated. It is regarded as the last calculated value of ${}^{t+\Delta t}\boldsymbol{U}^{(i)}$ [36].

5.7 Solution Algorithm

Constrained nodes are not included in the stiffness matrix, so further mathematical operations of the finite element model take place within the unconstrained ones in order to save memory. In this way an array including all degree of freedoms per unconstrained node is established. Then element connectivity array is constructed. This matrix is a kind of compact addressing system that links the mesh elements to the corresponding nodes that they are enclosed with.

Global stiffness matrix is simply computed as

$$\boldsymbol{K} = \sum_{i} \boldsymbol{K}^{i} \tag{5.104}$$

where the matrix $\boldsymbol{K}^{i}$ is the stiffness matrix of the ith element and summation goes over all elements in the assemblage. Since the matrix is symmetric, only the data above the diagonal of the stiffness matrix $\boldsymbol{K}$ (k_{ij}), is stored. To locate the rows with zero elements, m_k, half-bandwidth of the stiffness matrix is introduced. For $j > i + m_k$, the elements of $\boldsymbol{K}$ are zero. Defining by m_i, the row number of the first nonzero element in column i, the variables m_i, $i = 1,\ldots,n$, define the skyline of the matrix, and the variables $i - m_i$ are the column heights. The column heights are determined from the connectivity arrays of the elements by evaluating m_i, from the previously mentioned formula. Furthermore, half-bandwidth of the stiffness matrix, m_k equals $\max\{i - m\}$, $i = 1,,n$; it is equal to the maximum difference in global degrees of freedom pertaining to any one of the finite elements in the mesh. After the determination of the column heights of the stiffness matrix $\boldsymbol{K}$, all the elements below the skyline of the matrix $\boldsymbol{K}$ is stored in a one-dimensional array [38]. The addresses of this one-dimensional array are also stored in another array.

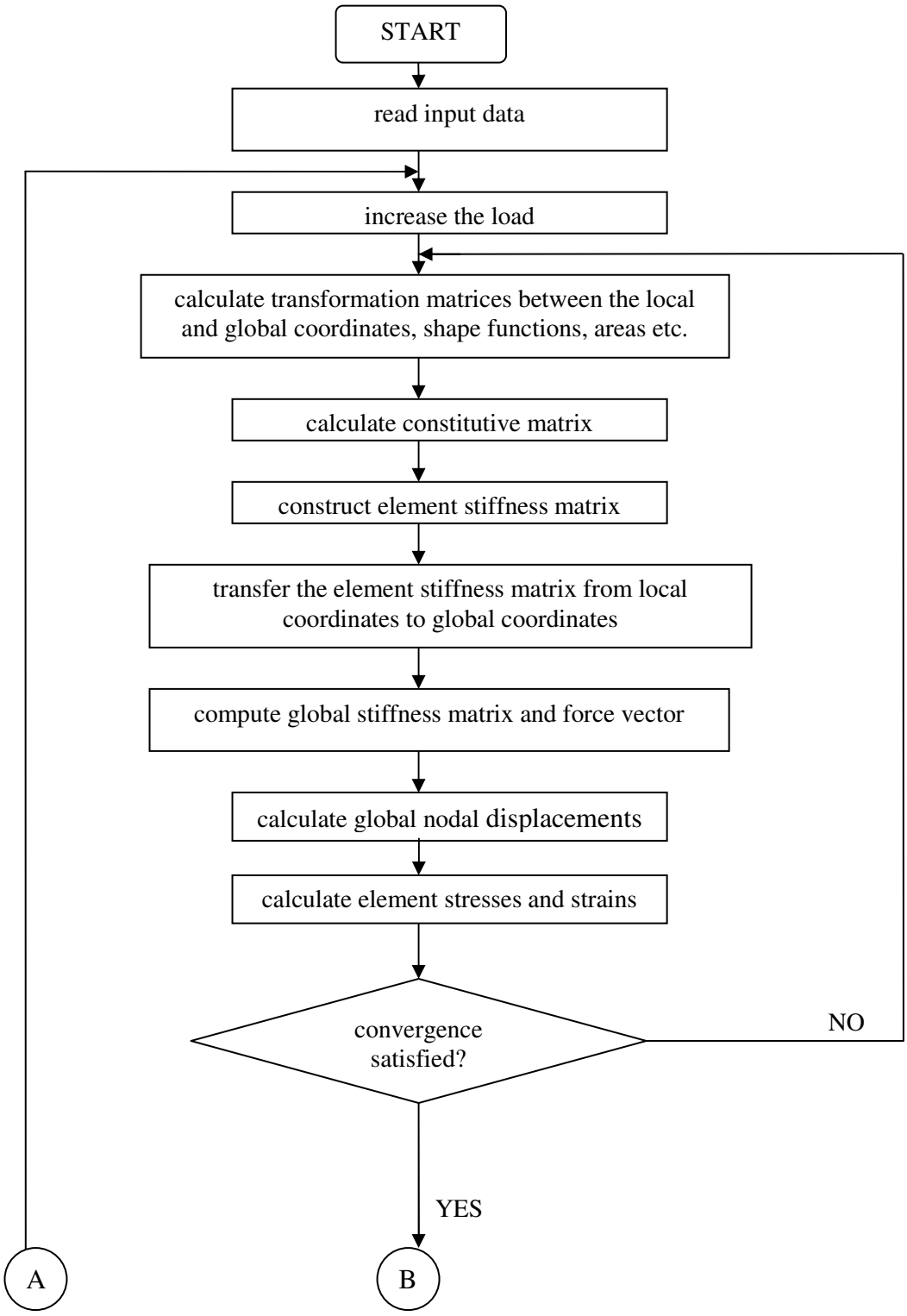

Figure 5.9.1 Program flowchart

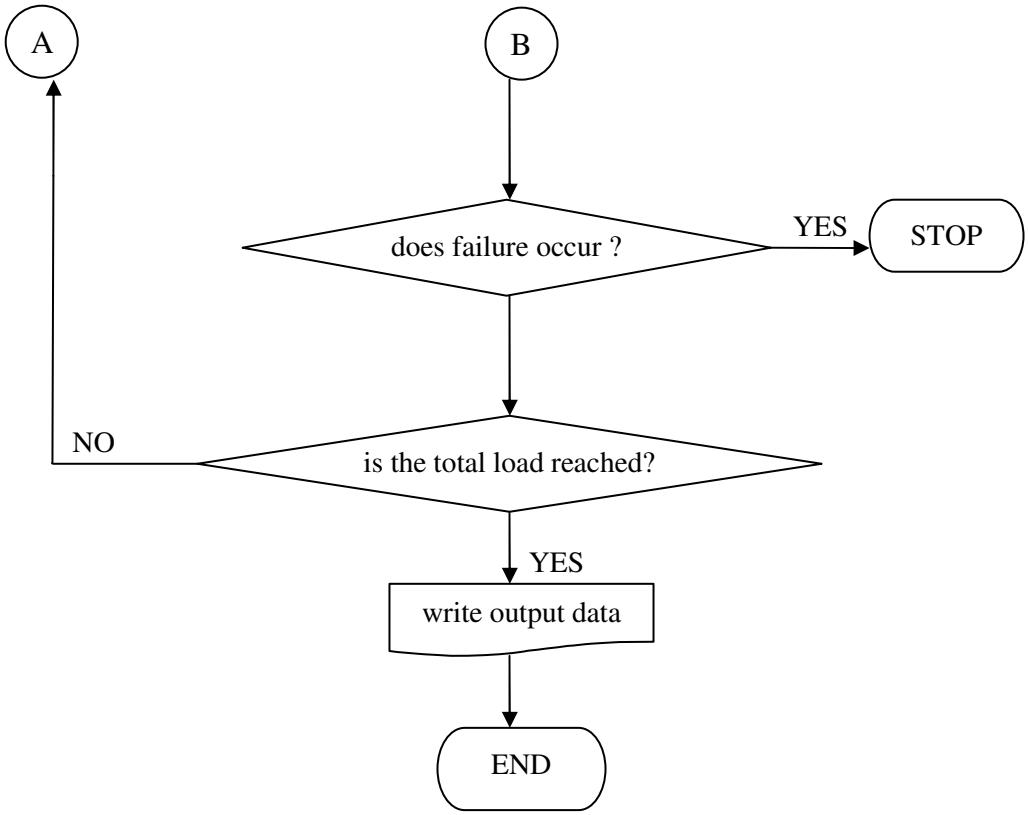

Figure 5.9.1 Program flowchart (continued)

CHAPTER 6

RESULTS AND DISCUSSION

Several laminates each constructed of glass/epoxy (Table 6.1) are considered with different orientation angles and boundary conditions. Deformed shapes of 2.8 mm thick 14-layered symmetric laminates having in-plane dimensions of $300\,mm$ x $100\,mm$ are depicted for the stacking sequences of $[0/90/0/90/0/90/0]_s$, $[15/-15/15/-15/-15/-15/15]_s$, $[30/-30/30/-30/-30/-30/30]_s$, $[45/-45/45/-45/-45/-45/45]_s$ and $[60/-60/60/-60/-60/-60/60]_s$ and results are compared with the results of the ANSYS software. First ply failure loads are determined for each laminate, and load-deflection characteristics are compared. Since ANSYS does not recommend using triangular element mesh with the finite strain shell, the mesh is built up with four-node elements in order to prevent any misleading consequences (Figure 6.1). In ANSYS, the material is defined as orthotropic and nonlinear-large displacement-static analysis case is selected as the solution scheme. The results of the developed code and ANSYS 8.1 are compared and in every combination, a good convergence level and an acceptable range of error percentage are obtained. The element mesh used for the developed code is shown in Figure 6.2.

Three different failure theories are considered to determine the first ply failure load for all laminates by the developed code. Then the related plot is depicted by the application of the maximum allowable load obtained by the Tsai-Wu theory. The same load is also used as the input force into the commercial finite element program, and the failure index values are listed in tabular form.

Table 6.1 Material Properties of Glass/Epoxy

$E_1 = 40\ GPa$
$E_2 = E_3 = 10\ GPa$
$G_{12} = G_{23} = G_{13} = 5\ GPa$
$X_T = 300\ MPa$
$X_C = 120\ MPa$
$Y_T = 200\ MPa$
$Y_C = 110\ MPa$
$S = 55\ MPa$

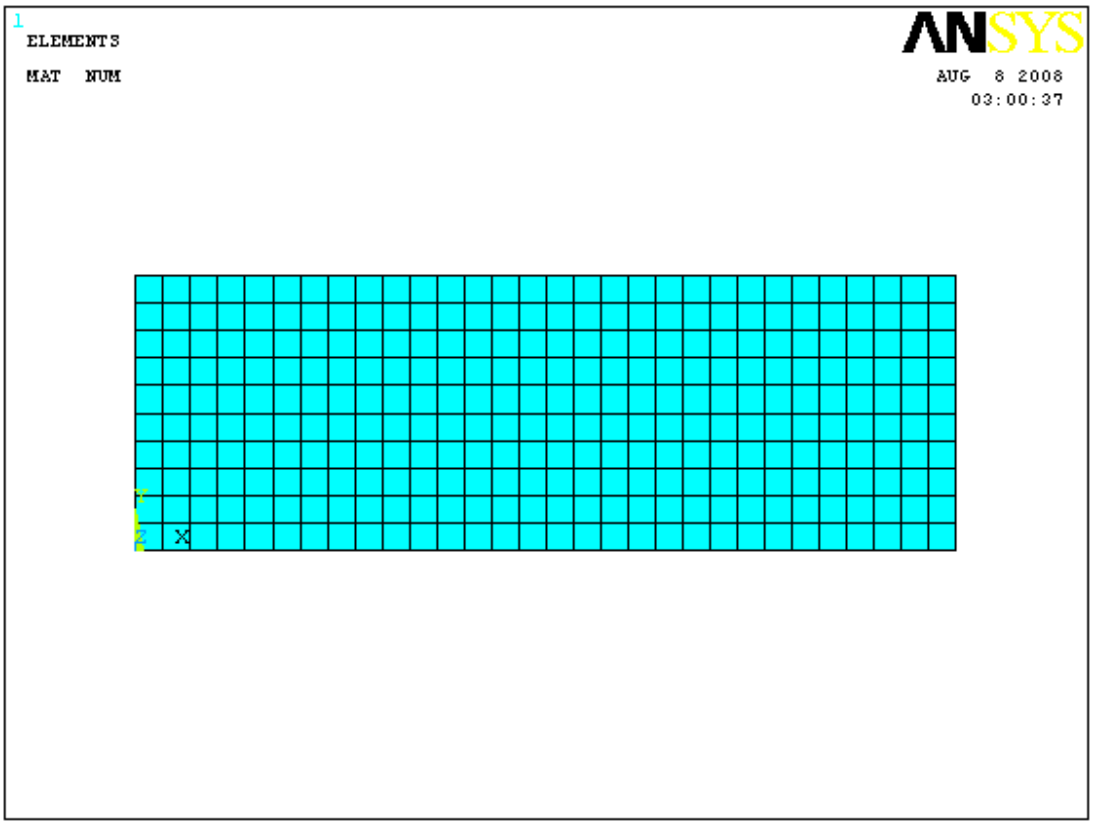

Figure 6.1 Finite element mesh for ANSYS (not to scale)

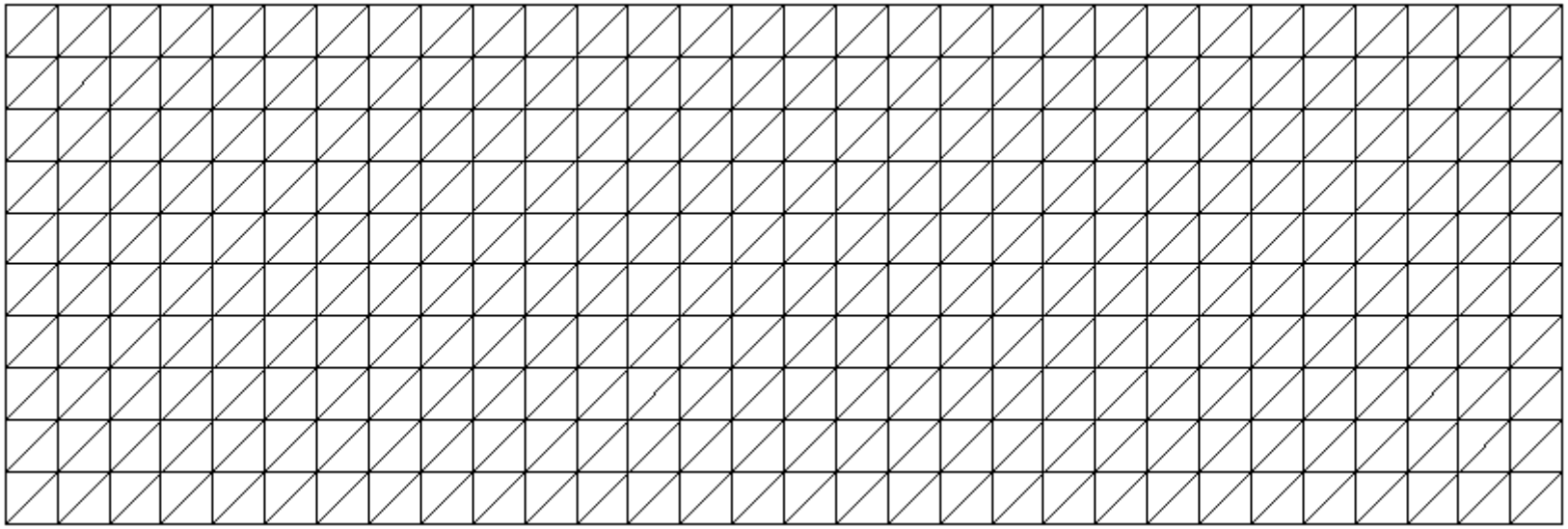

Figure 6.1 Finite element mesh for the developed code (not to scale)

6.1 Case I: One End Clamped

During the analyses of this case, the flat composite shells with different ply angles are loaded uniformly along one of the ends up to first ply failure and fully constrained from the other ends as shown in Figure 6.1.1. The first ply failure loads of 14-ply 2.8 mm thick laminates with the fiber angle orientations $[0/90/0/90/0/90/0]_s$, $[15/-15/15/-15/15/-15/15]_s$, $[30/-30/30/-30/30/-30/30]_s$, $[45/-45/45/-45/45/-45/45]_s$, $[60/-60/60/-60/60/-60/60]_s$ are generated according to the maximum stress, Tsai-Wu and Tsai-Hill failure theories. All the deformed shapes of the shells are determined by using Tsai-Wu criterion.

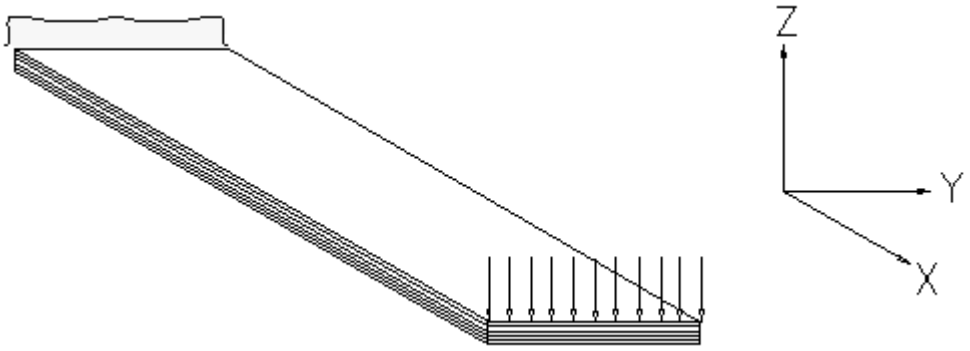

Figure 6.1.1 Schematic representation of Case I

For the composite shell with the fiber angle orientation $[0/90/0/90/0/90/0]_s$, the first ply failure loads that are obtained from the developed code using maximum stress, Tsai-Wu and Tsai-Hill failure criteria are given in Table 6.1.1. Applying the failure load determined by Tsai-Wu criterion, tip displacements and maximum failure index values found by both developed code and ANSYS are given in and 6.1.2. Failure onset is observed at the bottom layers along the supported edge. For the same fiber orientation, the deformed shape of the composite shell obtained from the code and ANSYS that are given in Figure 6.1.2. It is observed that the results are in good agreement.

Table 6.1.1 First Ply Failure (Results from Code)

Criterion	***Load (N)***	***Tip Displacement (mm)***	***Failure Index***
Maximum Stress	36.30	61.87	1.00213
Tsai-Wu	35.75	61.02	1.00601
Tsai-Hill	40.15	67.69	1.01804

Table 6.1.2 First Ply Failure (Results from ANSYS)

Criterion	***Load (N)***	***Tip Displacement (mm)***	***Failure Index***
Maximum Stress	35.75	59.43	0.88969
Tsai-Wu	35.75	59.43	0.85329

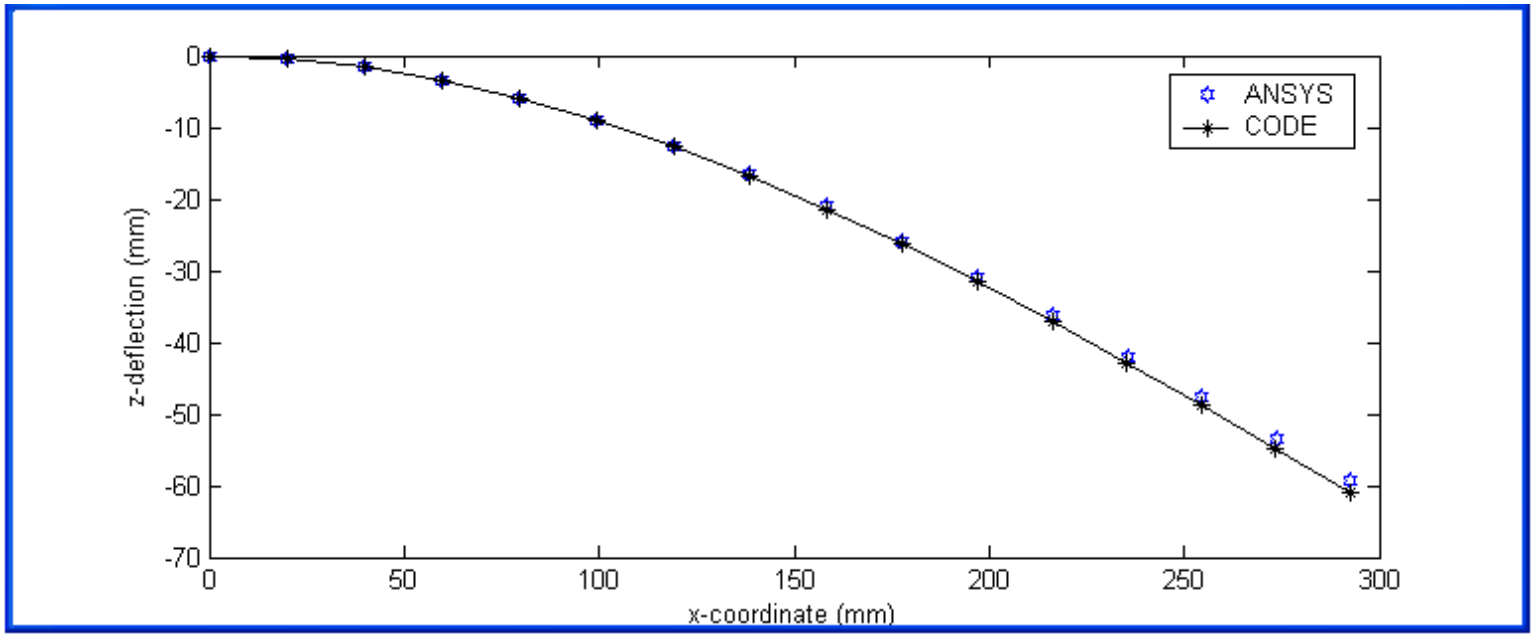

Figure 6.1.2 Deflected coordinates of the $[0/90/0/90/0/90/0]_s$ laminate. B.C: Left end fixed

The deformed shapes of the composite shell with the fiber angle orientation $[15/-15/15/-15/15/-15/15]_s$ obtained from the developed code and ANSYS are given in Figure 6.1.3. It is shown that ANSYS gives slight smaller displacements and failure indexes (Tables 6.1.3 and 6.1.4) according to the load that is determined by the Tsai-Wu criterion through the developed code. Failure onset is observed at the bottom layers along the supported edge in both of the programs and comparisons have shown adequate agreement between the two sets of results.

Table 6.1.3 First Ply Failure (Results from Code)

Criterion	***Load (N)***	***Tip Displacement (mm)***	***Failure Index***
Maximum Stress	48.84	65.68	1.00112
Tsai-Wu	47.41	63.99	1.00120
Tsai-Hill	54.34	72.03	1.00110

Table 6.1.4 First Ply Failure (Results from ANSYS)

Criterion	***Load (N)***	***Tip Displacement (mm)***	***Failure Index***
Maximum Stress	47.41	61.77	0.90635
Tsai-Wu	47.41	61.77	0.89329

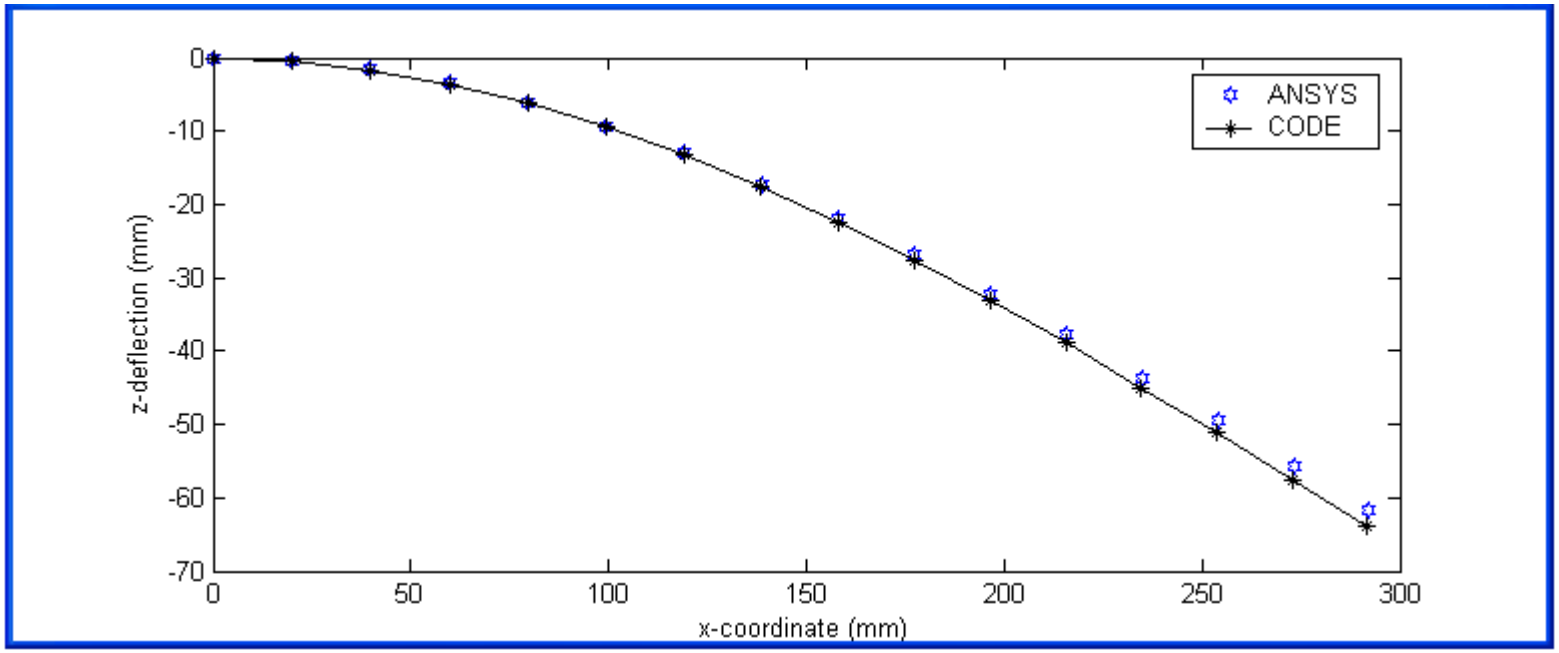

Figure 6.1.3 Deflected coordinates of the $[15/-15/15/-15/15/-15/15]_s$ laminate. B.C: Left end fixed

Tip displacements and maximum failure index values found by both developed code and ANSYS are given in Tables 6.1.5 and 6.1.6 for the composite shell with the fiber angle orientation $[30/-30/30/-30/30/-30/30]_s$. First ply failure is observed at the bottom layers along the supported edge in fiber direction in the form of compression. Deflection outputs of the code are appeared to be less than ANSYS; the difference is less than 3.5%. The deformed shape of the composite shell is illustrated in Figure 6.1.4.

Table 6.1.5 First Ply Failure (Results from Code)

Criterion	***Load (N)***	***Tip Displacement (mm)***	***Failure Index***
Maximum Stress	47.41	81.85	1.00163
Tsai-Wu	44.11	74.26	1.00001
Tsai-Hill	54.34	91.12	1.00063

Table 6.1.6 First Ply Failure (Results from ANSYS)

Criterion	***Load (N)***	***Tip Displacement (mm)***	***Failure Index***
Maximum Stress	44.11	76.86	0.93634
Tsai-Wu	44.11	76.86	1.00180

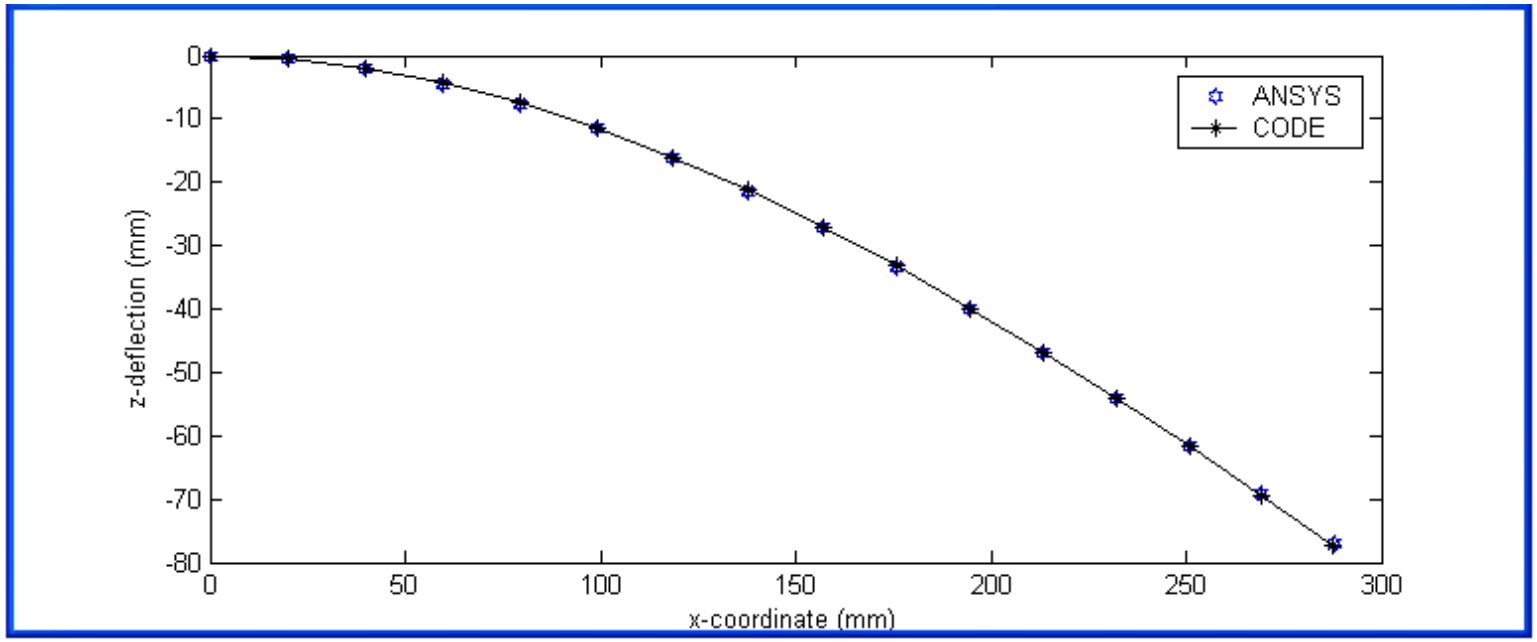

Figure 6.1.4 Deflected coordinates of the $[30/-30/30/-30/30/-30/30]_s$ laminate. B.C: Left end fixed

For the composite shell with the fiber angle orientation $[45/-45/45/-45/45/-45/45]_s$, the failure loads, tip displacements and maximum failure index values found by both developed code and ANSYS are presented in Tables 6.1.7 and 6.1.8, and the deformed shape is given in Figure 6.1.5. Failure is caused by the excess stress in fiber direction and is observed at the bottom layers along the supported edge. Despite a deviation of 5.5% in displacements, the results are compatible, and damage initiated at the same element in ANSYS and code.

Table 6.1.7 First Ply Failure (Results from Code)

Criterion	***Load (N)***	***Tip Displacement (mm)***	***Failure Index***
Maximum Stress	42.90	104.48	1.0026
Tsai-Wu	39.60	98.46	1.0036
Tsai-Hill	50.05	116.65	1.0048

Table 6.1.8 First Ply Failure (Results from ANSYS)

Criterion	***Load (N)***	***Tip Displacement (mm)***	***Failure Index***
Maximum Stress	39.60	103.93	0.85429
Tsai-Wu	39.60	103.93	1.03280

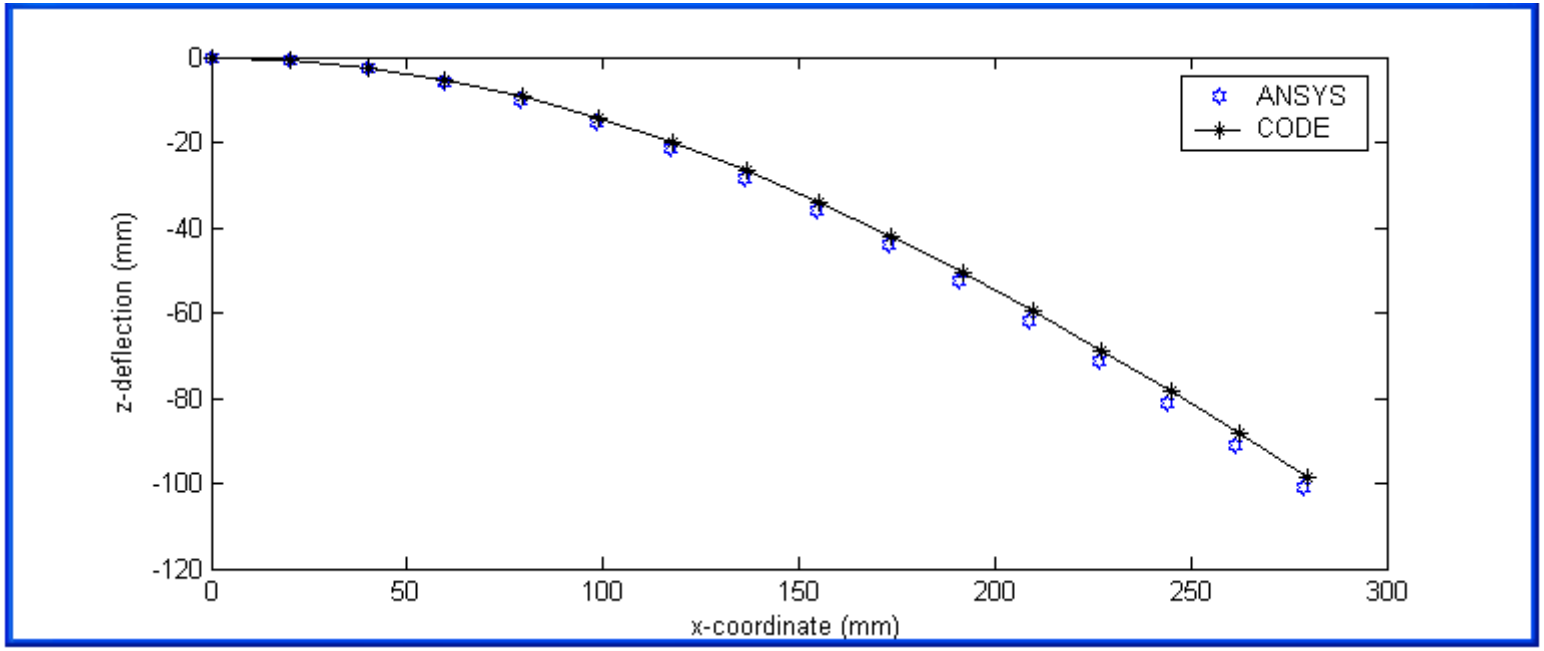

Figure 6.1.5 Deflected coordinates of the $[45/-45/45/-45/45/-45/45]_s$ laminate. B.C: Left end fixed

The composite shell with the fiber angle orientation $[60/-60/60/-60/60/-60/60]_s$ is analyzed with developed code and ANSYS, and failure loads, tip displacements and maximum failure index values found by both developed code and ANSYS are given in Tables 6.1.9 and 6.1.10. Satisfying results are achieved since first ply failure is observed at the same elements of the bottom layers along the supported edge by both of the programs. For the same fiber orientation, the deformed shape of the composite shell obtained from the code and ANSYS that are given in Figure 6.1.6. 2.28% difference is observed between the results.

Table 6.1.9 First Ply Failure (Results from Code)

Criterion	***Load (N)***	***Tip Displacement (mm)***	***Failure Index***
Maximum Stress	48.84	149.63	1.01690
Tsai-Wu	40.08	126.84	1.00008
Tsai-Hill	56.87	154.56	1.00044

Table 6.1.10 First Ply Failure (Results from ANSYS)

Criterion	***Load (N)***	***Tip Displacement (mm)***	***Failure Index***
Maximum Stress	40.08	123.94	0.58686
Tsai-Wu	40.08	123.94	0.86284

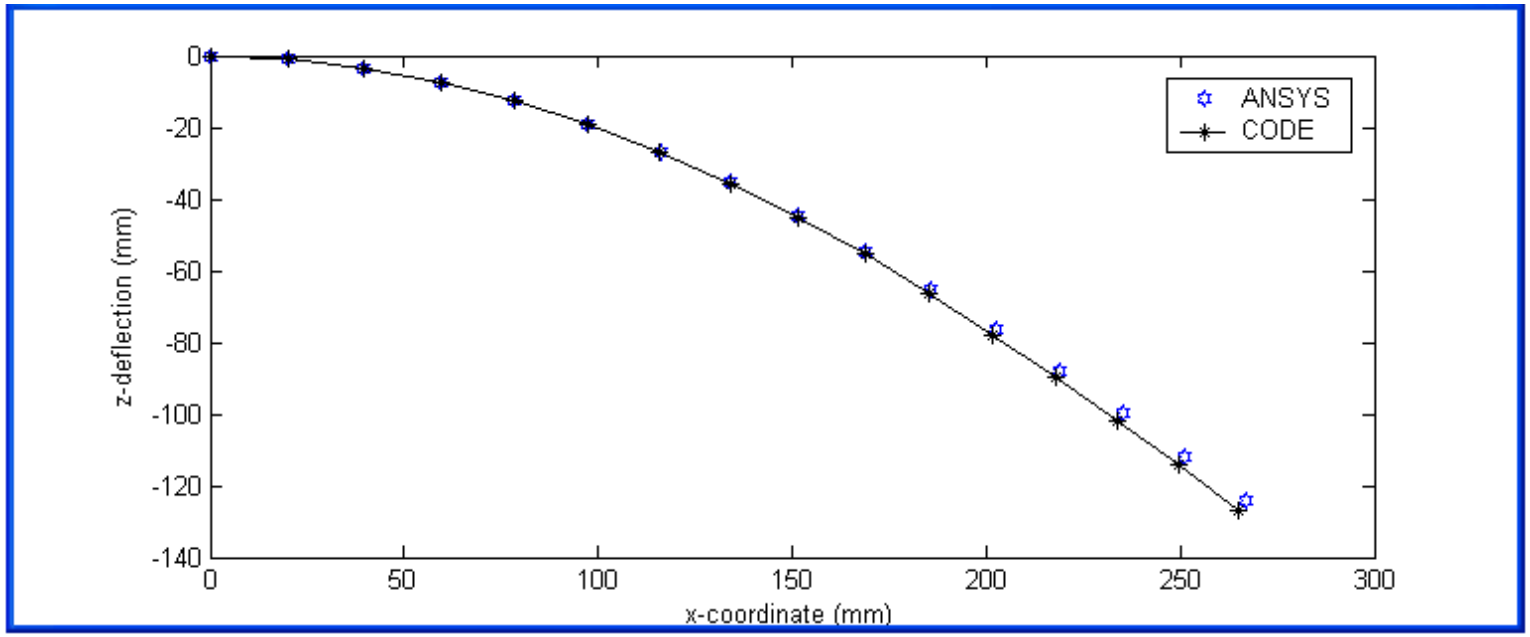

Figure 6.1.6 Deflected coordinates of the $[60/-60/60/-60/60/-60/60]_s$ laminate. B.C: Left end fixed

6.2 Case II: Clamped-Clamped

Case II includes the loading of the both ends fixed laminates along the middle line (Figure 6.2.1). 14-ply 2.8 mm thick laminates with the fiber angle orientations $[0/90/0/90/0/90/0]_s$, $[15/-15/15/-15/-15/-15/15]_s$, $[30/-30/30/-30/-30/-30/30]_s$, $[45/-45/45/-45/-45/-45/45]_s$, $[60/-60/60/-60/-60/-60/60]_s$ are loaded in an incremental iterative way and first ply failure loads and nonlinear deflection characteristics are detected according to the maximum stress, Tsai-Wu and Tsai-Hill failure theories. Graphs (Figures 6.2.2-6.2.6) are constructed by the application of the failure load obtained by Tsai-Wu criterion from the written code as an input load to the ANSYS. The output failure loads of the written code and ANSYS are listed in tabular form (Tables 6.2.1-6.2.10) together with the failure indexes, and a graph representing the deformed X-Z coordinates of the laminate up to damage onset is also plotted for each case.

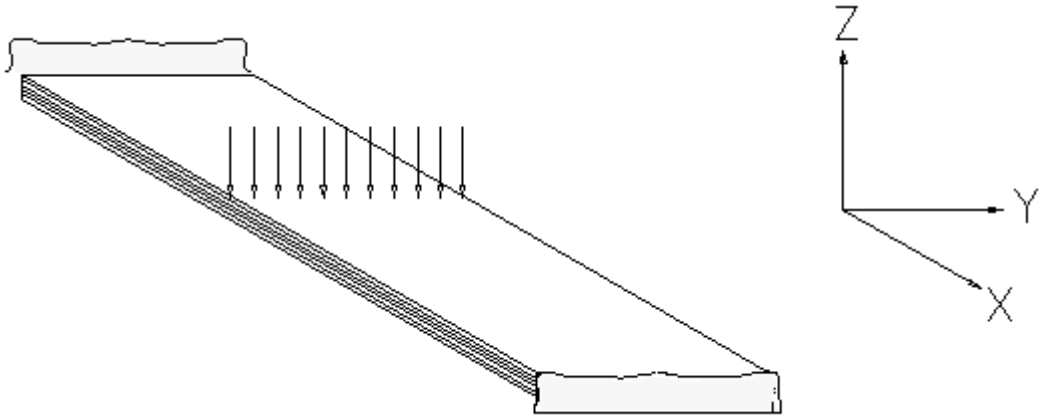

Figure 6.2.1 Schematic representation of Case II

For the composite shell with the fiber angle orientation $[0/90/0/90/0/90/0]_s$, the failure loads are obtained from the developed code and for this failure load, midpoint displacements and maximum failure index values found by both developed code and ANSYS are given in Tables 6.2.1 and 6.2.2, while the deformed shape is depicted in Figure 6.2.2. Failure onset is observed at the bottom layers at the midpoint of the laminate in tension form along the fiber direction according to the three criteria. Minimum stresses belong to maximum stress theory and the maximum ones to Tsai-Wu, because of the increasing loads. Results are at good agreement level.

Table 6.2.1 First Ply Failure (Results from Code)

Criterion	***Load (N)***	***Midpoint Displacement (mm)***	***Failure Index***
Maximum Stress	2018.50	8.35	1.00070
Tsai-Wu	2535.50	9.11	1.00100
Tsai-Hill	2167.00	8.57	1.00024

Table 6.2.2 First Ply Failure (Results from ANSYS)

Criterion	***Load (N)***	***Midpoint Displacement (mm)***	***Failure Index***
Maximum Stress	2535.50	8.9884	1.00920
Tsai-Wu	2535.50	8.9884	0.95272

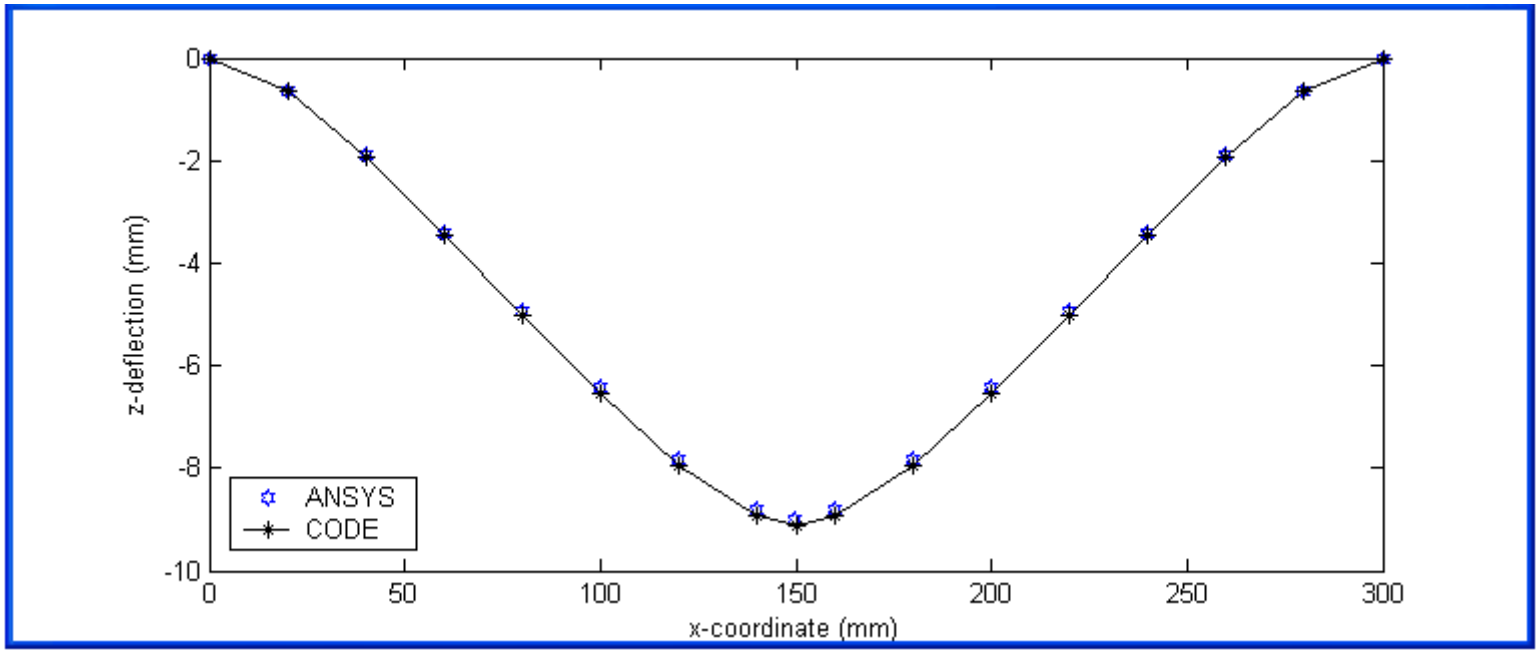

Figure 6.2.2 Deflected coordinates of the $[0/90/0/90/0/90/0]_s$ laminate. B.C: Both ends fixed

For the composite shell with the fiber angle orientation $[15/-15/15/-15/15/-15/15]_s$, the failure loads are obtained from the developed code and for this failure load, midpoint displacements and maximum failure index values found by both developed code and ANSYS are given in Tables 6.2.3 and 6.2.4. Failure onset is observed at the bottom layers along the left end by the compressive stress in fiber direction. For the same fiber orientation, the deformed shape of the composite shell obtained from the code and ANSYS that are given in Figure 6.2.3. Results form code and ANSYS are compatible.

Table 6.2.3 First Ply Failure (Results from Code)

Criterion	***Load (N)***	***Midpoint Displacement (mm)***	***Failure Index***
Maximum Stress	3201.00	9.14	1.00066
Tsai-Wu	3043.70	8.95	1.00000
Tsai-Hill	3493.60	9.45	1.00000

Table 6.2.4 First Ply Failure (Results from ANSYS)

Criterion	***Load (N)***	***Midpoint Displacement (mm)***	***Failure Index***
Maximum Stress	3043.70	8.65	0.87194
Tsai-Wu	3043.70	8.65	0.95245

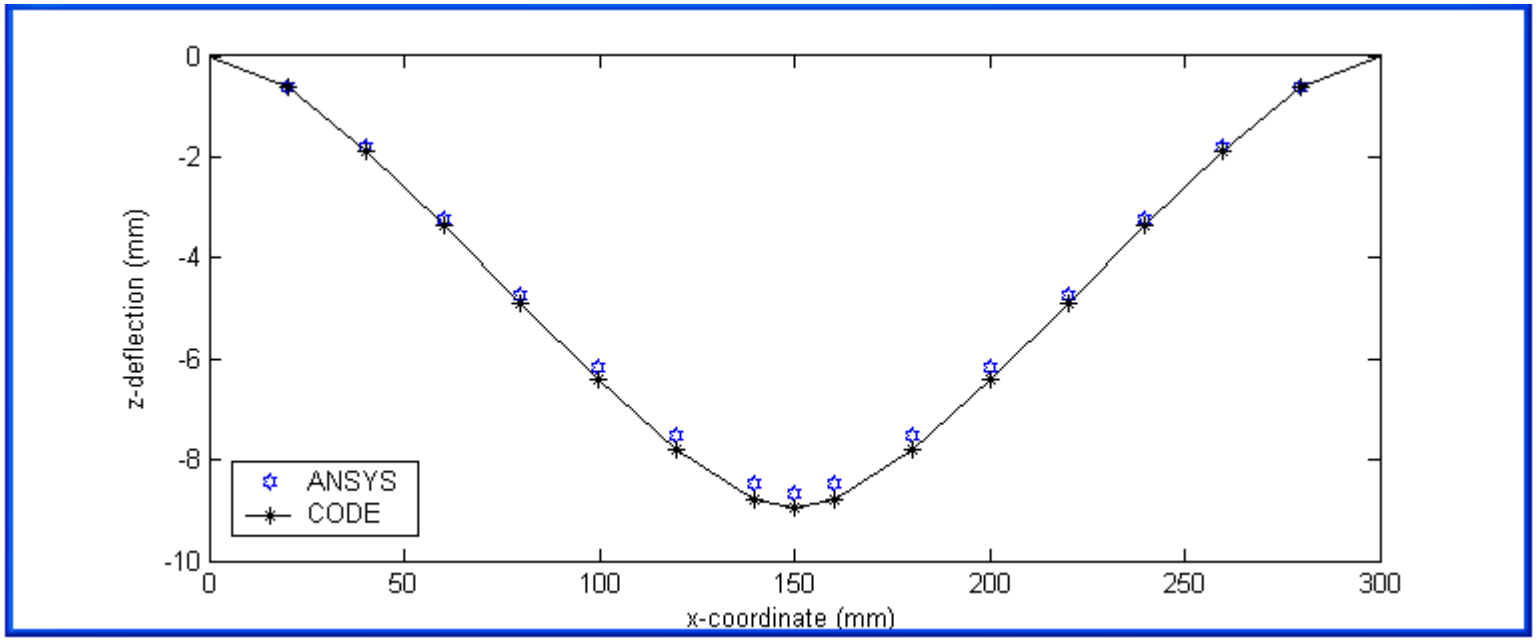

Figure 6.2.3 Deflected coordinates of the [*15/-15/15/-15/15/-15/15*]$_s$ laminate. B.C: Both ends fixed

For the composite shell with the fiber angle orientation $[30/-30/30/-30/-30/-30/30]_s$, the failure loads are obtained from the developed code and for this failure load, midpoint displacements and maximum failure index values found by both developed code and ANSYS are given in Tables 6.2.5 and 6.2.6. Failure onset is observed at the bottom layers near along the right hand side by the tensile stress in fiber direction. Also, a significant amount of shear stress is noted. For the same fiber orientation, the deformed shape of the composite shell obtained from the code and ANSYS that are given in Figure 6.2.4. The difference between the results are less than 3.2%.

Table 6.2.5 First Ply Failure (Results from Code)

Criterion	***Load (N)***	***Midpoint Displacement (mm)***	***Failure Index***
Maximum Stress	2530.00	9.59	1.00023
Tsai-Wu	2285.80	9.20	1.00007
Tsai-Hill	2722.50	9.86	1.00211

Table 6.2.6 First Ply Failure (Results from ANSYS)

Criterion	***Load (N)***	***Midpoint Displacement (mm)***	***Failure Index***
Maximum Stress	2285.80	8.91	0.95181
Tsai-Wu	2285.80	8.91	0.89099

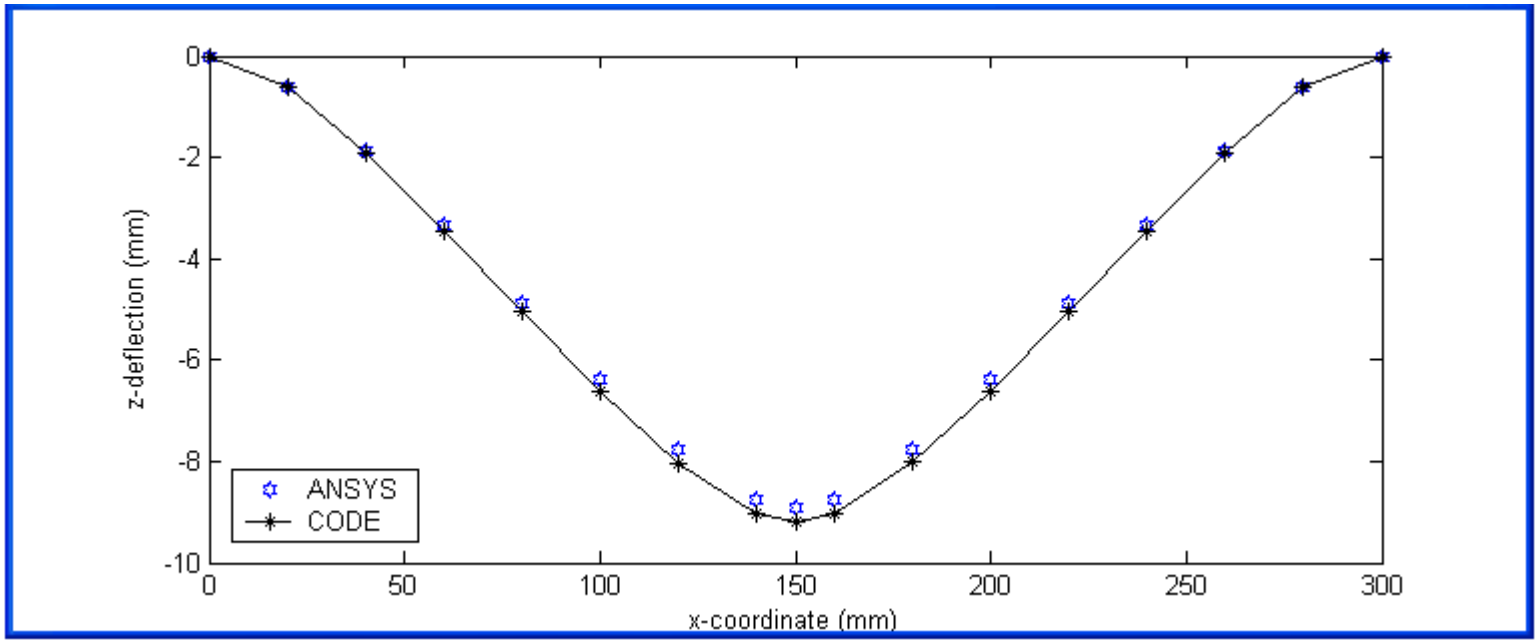

Figure 6.2.4 Deflected coordinates of the $[30/-30/30/-30/30/-30/30]_s$ laminate. B.C: Both ends fixed

The composite shell with the fiber angle orientation $[45/-45/45/-45/45/-45/45]_s$, the failure loads, midpoint displacements and maximum failure index values found by both developed code and ANSYS are given in Tables 6.2.7 and 6.2.8. First ply failure initiated at the bottom layers along the right hand side of the laminate as a result of excess compressive stress in fiber direction. For the same fiber orientation, the deformed shape of the composite shell obtained from the code and ANSYS are given in Figure 6.2.5. Comparisons have shown good agreement.

Table 6.2.7 First Ply Failure (Results from Code)

Criterion	***Load (N)***	***Midpoint Displacement (mm)***	***Failure Index***
Maximum Stress	2508.00	11.27	1.00044
Tsai-Wu	1967.50	10.24	1.00019
Tsai-Hill	3019.50	12.01	1.00126

Table 6.2.8 First Ply Failure (Results from ANSYS)

Criterion	***Load (N)***	***Midpoint Displacement (mm)***	***Failure Index***
Maximum Stress	1967.50	10.13	1.21030
Tsai-Wu	1967.50	10.13	1.02450

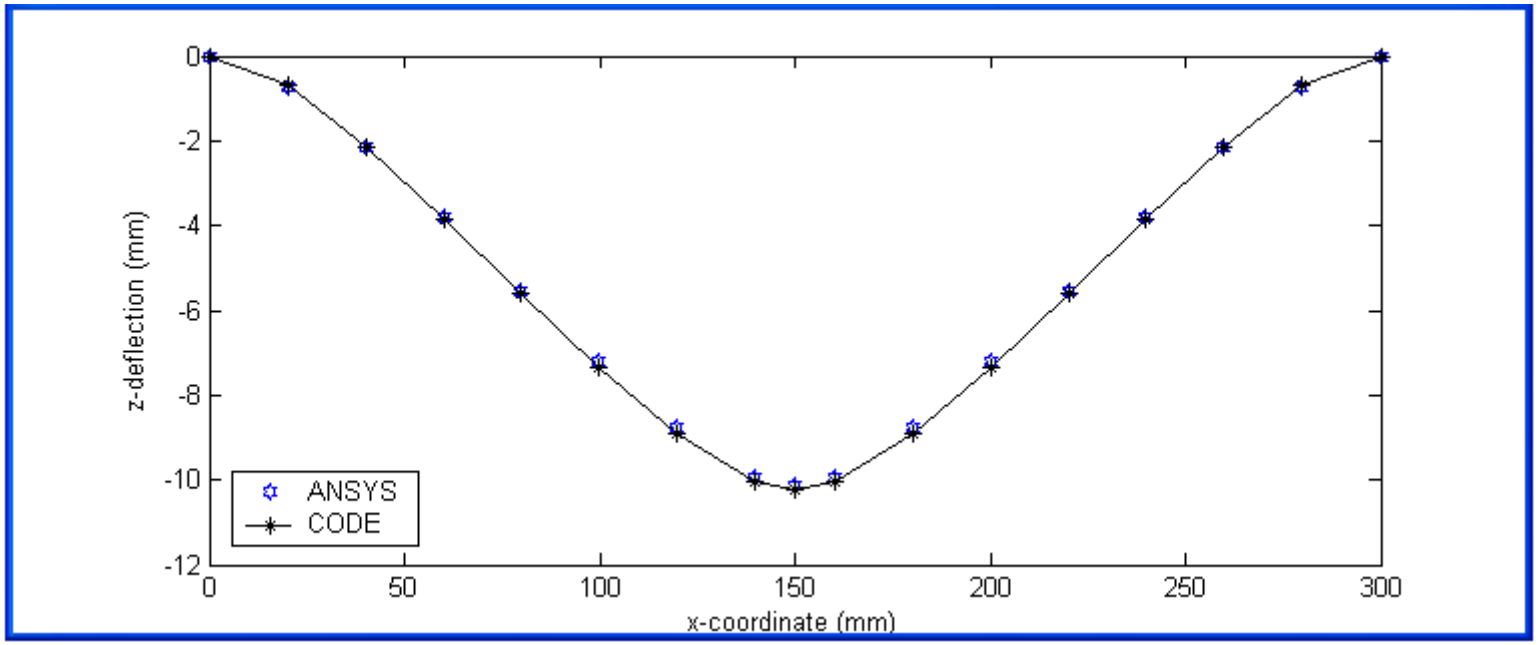

Figure 6.2.5 Deflected coordinates of the $[45/-45/45/-45/45/-45/45]_s$ laminate. B.C: Both ends fixed

The failure loads, midpoint displacements and maximum failure index values found by both developed code and ANSYS are given in Tables 6.2.9 and 6.2.10 for the composite shell with the fiber angle orientation $[60/-60/60/-60/-60/-60/60]_s$. The deformed shapes of the composite shell obtained from the code and ANSYS are given in Figure 6.2.6. Failure is observed at the bottom layers along the right hand side of the shell in all theories. Good agreement is observed between the results of the developed code and ANSYS.

Table 6.2.9 First Ply Failure (Results from Code)

Criterion	***Load (N)***	***Midpoint Displacement (mm)***	***Failure Index***
Maximum Stress	3437.50	14.25	1.00018
Tsai-Wu	2975.50	13.49	1.00014
Tsai-Hill	4004.00	15.09	1.00005

Table 6.2.10 First Ply Failure (Results from ANSYS)

Criterion	***Load (N)***	***Midpoint Displacement (mm)***	***Failure Index***
Maximum Stress	2975.50	13.35	1.39810
Tsai-Wu	2975.50	13.35	1.61570

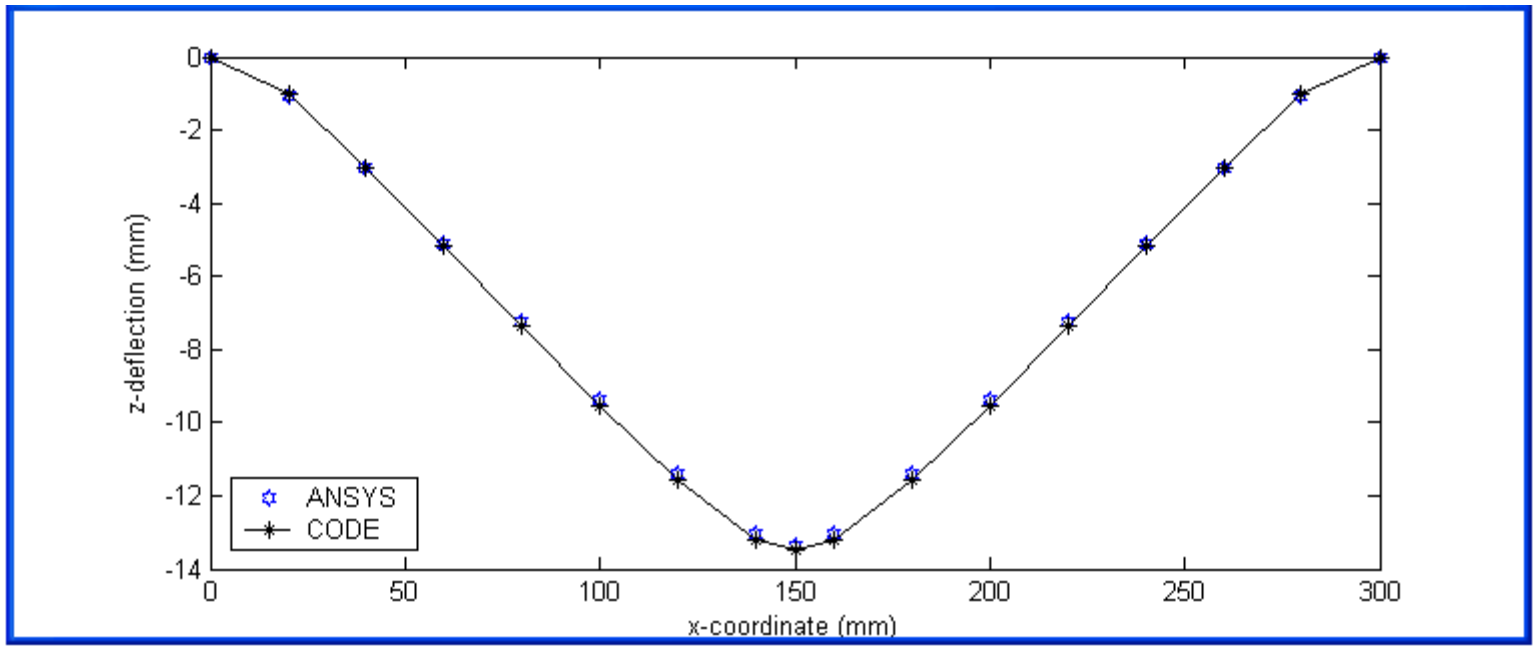

Figure 6.2.6 Deflected coordinates of the $[60/-60/60/-60/60/-60/60]_s$ laminate. B.C: Both ends fixed

6.3 Case III: Clamped-Roller

In Case-III, the structure is fully restricted on the left end while the other end is allowed to translate among X and Y axes, and rotate about Y (Figure 6.3.1). Loads are applied to the nodes lying on the middle line of the laminate, and failure responses and deformation characteristics are observed. 14-ply 2.8 mm thick laminates with the fiber angle orientations $[0/90/0/90/0/90/0]_s$, $[15/-15/15/-15/-15/-15/15]_s$, $[30/-30/30/-30/-30/-30/30]_s$, $[45/-45/45/-45/-45/-45/45]_s$, $[60/-60/60/-60/-60/-60/60]_s$ are examined according to the maximum stress, Tsai-Wu and Tsai-Hill failure theories. The output failure loads of the developed code and ANSYS are listed in tabular form together with the failure indexes, and a graph representing the deformed shape of the laminate up to damage initiation is also plotted for each case. Graphs are constructed by the application of the failure load obtained by Tsai-Wu criterion from the developed code as an input load to the ANSYS. Failure initiated at the bottom layers starting from the fixed ends of the laminates.

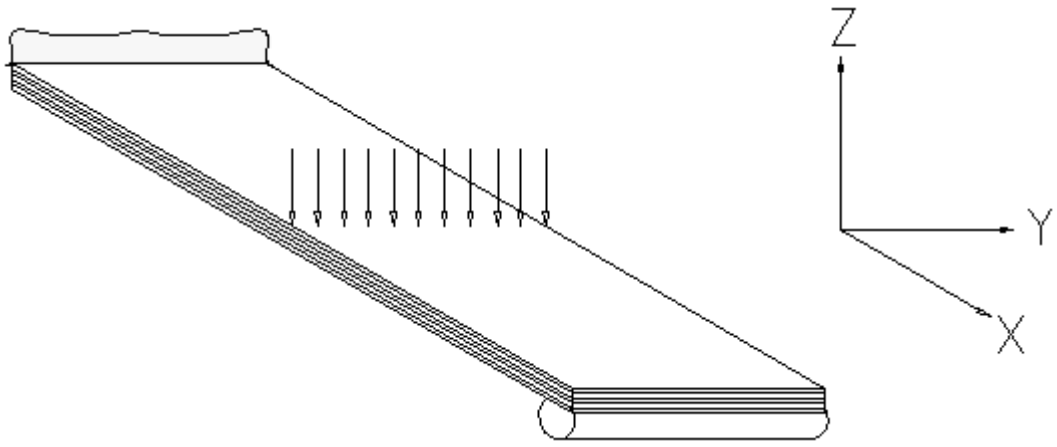

Figure 6.3.1 Schematic representation of Case III

Failure loads, midpoint displacements and maximum failure index values found by both developed code and ANSYS are given in Tables 6.3.1 and 6.3.2 and a schematic representation of the deformed shapes of the composite shell obtained from the code and ANSYS is given in Figure 6.3.2 for the composite shell with the fiber angle orientation $[0/90/0/90/0/90/0]_s$. Failure is caused by the compressive stress in fiber direction at the bottom layers along the fixed end, and initiated at the same element in all theories. Results are in good agreement.

Table 6.3.1 First Ply Failure (Results from Code)

Criterion	*Load (N)*	*Midpoint Displacement (mm)*	*Failure Index*
Maximum Stress	208.60	9.82	1.00129
Tsai-Wu	203.50	9.66	1.00108
Tsai-Hill	225.50	10.67	1.00376

Table 6.3.2 First Ply Failure (Results from ANSYS)

Criterion	*Load (N)*	*Midpoint Displacement (mm)*	*Failure Index*
Maximum Stress	203.50	9.54	0.91461
Tsai-Wu	203.50	9.54	0.88579

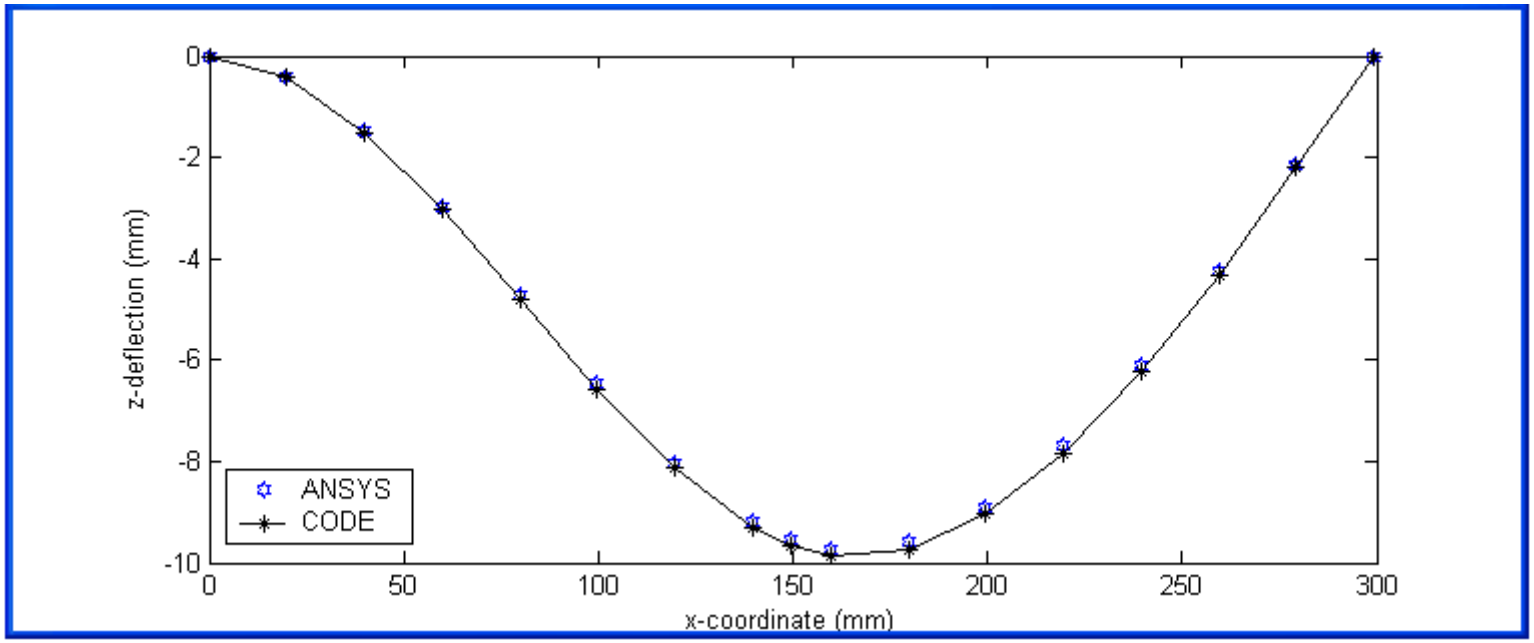

Figure 6.3.2 Deflected coordinates of the $[0/90/0/90/0/90/0]_s$ laminate. B.C: Fixed-roller

For the composite shell with the fiber angle orientation $[15/-15/15/-15/-15/-15/15]_s$, the failure loads, midpoint displacements and maximum failure index values found by both developed code and ANSYS are given in Tables 6.3.3 and 6.3.4, and the deformed shape is plotted in Figure 6.3.3. Failure started at the bottom layers along the fixed end by the excess compressive stress in fiber direction, and initiated at the same element in all theories. Deformed shapes obtained from developed code and ANSYS are in good agreement.

Table 6.3.3 First Ply Failure (Results from Code)

Criterion	***Load (N)***	***Midpoint Displacement (mm)***	***Failure Index***
Maximum Stress	273.90	8.54	1.00015
Tsai-Wu	266.20	8.32	1.00006
Tsai-Hill	303.60	11.28	1.00140

Table 6.3.4 First Ply Failure (Results from ANSYS)

Criterion	***Load (N)***	***Midpoint Displacement (mm)***	***Failure Index***
Maximum Stress	266.20	9.75	0.92579
Tsai-Wu	266.20	9.75	0.95794

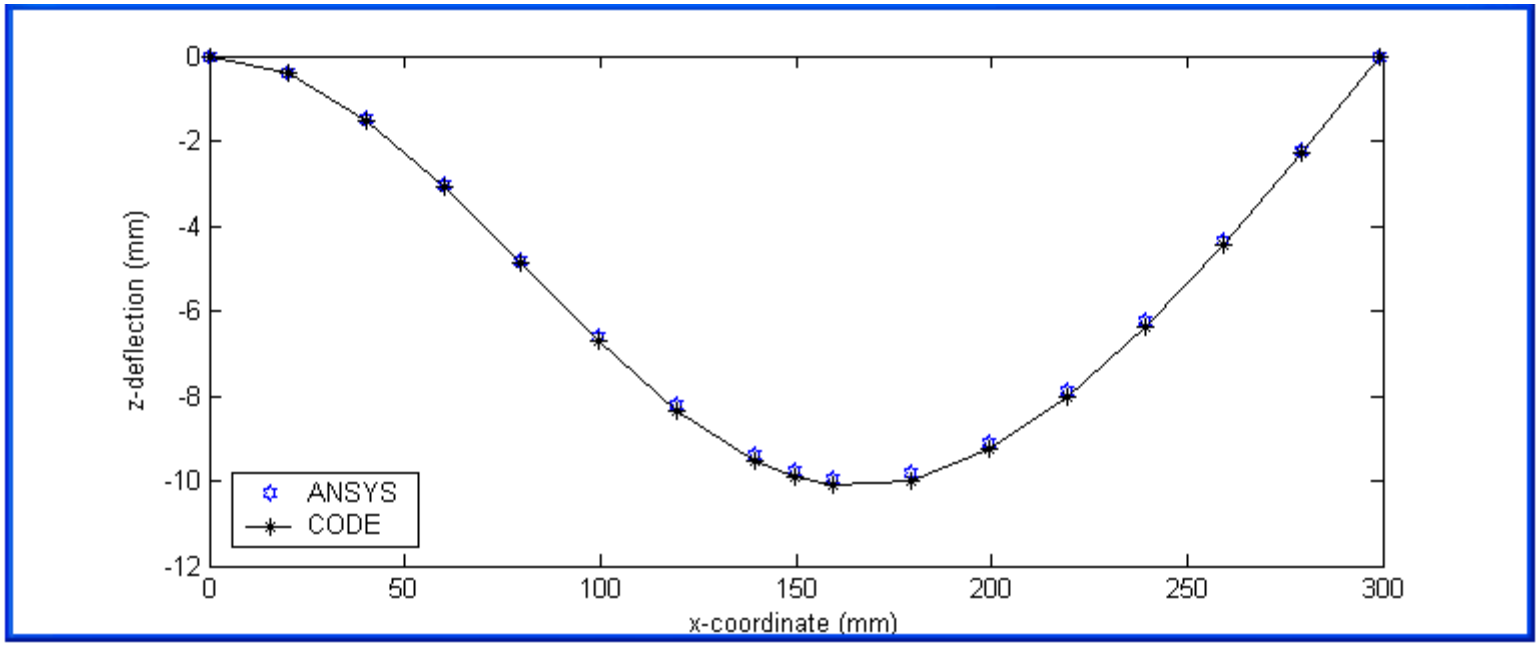

Figure 6.3.3 Deflected coordinates of the $[15/-15/15/-15/15/-15/15]_s$ laminate. B.C: Fixed-roller

For the composite shell with the fiber angle orientation $[30/-30/30/-30/-30/-30/30]_s$, the failure loads are obtained from the developed code and for this failure load, tip displacements and maximum failure index values found by both developed code and ANSYS are given in Tables 6.3.5 and 6.3.6. For the same fiber orientation, the deformed shape of the composite shell obtained from the code and ANSYS that are given in Figure 6.3.4. Both results are in good agreement. Failure onset is observed at the bottom layers along the fixed end in fiber-direction-compression form.

Table 6.3.5 First Ply Failure (Results from Code)

Criterion	***Load (N)***	***Midpoint Displacement (mm)***	***Failure Index***
Maximum Stress	249.15	10.13	1.00194
Tsai-Wu	243.30	11.62	1.00193
Tsai-Hill	281.08	13.78	1.00025

Table 6.3.6 First Ply Failure (Results from ANSYS)

Criterion	***Load (N)***	***Midpoint Displacement (mm)***	***Failure Index***
Maximum Stress	243.30	11.69	0.90996
Tsai-Wu	243.30	11.69	0.96361

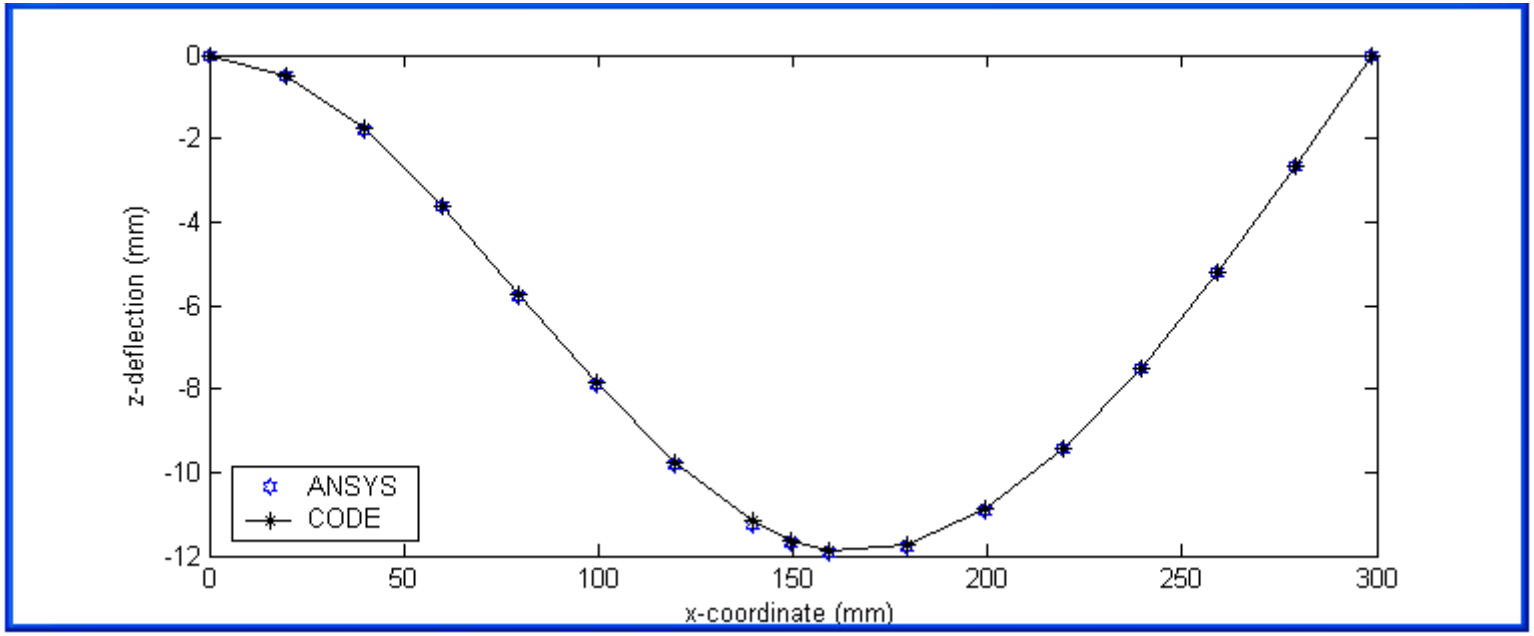

Figure 6.3.4 Deflected coordinates of the $[30/-30/30/-30/30/-30/30]_s$ laminate. B.C: Fixed-roller

Failure loads, midpoint displacements and maximum failure indexes of the composite shell with the fiber angle orientation $[45/-45/45/-45/-45/45/45]_s$ found by both developed code and ANSYS are given in Tables 6.3.7 and 6.3.8. First ply failure is observed at the bottom layers along the fixed end in fiber-compression-direction. For the same fiber orientation, the deformed shape of the composite shell obtained from the code and ANSYS are given in Figure 6.3.5. A deviation of 6.15 % is detected during the displacement comparisons, but results are in adequate agreement in both of the programs.

Table 6.3.7 First Ply Failure (Results from Code)

Criterion	***Load (N)***	***Midpoint Displacement (mm)***	***Failure Index***
Maximum Stress	223.30	16.04	1.00004
Tsai-Wu	210.30	15.18	1.00011
Tsai-Hill	253.00	17.98	1.00491

Table 6.3.8 First Ply Failure (Results from ANSYS)

Criterion	***Load (N)***	***Midpoint Displacement (mm)***	***Failure Index***
Maximum Stress	210.30	16.112	0.84186
Tsai-Wu	210.30	16.112	1.03390

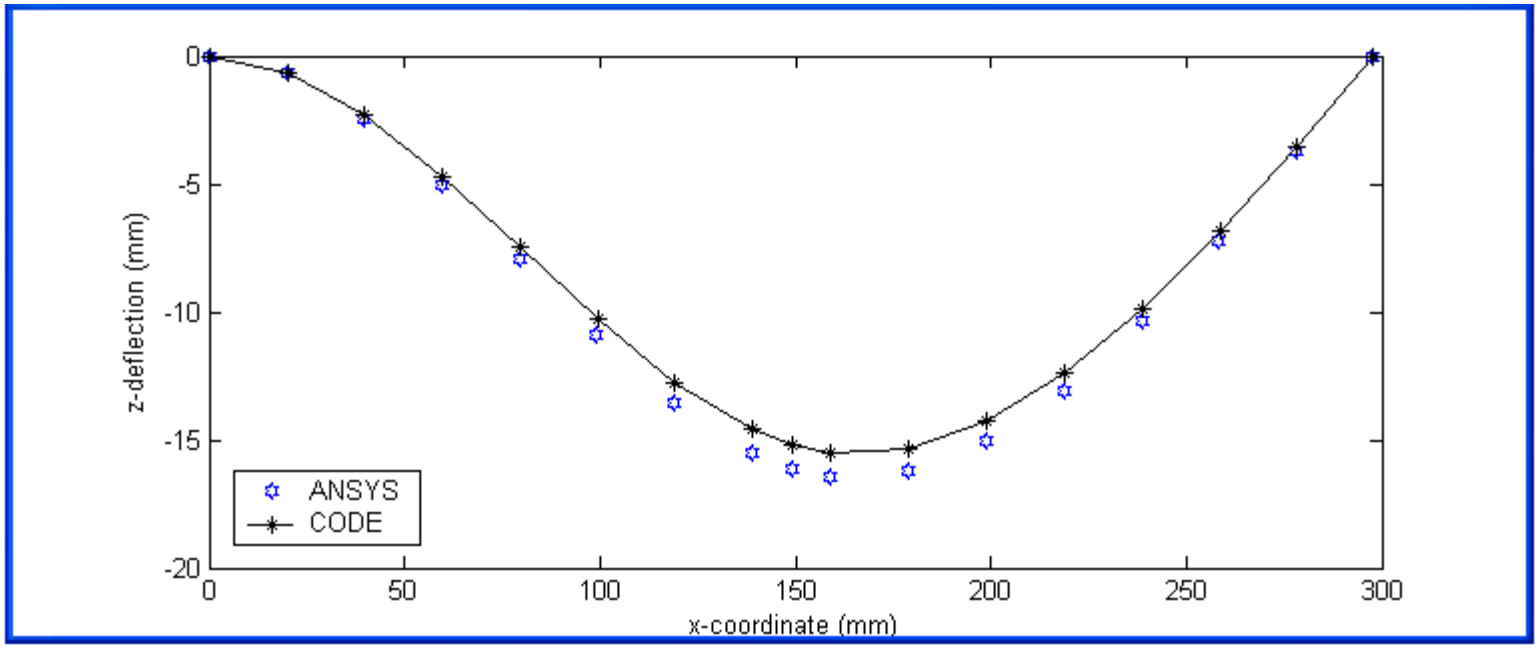

Figure 6.3.5 Deflected coordinates of the $[45/-45/45/-45/45/-45/45]_s$ laminate. B.C: Fixed-roller

For the composite shell with the fiber angle orientation $[60/-60/60/-60/-60/-60/60]_s$, the failure loads are obtained from the developed code and for this failure load, midpoint displacements and maximum failure index values found by both developed code and ANSYS are given in Tables 6.3.9 and 6.2.10. Damage onset is observed at the bottom layers along the fixed end and the failure stress is in compression form. For the same fiber orientation, the deformed shape of the composite shell obtained from the code and ANSYS that are given in Figure 6.3.6. The maximum difference between the results is about 6.47%.

Table 6.3.9 First Ply Failure (Results from Code)

Criterion	***Load (N)***	***Midpoint Displacement (mm)***	***Failure Index***
Maximum Stress	239.80	23.88	1.00363
Tsai-Wu	205.48	20.80	1.00033
Tsai-Hill	268.40	26.39	1.00563

Table 6.3.10 First Ply Failure (Results from ANSYS)

Criterion	***Load (N)***	***Midpoint Displacement (mm)***	***Failure Index***
Maximum Stress	205.48	22.24	0.63400
Tsai-Wu	205.48	22.24	1.00600

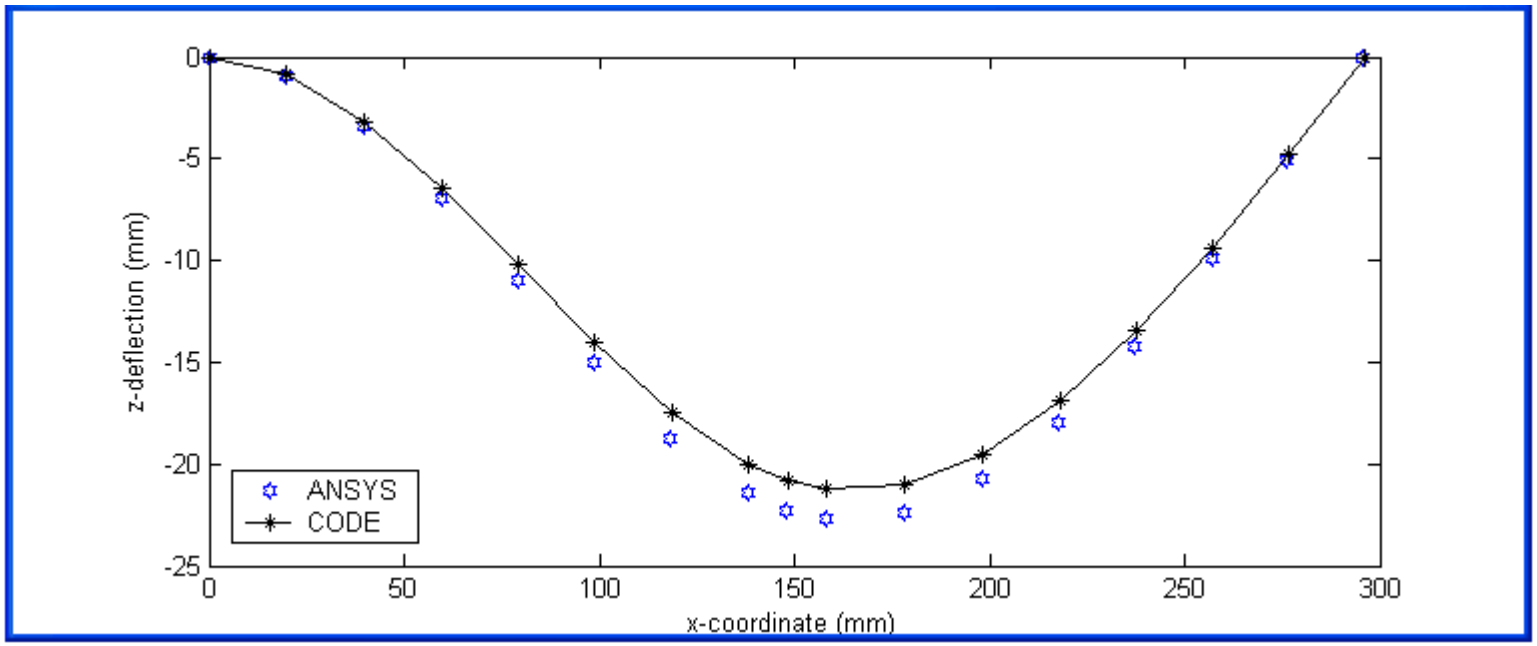

Figure 6.3.6 Deflected coordinates of the $[60/-60/60/-60/60/-60/60]_s$ laminate. B.C: Fixed-roller

6.4 Case IV: Simply Supported

Case IV includes the loading of 14-ply 2.8 mm thick laminates having the fiber angle orientations $[0/90/0/90/0/90/0]_s$, $[15/-15/15/-15/-15/-15/15]_s$, $[30/-30/30/-30/-30/-30/30]_s$, $[45/-45/45/-45/-45/-45/45]_s$, $[60/-60/60/-60/-60/-60/60]_s$ with the imposed boundary condition "simply supported" (Figure 6.4.1). The left hand side nodes are pinned allowing the Y-axis rotation, and that of the other end are restricted by a roller constraining the X and Z rotations and X-axis translation. The laminates are loaded incrementally until the first ply failure initiation with respect to maximum stress, Tsai-Wu and Tsai-Hill theories. All models started to fail at the top layer; and the failed coordinates are along the middle of the laminates. The output failure loads of the written code and ANSYS are listed in tabular form together with the failure indexes, and a graph representing the deformed shape of the laminate up to damage initiation is also plotted for each case. Graphs are constructed by the application of the failure load obtained by Tsai-Wu criterion from the written code as an input load to the ANSYS.

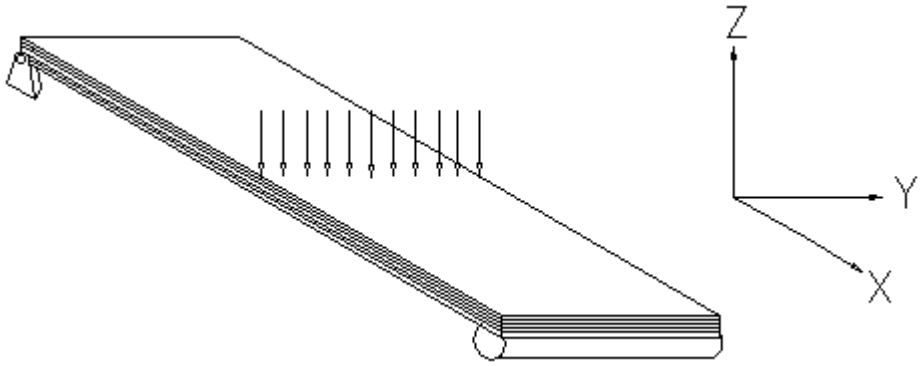

Figure 6.4.1 Schematic representation of Case IV

The composite shell with the fiber angle orientation $[0/90/0/90/0/90/0]_s$ is loaded until the first ply failure, and the resultant loads, midpoint displacements and maximum failure index values found by both developed code and ANSYS are given in Tables 6.4.1 and 6.4.2. For the same fiber orientation, the deformed shape of the composite shell obtained from the code and ANSYS that are given in Figure 6.4.2. Failure is initiated by the stress in the fiber direction at the top layers along the loading line. Results are in good agreement with a difference less than 2 % .

Table 6.4.1 First Ply Failure (Results from Code)

Criterion	*Load (N)*	*Midpoint Displacement (mm)*	*Failure Index*
Maximum Stress	152.90	16.62	1.00307
Tsai-Wu	150.70	16.39	1.00091
Tsai-Hill	165.00	17.85	1.00646

Table 6.4.2 First Ply Failure (Results from ANSYS)

Criterion	*Load (N)*	*Midpoint Displacement (mm)*	*Failure Index*
Maximum Stress	150.70	16.08	0.92332
Tsai-Wu	150.70	16.08	0.89663

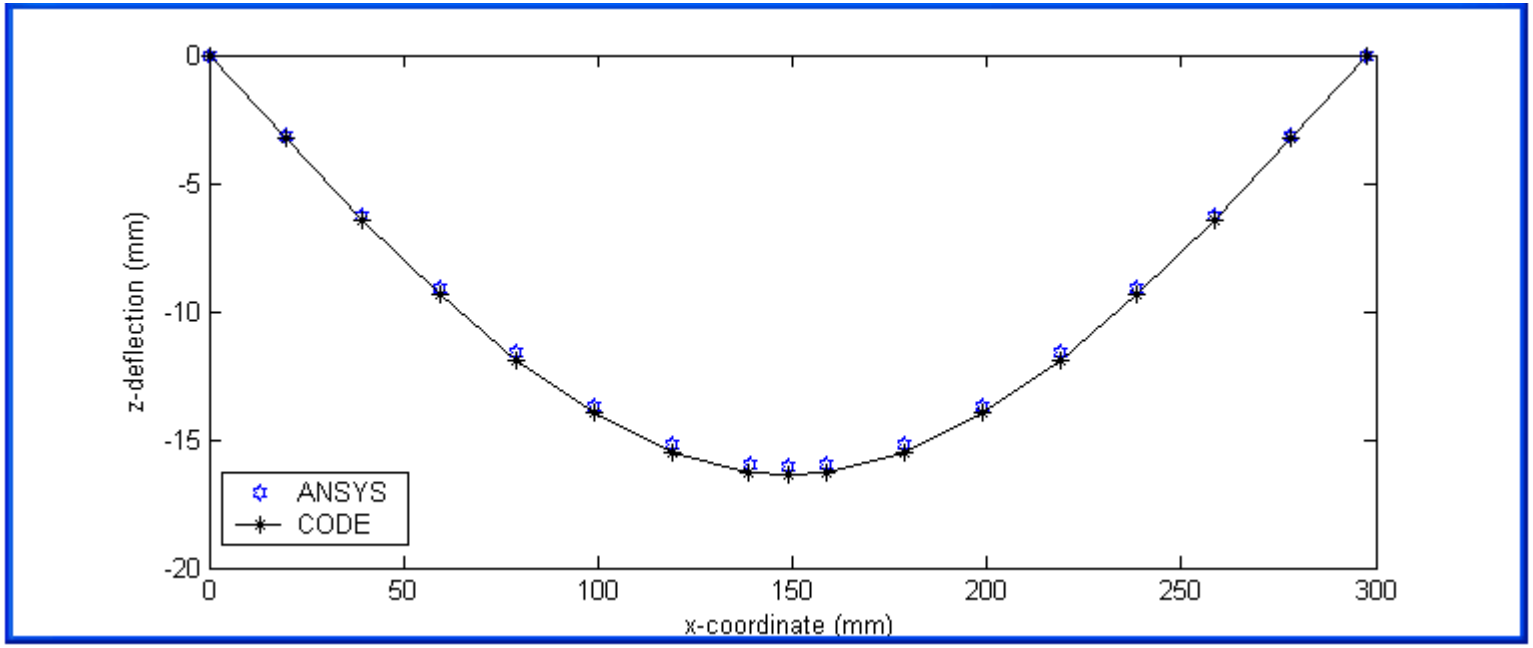

Figure 6.4.2 Deflected coordinates of the $[0/90/0/90/0/90/0]_s$ laminate. B.C: Simply supported

Failure loads, midpoint displacements and maximum failure indexes found by both developed code and ANSYS are given in Tables 6.4.3 and 6.4.4 for the composite shell with the fiber angle orientation $[15/-15/15/-15/15/-15/15]_s$. Deformed shape of the laminate obtained from the code and ANSYS that are given in Figure 6.4.3. Failure onset is detected at the top layers along the loading line. Results are observed to be in good agreement.

Table 6.4.3 First Ply Failure (Results from Code)

Criterion	***Load (N)***	***Midpoint Displacement (mm)***	***Failure Index***
Maximum Stress	217.80	18.45	1.00490
Tsai-Wu	211.86	17.97	1.00203
Tsai-Hill	239.80	20.19	1.00058

Table 6.4.4 First Ply Failure (Results from ANSYS)

Criterion	***Load (N)***	***Midpoint Displacement (mm)***	***Failure Index***
Maximum Stress	211.86	17.64	0.95034
Tsai-Wu	211.86	17.64	0.95794

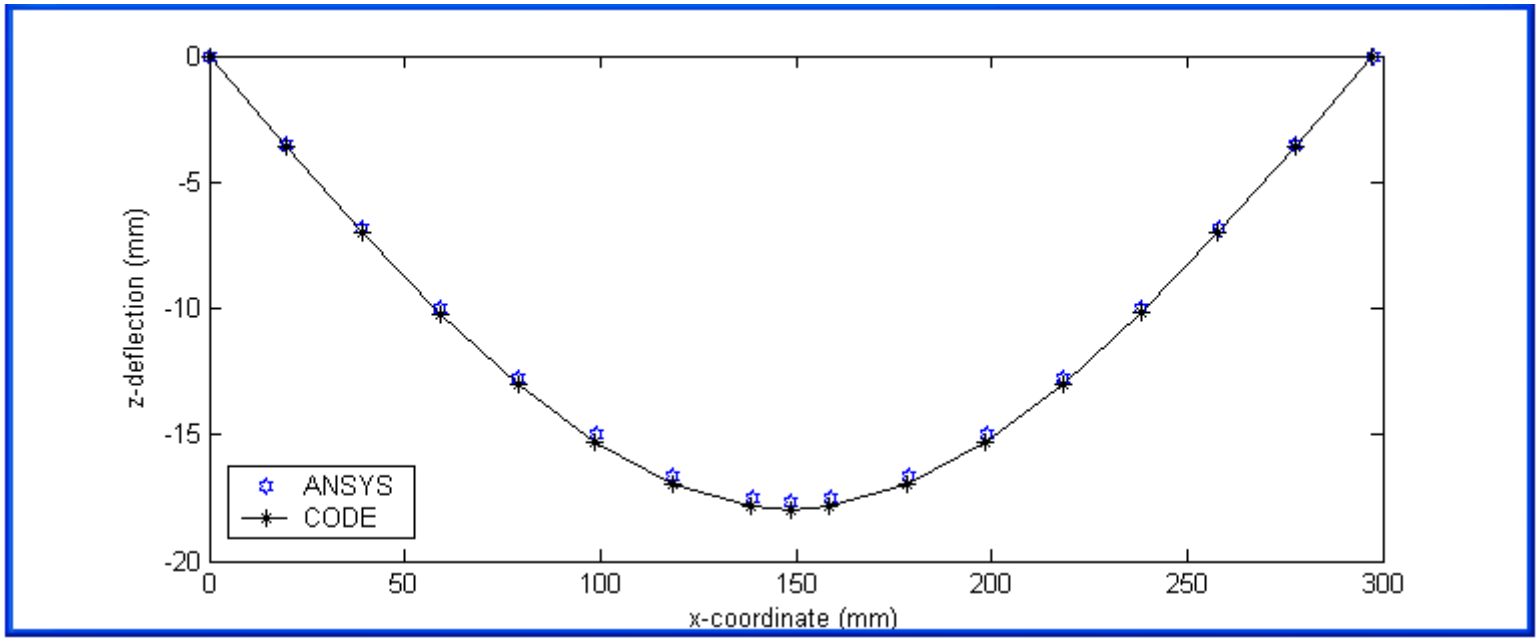

Figure 6.4.3 Deflected coordinates of the $[15/-15/15/-15/15/-15/15]_s$ laminate. B.C: Simply supported

The composite shell with the fiber angle orientation $[30/-30/30/-30/30/-30/30]_s$ is loaded to detect its first ply failure characteristics. Loads obtained from the developed code and for this failure load, midpoint displacements and maximum failure indexes found by both developed code and ANSYS are listed in Tables 6.4.5 and 6.4.6, and the deformed shape of the composite shell plotted by the data obtained from the code and ANSYS are given in Figure 6.4.4. Damage onset is observed at the top layers along the loading line in fiber direction in the form of compression. Results have shown good agreement.

Table 6.4.5 First Ply Failure (Results from Code)

Criterion	***Load (N)***	***Midpoint Displacement (mm)***	***Failure Index***
Maximum Stress	189.20	21.13	1.0025
Tsai-Wu	180.95	20.30	1.0004
Tsai-Hill	211.20	23.32	1.0014

Table 6.4.6 First Ply Failure (Results from ANSYS)

Criterion	***Load (N)***	***Midpoint Displacement (mm)***	***Failure Index***
Maximum Stress	180.95	20.50	0.89871
Tsai-Wu	180.95	20.50	0.97364

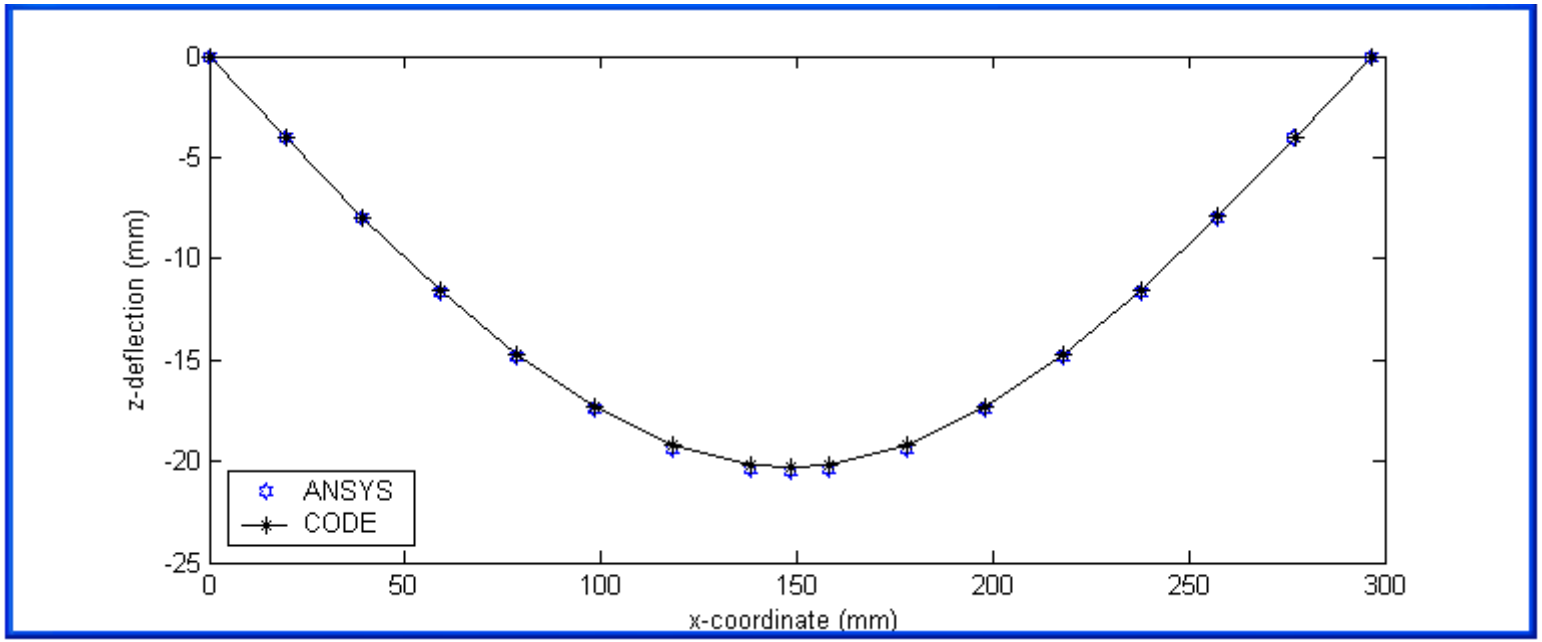

Figure 6.4.4 Deflected coordinates of the $[30/-30/30/-30/30/-30/30]_s$ laminate. B.C: Simply supported

For the composite shell with the fiber angle orientation $[45/-45/45/-45/45/-45/45]_s$, the failure loads are obtained from the developed code and for this failure load, midpoint displacements and maximum failure index values found by both developed code and ANSYS are presented in Tables 6.4.7 and 6.4.8. Damage is initiated by the excess compressive stresses at the top layers along the loading line. For the same fiber orientation, the deformed shape of the composite shell obtained from the code and ANSYS that are given in Figure 6.4.5. The maximum difference between the results obtained from the two sets of results is less than 7.5 %.

Table 6.4.7 First Ply Failure (Results from Code)

Criterion	***Load (N)***	***Midpoint Displacement (mm)***	***Failure Index***
Maximum Stress	189.20	30.48	1.00477
Tsai-Wu	177.13	28.17	1.00000
Tsai-Hill	211.20	33.49	1.00270

Table 6.4.8 First Ply Failure (Results from ANSYS)

Criterion	***Load (N)***	***Midpoint Displacement (mm)***	***Failure Index***
Maximum Stress	177.13	30.25	0.89639
Tsai-Wu	177.13	30.25	1.20720

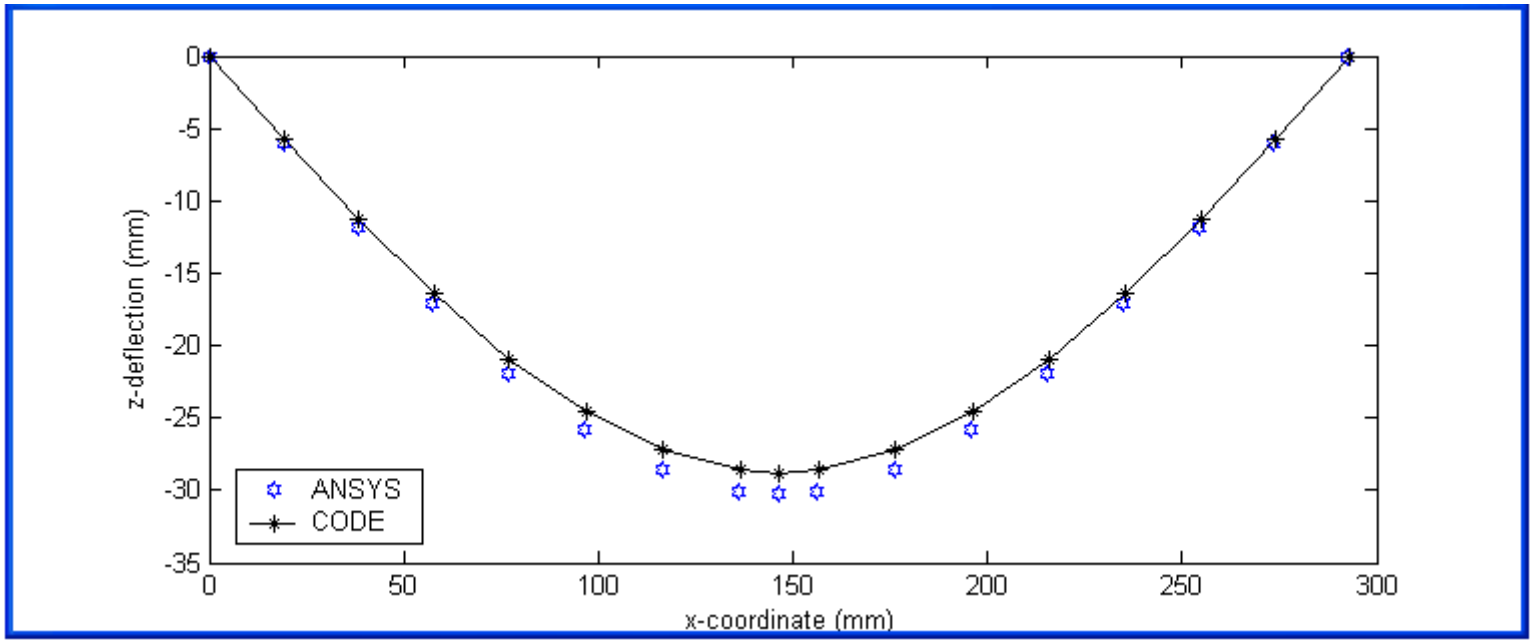

Figure 6.4.5 Deflected coordinates of the $[45/-45/45/-45/45/-45/45]_s$ laminate. B.C: Simply supported

The laminated composite shell with the fiber angle orientation $[60/-60/60/-60/60/-60/60]_s$ is loaded up the first ply failure. Loads, midpoint displacements and maximum failure index values corresponding to this failure load that are found by both developed code and ANSYS are given in Tables 6.4.9 and 6.4.10. Failure onset is observed at the top layers along the loading line. For the same fiber orientation, the deformed shape of the composite shell obtained from the code and ANSYS that are given in Figure 6.4.6. A difference of 6.6% is detected in the deflection amounts.

Table 6.4.9 First Ply Failure (Results from Code)

Criterion	*Load (N)*	*Midpoint Displacement (mm)*	*Failure Index*
Maximum Stress	201.30	43.18	1.00191
Tsai-Wu	172.37	38.08	1.00031
Tsai-Hill	220.00	46.30	1.00046

Table 6.4.10 First Ply Failure (Results from ANSYS)

Criterion	*Load (N)*	*Midpoint Displacement (mm)*	*Failure Index*
Maximum Stress	172.37	40.50	0.64101
Tsai-Wu	172.37	40.50	1.15940

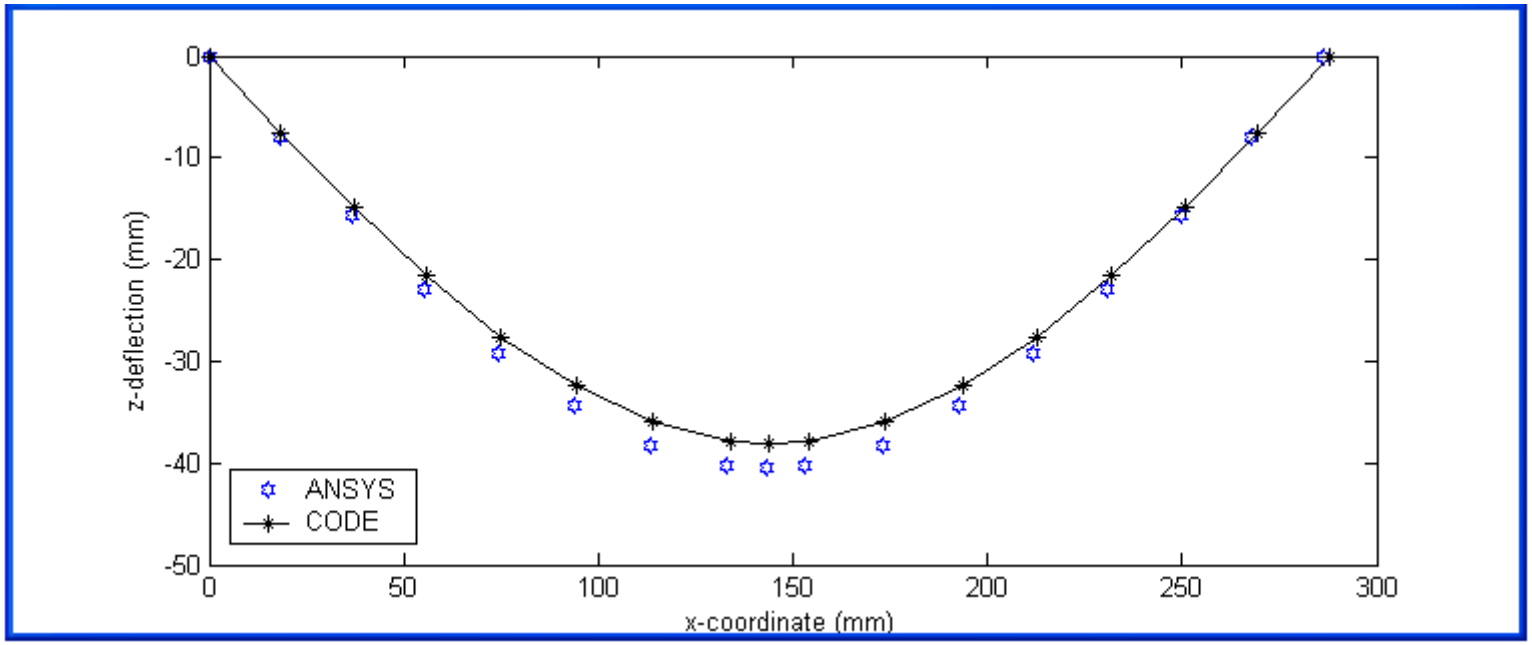

Figure 6.4.6 Deflected coordinates of the $[60/-60/60/-60/60/-60/60]_s$ laminate. B.C: Simply supported

6.5 Case V: Pinched Cylinder

In Case V, pinched cylinder problem is inspected with the use of the developed code and ANSYS. This case is considered in order to check the ability of the constructed model whether it can sustain membrane loads as well as the bending loads. The cylindrical shell subjected to the compressive load P is shown in Figure 6.5.1. The problem is modeled taking the advantages of symmetric boundary conditions, using the 1/8 portion of the shell as shown in Figure 6.5.2, and applying P/4 to the point A. A 14-layered-2.8 mm thick cylindrical shell with the fiber angle orientation $[0/90/0/90/0/90/0]_s$, having dimensions of R = 50 mm, L= 200 mm is loaded with a force of P/4 = 161.0 N and radial displacement results of the developed code and ANSYS are compared.

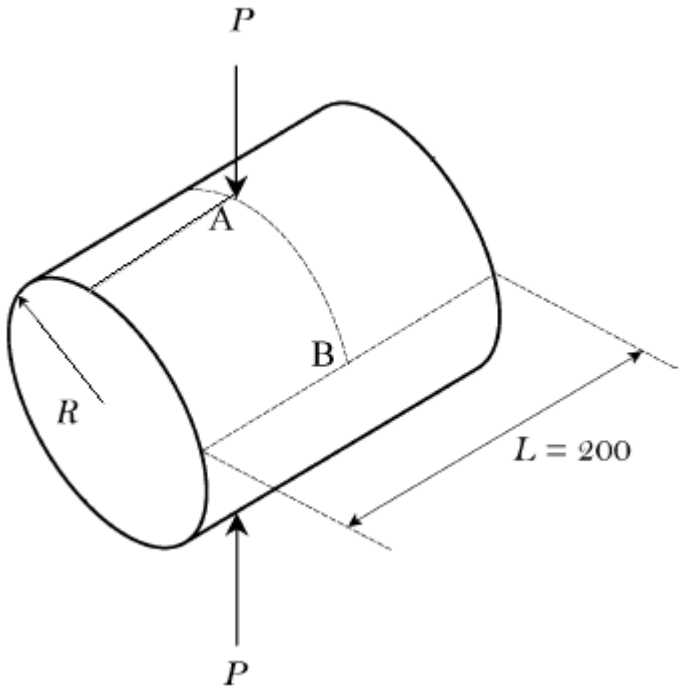

Figure 6.5.1 Pinched cylinder (not to scale) [39]

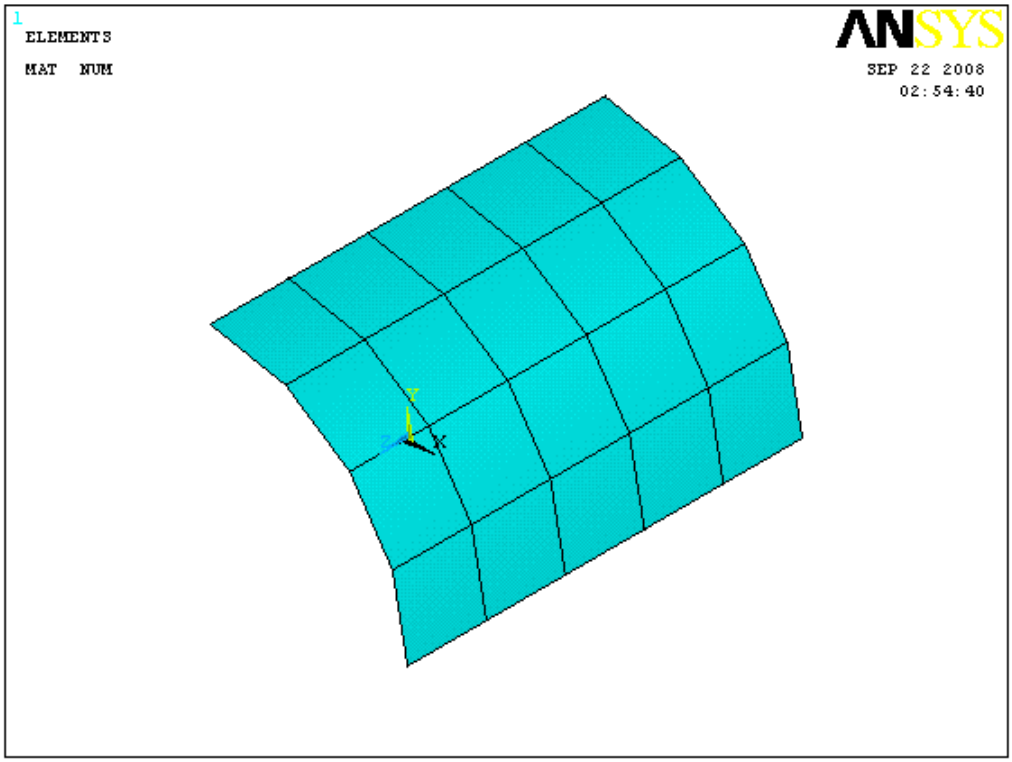

Figure 6.5.2 Illustration of the 1/8 of the cylindrical shell in ANSYS

A load of 161.0 N is applied to both programs and radial displacement values are plotted together from point A to B, with the undeformed shape in Figure 6.5.3. Results from the two data sets have shown good agreement.

Failure loads, midpoint displacements and maximum failure indexes of the composite shell with the fiber angle orientation $[0/90/0/90/0/90/0]_s$ found by both developed code and ANSYS are given in Tables 6.5.1 and 6.5.2. For the same fiber orientation, the deformed shape of the composite shell obtained from the code and ANSYS are given in Figure 6.5.3.

Table 6.5.1 First Ply Failure (Results from Code)

Criterion	*Load (N)*	*Radial Displacement (mm)*	*Failure Index*
Maximum Stress	162.25	4.37	1.00033
Tsai-Wu	161.00	4.32	1.00017
Tsai-Hill	169.8	4.65	1.00066

Table 6.5.2 First Ply Failure (Results from ANSYS)

Criterion	*Load (N)*	*Radial Displacement (mm)*	*Failure Index*
Maximum Stress	161.00	3.93	0.85652
Tsai-Wu	161.00	3.93	0.81035

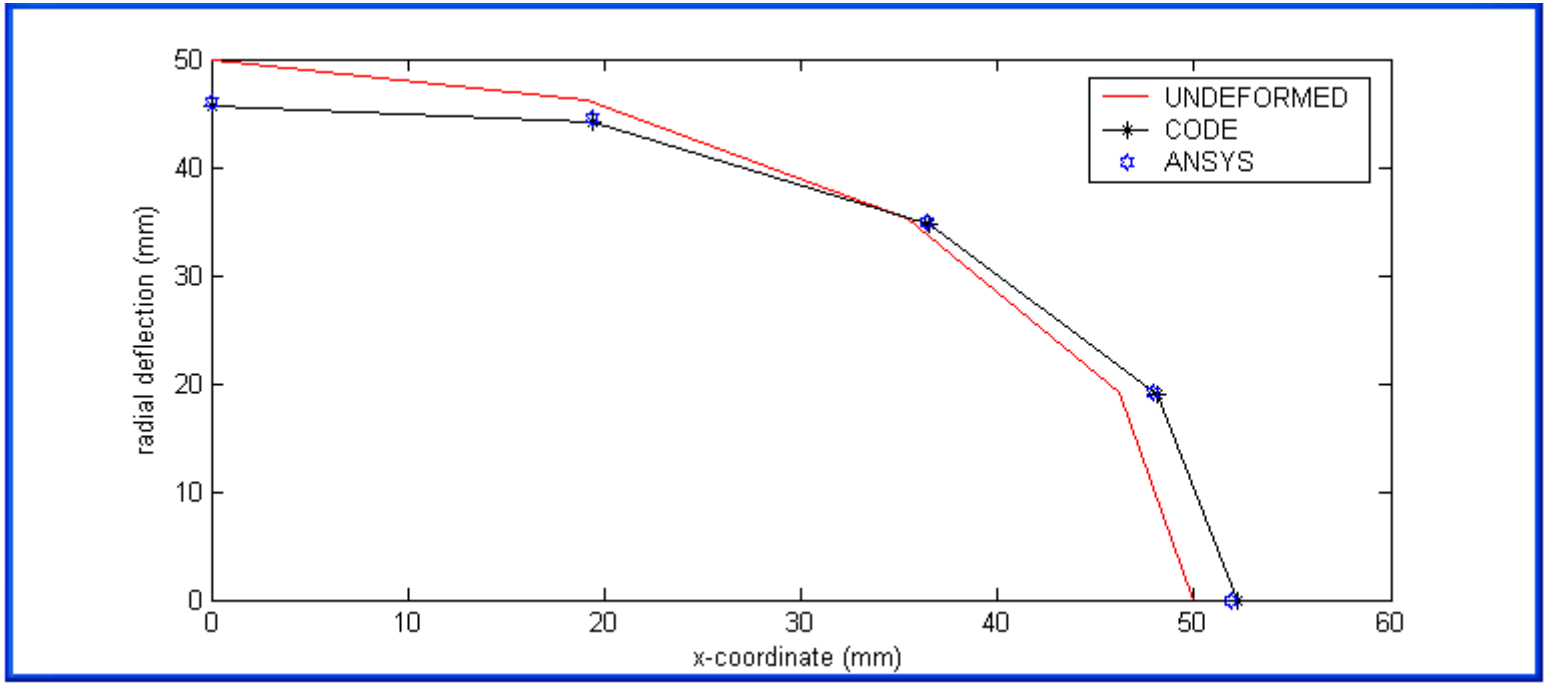

Figure 6.5.3 Deflected coordinates of the [0/90/0/90/0/90/0]s pinched cylinder

CHAPTER 7

CONCLUSIONS

In the content of this study, the first ply failure and large displacement characteristics of the laminated flat composite shells made up of glass/epoxy are investigated through the use of the developed code, and the commercial finite element program, ANSYS. According to the current work, the following conclusions have been acquired:

1. Deflections and failure indexes obtained by ANSYS and developed code are very close to each other which yield almost the same stress states for the same load. The small differences may arise from the fact that mesh elements have different geometries and programs govern different iteration-solution techniques in each solution scheme.

2. It is found out that the dominant mode in first ply failure is mostly originated from fiber-directed compressive stress.

3. Whatever the boundary condition is, it is observed that out-of-plane stresses are considerably small values as compared to those in material coordinates for the laminate with the fiber angle orientation $[0/90/0/90/0/90/0]_{s.}$. For the angle-ply laminates this situation is also valid, but the shear stress components become more significant.

4. In all cases except for the simply supported one, damage initiated at the bottom layer regardless of the fiber orientation. On the contrary, the laminates

with the simply supported boundary condition started to fail from the top layer.

5. It can be noted that, among all the theories applied, Tsai-Hill criterion lead to the maximum failure load most of the time.

6. It is proved that the entrance of shear correction factor into the constitutive relations has improved the results.

7. It is observed that, as the laminate gets thinner, results obtained with higher load steps diverges from the actual results apparently because of the shear locking problem. But the imposition of the smaller load increments causes an incredible increase in the CPU time, so a precise compromise should be authorized by the user. During the FORTRAN executions, the load step must be chosen as small as possible in order to achieve exact results.

8. The model is proved to work well with both flat and curved shells.

9. Comparisons are found to have shown adequate agreement between the outputs of the modified computer program and the simulation tool ANSYS 8.1.

The extension of the current work may include progressive damage analysis which is based on the stiffness reduction of the element mesh, since the developed program is applicable for this kind of process.

REFERENCES

[1] Gibson, R.F., Principles of Composite Material Mechanics, McGraw-Hill, 1994

[2] Schwartz, M.M., Composite Materials, Volume II: Processing, Fabrication and Applications, Prentice Hall, 1997

[3] Mazumdar, S.K., Composites Manufacturing, CRC Press, 2001

[4] Schwartz, M.M., Composite Materials Handbook, McGraw-Hill, 1984

[5] Noton, B.R., Engineering Applications of Composite Materials, Academic Press, 1974

[6] Masud, A., Tham, C.L., Liu, W.K., *A Stabilized 3-D Co-Rotational Formulation for Geometrically Nonlinear Analysis of Multi-Layered Composite Shells,* Computational Mechanics, Vol. 26, pp 1-12, 2001

[7] Kumar, W.P., Palaninathan, R., *Finite Element Analysis of Laminated Shells with Exact Through-Thickness Integration,* Computers and Structures, Vol. 63, pp 173-184, 1997

[8] Hossain, S.J., Sinha, P.H., Sheikh, A.H., *A Finite Element Formulation for the Analysis of Laminated Composite Shells,* Computers and Structures, Vol. 82, pp 1623-1638, 2004

[9] Dau, F., Polit, O., Touratier, M., C^1 *Plate and Shell Finite Elements for Geometrically Nonlinear Analysis of Multilayered Structures,* Computers and Structures, Vol. 84, pp 1264-1274, 2006

[10] Klinkel, S., Gruttmann, F., Wagner, W., *A Continuum Based ThreeDimensional Shell Element for Laminated Structures,* Computers and Structures, Vol. 71, pp 43-62, 1999

[11] Brank, B., Carrera, E., *A Family of Shear-Deformable Shell Finite Elements for Composite Structures,* Computers and Structures, Vol. 76, pp 287-297, 2000

[12] Alfano, G., Auricchio, F., Rosati, L., Sacco, E., *MITC Finite Elements for Laminated Composite Plates,* International Journal for Numerical Methods in Engineering, Vol. 51, pp 707-738, 2001

[13] Yu, W., Hodges, D.H., Volovoi, V.V., *Asymptotically Accurate 3-D Recovery from Reissner-like Composite Plate Finite Elements,* Computers and Structures, Vol. 81, pp 439-454, 2003

[14] Wung, P.M., *Laminated Composite Structures by Continuum-Based Shell Elements with Transverse Deformation,* Computers and Structures, Vol. 62, pp 1073-1090, 1997

[15] Rohwer, K., Rolfes, R., *Calculating 3-D Stresses in Layered Composite Plates and Shells,* Mechanics of Composite Materials, Vol. 34, pp 355-362, 1998

[16] Goswami, S., *A C^0 Plate Bending Element with Refined Shear Deformation Theory for Composite Structures*, Composite Structures, Vol. 72, pp 375-382, 2006

[17] Chaudhuri, R.A., Hsia, R.L., *Effect of Thickness on the Large Elastic Deformation Behavior of Laminated Shells*, Composite Structures, Vol. 43, pp 117-128, 1998

[18] Malekzadeh, P., Setoodeh, A.R., *Large Deformation Analysis of Moderately Thick Laminated Plates on Nonlinear Elastic Foundations by DQM,* Composite Structures, Vol. 80, pp 569-579, 2007

[19] Parhi, P.K., Bhattacharyya, S.K., Sinha, P.K., *Failure Analysis of Multiple Delaminated Composite Plates Due to Bending and Impact,* Bull. Mater. Sci., Vol. 24, pp 143-149, 2001

[20] Huang, Z-M., *Failure Analysis of Laminated Structures by FEM Based on Nonlinear Constitutive Relationship,* Composite Structures, Vol. 77, pp 270-279, 2007

[21] Huang, Z-M., *Effect of Matrix Plasticity on Ultimate Strength of Composite Laminates*, Journal of Reinforced Plastics and Composites, Vol. 20, pp 304-320, 2001

[22] Lin, W-P., Hu, H-T., *Nonlinear Analysis of Fiber Reinforced Laminates Subjected to Uniaxial Tensile Load*, Journal of Composite Materials, Vol. 36, pp 1481-1503, 2001

[23] Padhi, G.S., Shenoi, R.A., Moy, S.S.J., and Hawkins, G.L., *Progressive Failure and Ultimate Collapse of Laminated Composite Plates in Bending,* Composite Structures, Vol. 40, pp 277-291, 1998

[24] Spottswood, M.S., Palazotto, A.N., *Progressive Failure Analysis of a Composite Shell, Composite Structures*, Vol. 53, pp 117-131, 2001

[25] Prusty, B.G., Satsangi, S.K., Ray, C., *First Ply Failure Analysis of Laminated Panels under Transverse Loading*, Journal of Reinforced Plastics and Composites, Vol. 20, pp 671-684, 2001

[26] Pal, P., Bhattacharyya, S.K., *Progressive Failure Analysis of Cross-ply Laminated Composite Plates by Finite Element Method*, Journal of Reinforced Plastics and Composites, Vol. 26, pp 465-477, 2007

[27] Pal, P., Ray, C., *Progressive Failure Analysis of Laminated Composite Plates by Finite Element Method*, Journal of Reinforced Plastics and Composites, Vol. 21, pp 1505-1513, 2002

[28] Reddy, J.N., *Mechanics of Laminated Composite Plates and Shells*, CRC Press

[29] Reddy, J.N., Finite Element Method, McGraw-Hill

[30] Lim, G.T., Reddy, J.N., *On Canonical Bending Relationships for Plates*, International Journal of Solids and Structures, Vol. 40, pp 3039-3067, 2003

[31] Roufaeil, O.L., Tran-Cong, T., *Finite Strip Elements for Laminated Composite Plates with Transverse Shear Strain Discontinuities,* Composite Structures, Vol. 56, pp 249-258, 2002

[32] Gdoudus, E.E., Pilakoutas, K., Rodopoulos, C.A., Failure Analysis of Industrial Composite Materials, McGraw-Hill

[33] Pisano, A.A., Fuschi, P., *A Numerical Approach for Limit Analysis of Orthotropic Composite Laminates,* International Journal for Numerical Methods in Engineering, 2006

[34] Naik, N.G., Murty, A.V.K., *A Failure Mechanism-based Approach for Design of Composite Laminates,* Composite Structures, Vol. 45, pp 71-80, 1999

[35] Jones, R.M., Mechanics of Composite Materials, McGraw-Hill, 1975

[36] Darendeliler, H., Oral, S., Turgut, A., *A Pseudo-Layered, Elastic-Plastic, Flat-Shell Finite Element,* Computational Methods in Applied Mechanics and Engineering, Vol.174, pp 211-218, 1999

[37] Hoque, M.M., *3-D Nonlinear Mixed Finite Element Analysis of RC Beams and Plates with and without FRP Reinforcement*, 2006

[38] Bathe, K.J., Finite Element Procedures, Prentice Hall, 1996

[39] Pimenta, P.M., Campello, E.M.B., Wriggers, P., *A Fully Nonlinear Multi-Parameter Shell Model with Thickness Variation and a Triangular Shell Finite Element*, Computational Mechanics, Vol. 34, pp 181-193, 2004